UNIVERSIDAD NACIONAL AUTÓNOMA DE MÉXICO

PROGRAMA DE MAESTRÍA Y DOCTORADO EN INGENIERÍA
INGENIERÍA ELÉCTRICA – CONTROL

TRANSPARENT TELEOPERATION WITH UNKNOWN SURFACES AND FORCE ESTIMATION

TESIS
QUE PARA OPTAR POR EL GRADO DE:
DOCTOR EN INGENIERÍA

PRESENTA:
M.I. IVÁN ALEJANDRO GUTIÉRREZ GILES

TUTOR PRINCIPAL
DR. MARCO ANTONIO ARTEAGA PÉREZ, FACULTAD DE INGENIERÍA, UNAM
COMITÉ TUTOR
DR. ALEJANDRO RODRÍGUEZ ÁNGELES, CINVESTAV, IPN
DR. YU TANG XU, FACULTAD DE INGENIERÍA, UNAM

MÉXICO, D. F. JUNIO 2016

JURADO ASIGNADO:

Presidente:	DR. GERARDO RENÉ ESPINOSA PÉREZ
Secretario:	DR. YU TANG XU
Vocal:	DR. MARCO ANTONIO ARTEAGA PÉREZ
1er. Suplente:	DR. ALEJANDRO RODRÍGUEZ ÁNGELES
2do. Suplente:	DR. RUBÉN ALEJANDRO GARRIDO MOCTEZUMA

Lugar o lugares donde se realizó la tesis: FACULTAD DE INGENIERÍA, UNAM

TUTOR DE TESIS:

DR. MARCO ANTONIO ARTEAGA PÉREZ

FIRMA

Abstract

Teleoperation means operating at a distance. In the context of robotics, teleoperation is commonly carried out by means of robotic arms and a human–machine interface. To exploit to the maximum the capabilities of a teleoperation system, the control engineering discipline analyzes, through the development of mathematical models, the system dynamics to design algorithms in order to improve the performance or to induce some predefined behavior. In the present work, a robotic teleoperation system is studied, which is composed of two manipulators called *master* and *slave*, a *human operator* that moves the master, a *remote environment* over which the slave operates, and a *communication channel* between the controllers of each robot.

The main objective of this work is to design a control algorithm for a master–slave teleoperation system that operates over rigid surfaces with unknown geometry. Additionally, it is desired that the designed algorithm does not require velocity nor force sensors at the slave side, *i.e.*, using only joint position measurements for the slave robot. To achieve this objective, a dynamic extension and a high–gain observer were employed, which jointly are known in the literature as Generalized Proportional Integral (GPI) observers. For the movement control and force tracking, a hybrid position/force controller based on an orthogonal decomposition of the task space was employed. The GPI observer allows, besides simultaneous estimation of slave robot joint velocity and the contact force over the remote environment, to reconstruct the geometry of the remote surface by means of an on line estimator. In other words, the proposed algorithm achieves movement of the slave robot over the surface and simultaneous application of a force desired by the human operator, while at the same time it performs an estimation of the velocity and force signals, and the gradient of the unknown surface.

A mathematical analysis was carried out, which guarantees locally uniform ultimate boundedness of all signals. Furthermore, it was formally proven that the final bound of the tracking and estimation errors can be made arbitrarily small, which means approximate but arbitrarily close position and force tracking and also arbitrarily close estimation of slave joint velocities, contact force, and the gradient of the surface.

The proposed scheme was validated both through numerical simulations and experiments, with satisfactory results. The simulations show that the proposed method has an excellent performance under ideal conditions. On the other hand, the experimental results supports the pertinence of the assumptions made for the design and analysis of the system, also obtaining a good performance, given the simplicity of the proposed method. Among some other advantages, the designed scheme is easy to tune and to implement, which makes it very attractive for the practitioners over other existing solutions available in the literature.

Resumen

Teleoperación significa literalmente operar a distancia. En el contexto de la robótica, la teleoperación se realiza comúnmente a través de brazos manipuladores mediante una interfaz humano–máquina. Para aprovechar al máximo las capacidades de un sistema de teleoperación, la ingeniería de control se encarga, mediante el uso de modelos matemáticos, de analizar la dinámica del sistema y diseñar algoritmos para obtener mejoras o inducir un comportamiento específico de acuerdo con un objetivo preestablecido. En este trabajo se estudia un sistema de teleoperación robótica compuesto por dos manipuladores llamados *maestro* y *esclavo*, un *operador humano* que mueve al maestro, un *ambiente remoto* sobre el que opera el esclavo y un *canal de comunicación* entre los sistemas que controlan a cada uno de los robots.

El objetivo de este trabajo consistió en diseñar un algoritmo de control para un sistema de teleoperación maestro–esclavo sobre superficies rígidas con geometría desconocida. Se desea además que el algoritmo no emplee sensores de velocidad ni de fuerza, es decir, utilizando sólo mediciones de posición en caso del robot esclavo. Para lograr este objetivo se utilizó una extensión dinámica del estado y un observador de alta ganancia, que en conjunto son conocidos como observadores Proporcionales Integrales Generalizados (GPI, por sus siglas en inglés). Para lograr el control de movimiento y de la fuerza de contacto se utilizó un controlador híbrido de posición/fuerza basado en la descomposición ortogonal del espacio de trabajo. El observador GPI permite, además de estimar simultáneamente la velocidad articular del robot esclavo y la fuerza de contacto sobre la superficie remota, reconstruir la geometría de dicha superficie mediante la introducción de un estimador en línea. En otras palabras, el algoritmo logra que el robot esclavo se mueva sobre la superficie, de acuerdo con la trayectoria deseada por el operador humano, ejerciendo al mismo tiempo una fuerza también comandada por el operador sobre ésta, mientras estima las señales de velocidad y de fuerza y la geometría de la superficie.

Se llevó a cabo un análisis matemático que garantiza localmente el acotamiento uniforme de todas las señales. Adicionalmente, se demostró que la cota final de los errores de estimación

y de seguimiento de posición y de fuerza puede hacerse arbitrariamente pequeña, lo que significa que se obtiene un seguimiento aproximado pero arbitrariamente cercano de las trayectorias deseadas así como una estimación de la velocidad articular, la fuerza de contacto y el gradiente de la superficie.

El esquema propuesto fue validado tanto en simulación numérica como experimentalmente con resultados satisfactorios. Las simulaciones muestran que el método propuesto presenta un excelente desempeño en condiciones ideales. Por otro lado, los resultados experimentales apoyan la validez de las suposiciones realizadas, obteniendo asimismo un buen desempeño tomando en cuenta la simplicidad del algoritmo propuesto. Entre las principales ventajas del método propuesto destaca su facilidad de sintonización e implementación, lo que lo hace atractivo para la práctica en contraste con otras soluciones existentes en la literatura.

Acknowledgments

Firstly, I would like to express my sincere gratitude to my mentor Dr. Marco Arteaga, for all his support, for sharing his knowledge and above all for being a great person. I could not have imagined having a better advisor for my doctoral studies.

I want also like to thank my thesis committee, Dr. Alejandro Rodríguez, Dr. Yu Tang, Dr. Rubén Garrido, and Dr. Gerardo Espinosa, whose invaluable comments and insightful suggestions helped me to improve in a significant way this document.

A special thanks to the Automatic Control Group at UNAM for all their support and kindness. I would like to thank in particular to Dr. Gerardo Espinosa for his continuous advice and encouragement.

Last but not least, my sincere thanks goes also to my *alma mater*, the National Autonomous University of Mexico (UNAM) for giving me the priceless opportunity to be a better human being.

This work was based on a research supported by CONACyT under scholarship CVU No. **334785** and DGAPA-UNAM under Grant **IN116314**.

Table of contents

Chapter 1

Introduction

In the context of robotics, a *teleoperation system* consists of one or many robotic manipulators operated by a human and one or many manipulators in a remote place. A common configuration is composed by the human operator, a local manipulator which is called *master*, a remote manipulator, called *slave*, a communication channel between the input and output signals of the two robots, and a remote environment over which the slave robot operates (see Figure 1.1).

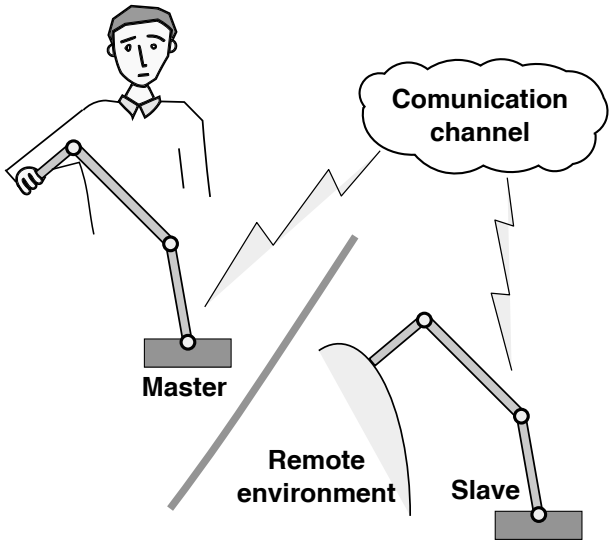

Figure 1.1: Master–slave teleoperation system.

In this scenario, the slave is intended to mimic the movements of the master robot, so that the whole configuration is known as a *master–slave teleoperation system.* If in addition

the contact force that the slave robot exerts over the environment is reflected to the human operator through the master manipulator then the teleoperation is called *bilateral* [1].

The sensation for the human operator of being directly manipulating the remote environment is known as *telepresence*. If he/she cannot feel neither the dynamic effects of the involved manipulators nor any other force than the one exerted over the remote surface, then the system is said to be *transparent*. In this sense, transparency acts as a measure of telepresence.

From the control systems point of view there are two main challenges for a master–slave bilateral teleoperator, namely the *stability* and the *transparency* of system. One vastly studied problem is the effect of the delays in the communication channel on the stability of the system. In this regard, most control algorithms are designed to guarantee stability in spite of the destabilizing effects of both constant and variable time delays. It turns out that robust stability and transparency are two contradictory goals even in the non–delayed scenario [Lawrence, 1993], then it depends on the particular application which of these two goals is pursued.

1.1 State of the Art

The master–slave bilateral teleoperation problem has been extensively studied since the 1950s with the seminal work of Goertz [Goertz and Thompson, 1954; Goertz, 1954]. This first approach consisted of two mechanically coupled manipulators for toxic waste handling, and it was later improved to reflect the environment force by using electrical signals. In these first years, it was found that the delays in the communication channel could easily destabilize the system and thereupon a lot of *software* solutions proliferated in the literature. The most popular among this solutions was the so–called *supervisory control* [Ferrell and Sheridan, 1967]. The philosophy behind this solution was to divide a highly complex teleoperation task into a number of simple autonomous tasks, arbitrated by a supervisory high–level software.

It was not until 1986 that the robotic teleoperation problem was studied from the Lyapunov theory point of view in Miyazaki et al. [1986], where asymptotic stability of position tracking error is guaranteed for the delay–free case. Three years later, in Hannaford and Kim [1989] the *shared compliance control* was introduced to cope with the oscillations originated by the contact of the slave robot with a rigid surface. A low–pass filter was included in the control loop to obtain a stable behavior even in presence of delays in the communication.

[1] In general, the term *bilateral* means that some information (position, velocity and/or force) is transmitted in both directions of the communication channel.

In Anderson and Spong [1989] stability in presence of delays was formally guaranteed by introducing the *scattering variables* in the teleoperation architecture, a concept that was well known by the epoch in transmission lines theory. Independently, in Niemeyer and Slotine [1991] a closely related concept, the *wave variables*, was proposed to guarantee stability for the delayed case. In that work it was also introduced another concept from the transmission lines theory, the *impedance matching*, to minimize wave reflection, which is one of the main destabilizing effects in a delayed teleoperation system. Since then, the robotic teleoperation problem has been a very prolific research area (see Hokayem and Spong [2006] for a historical survey up to 2006). Most of the results that guarantee stability in spite of communication delays are based on the *Passivity Based Control* [Niemeyer and Slotine, 1998; Chopra et al., 2006, 2008; Nuño et al., 2009, 2011].

On the other hand, in Lawrence [1993] and Yokokohji and Yoshikawa [1994] it is established that a four channel architecture (position and force transmitted in both directions) is required for obtaining ideal transparency. The effect in improving transparency by using a local force control in one or both master and slave manipulators and the reliability of obtaining ideal transparency with a three channel architecture is studied in Hashtrudi-Zaad and Salcudean [2002].

The results of Hashtrudi-Zaad and Salcudean [2002] imply that if positions of both sides are transmitted through the communication channel, then the force of at least one side of the teleoperator must be included in the control algorithm to obtain the best transparency. Furthermore, most of the existing controllers require full–state measurements. Thus another important research direction is removing the necessity of sensors by employing state observers rather than directly measuring all the required signals.

In this context, contact force estimation is another important area in robotics research regardless if the estimation is utilized for teleoperation or for a single robot in an autonomous control scheme. One of the first works on force estimation was published in Huang and Tseng [1988, 1991], where a nonlinear transformation is employed to estimate the velocity and force of a constrained manipulator in an open–loop framework, without using the estimated signals for control. Later, in Ohishi et al. [1992] an acceleration $\mathscr{H}^{\infty}$ based controller is used to estimate the contact force in a closed loop system, but it still requires velocity and acceleration measurements and the closed loop stability is only experimentally tested. In Hacksel and Salcudean [1994] it is shown that velocity and force measurements can be eliminated altogether by applying the Nicosia–Tomei observer [Nicosia and Tomei, 1990] to the force/velocity estimation problem. The same idea is further improved in Alcocera et al. [2004]. A nonlinear state

transformation is proposed in de Queiroz et al. [1996] to track position and force trajectories with only joint position measurements. A velocity observer and a open loop force control is proposed in Martínez-Rosas et al. [2006] to deal with the hybrid position/force control for cooperative manipulation. An improvement of this method including a force observer in a controller–observer algorithm is presented in Martınez-Rosas and Arteaga [2008]. Finally, in Arteaga-Pérez et al. [2013] a nonlinear *PID* observer–based controller is employed to solve the output feedback hybrid position/force problem. In all the aforementioned approaches, the required signals are reconstructed using only joint position measurements and torque inputs, but force and velocity can also be reconstructed by directly measuring joint torques [Phong et al., 2012] or motor currents [Aksman et al., 2007]. For teleoperation, Hashtrudi-Zaad and Salcudean [1996] introduced an adaptive controller that does not require force but relies in position, velocity and acceleration measurements. On the other hand, in Daly and Wang [2014] a force and velocity observer for non–stiff remote environments is proposed, based on the second order sliding–mode velocity observer reported in Davila et al. [2005].

For a force/position controller to function properly, a geometric description of the environment is necessary. For compliant (non–stiff) environments the controller can be designed to be robust against uncertainties in this description, while for rigid surfaces it has been proved that slight uncertainties in the geometric description can easily lead to instability of the closed loop system [Wang and McClamroch, 1994]. One of the first works related to this problem [Yoshikawa and Sudou, 1993] made use of the information from position and force sensors to on line estimate the unknown constraint shape. Some other solutions include visual identification of the surface [Dean-León et al., 2006; Lippiello et al., 2007; Leite et al., 2009; Cheah et al., 2010] robustness against kinematic and/or dynamic uncertainties [Wang et al., 1998], and adaptive control [Chiu et al., 2004; Namvar and Aghili, 2005; Karayiannidis and Doulgeri, 2009, 2010; Pliego-Jiménez and Arteaga-Pérez, 2015]. Some adaptive schemes have been adopted for bilateral teleoperation when there are uncertainties in the kinematics or even in the dynamic model of the surface [Lee and Chung, 1998; Liu et al., 2010, 2014].

The basic idea behind the mentioned schemes, when no exact description of the constraint geometry is available, is to reconstruct the surface by means of position, velocity, visual and/or force measurements. In the case that only joint positions are measured the problem of uncertain surfaces, to the best of the author's knowledge, has been solved only for compliant environments. The existing solutions include an open loop force control with adaptive identification of the surface [Doulgeri and Karayiannidis, 2008] and extended active observers [Chan et al., 2013], among others.

1.2 Motivation and Problem Statement

As stated in the last section, the problem of contact force estimation is an active research area on its own. Removing the force sensor has a lot of advantages, such as reducing costs, weight, size, operation in noisy environments, etc. Another interesting problem is the force control over an unknown rigid surface, even in the case when position and force are measured. However, to the best of the author's knowledge, there are no results in the literature that combine both problems, *i.e.*, the force/position control problem over an unknown rigid environment with only joint position measurements. One motivation of this work is to solve this problem for a single robot manipulator under autonomous operation.

On the other hand, there are few works in the literature addressing the teleoperation problem combined with direct force control (the majority of teleoperation schemes use indirect force control or no force control at all), and those few works that employ this kind of control require at least position and contact force measurements. There are some advantages in using direct force control such as improved transparency, decoupling of the position/force tasks, better exactitude in position and force tracking, etc. In addition, the reported teleoperation schemes that employ this approach demand the exact knowledge of the constraint surface geometry, which is very restrictive for many applications.

Accordingly, the main objective of this thesis is to solve the non–delayed master–slave teleoperation problem using direct force control over an unknown rigid remote surface, with only joint position measurements on the slave side and to obtain the best achievable transparency. For the master manipulator, joint positions, velocities and accelerations are considered to be available. Nevertheless, these signals can also be obtained from position measurements by means of an state observer similar to the employed at the slave side.

Many applications for robotic teleoperation require that the control strategy takes into account the communication delays, such as *telesurgery* or remote control of *underwater vehicles*. However, there are a lot of applications for the non–delayed bilateral teleoperation studied in this work. For example, in space missions the astronauts are required to perform some tasks in outer space such as assembly, repair and maintenance, which can be performed remotely using lightweight robotic manipulators and therefore reducing the risk in the astronauts' safety [Hirzinger et al., 1993]. Handling hazardous materials is another important application when delays in communication can be neglected, for example in handling radioactive substances [Clement et al., 1985]. The proposed method can also be applied in *microsurgery*, where the additional advantage of removing the velocity and force sensors of the

scheme proposed in this work, makes it more suitable for this application than the existing algorithms in literature. Finally, the proposed approach can be applied to the control of robotic *exoskeletons*, which are intended not only for military purposes but to help elderly and disabled people walk, climb stairs, and carry things around [Guizzo and Goldstein, 2005].

1.3 Methodology

Before approaching the main objective of the thesis some less–complicated intermediate problems are addressed. First, the force and velocity estimation issue is taken into account for a single robot in autonomous operation. As mentioned in the state of the art, this problem has been solved in the past with different techniques. However, in this work an extended–state high–gain observer is proposed to carry out the velocity and force estimation. This philosophy is the core of the so–called *GPI Observers* [Sira-Ramírez et al., 2010], which have been proved to be an excellent solution to the robust control problem not only for robotic manipulation [Arteaga-Perez and Gutierrez-Giles, 2014; Ramírez-Neria et al., 2015; Gutierrez-Giles et al., 2016] but for non–holonomic [Ramirez-Neria et al., 2013; Sira-Ramírez et al., 2014], underactuated [Ramírez-Neria et al., 2014, 2016] and haptic mechanical systems [Rodriguez-Angeles and Garcia-Antonio, 2014], electronic power converters [Luviano-Juarez et al., 2010; Juárez-Abad et al., 2014], and electric machines [Sira-Ramirez et al., 2014; De La Guerra et al., 2016], among others.

A GPI observer was designed in Arteaga-Pérez et al. [2015] for the estimation of the velocity and one chamber's pressure of a differential pneumatic piston. Given the good results obtained for the pneumatic system, the same idea was employed to the force/velocity estimation for a robotic manipulator subject to holonomic constraints [Gutierrez-Giles et al., 2013]. The algorithm was further improved to deal with the noise amplification issue and a formal stability analysis was performed as reported in Gutiérrez-Giles and Arteaga-Pérez [2014].

Next, the problem of the remote surface unknown geometry was addressed. The basic idea of local approximation the surface by a plane was taken from Pliego-Jiménez and Arteaga-Pérez [2015]. However, in that work the surface reconstruction is carried out by means of force measurements, and thus some modifications were made to include the force estimated by the GPI Observer. A formal stability proof and some numerical simulations were performed with good results [Gutiérrez-Giles and Arteaga-Pérez, 2016b].

Finally, the transparent teleoperation problem was considered. For addressing this issue, the *virtual surfaces* approach reported in Rodríguez-Angeles et al. [2015] was taken as a starting

point. The advantages of using this approach are twofold: it is suitable for hybrid position/force control and it is centered in the transparency of the system. Some adaptations of the algorithm to include the GPI Observer and the surface estimator were carried out and the former stability proof was also extended to the master–slave teleoperation problem [Gutiérrez-Giles and Arteaga-Pérez, 2016a].

1.4 Contributions

The contributions of this work are summarized in the following:

- A force and velocity observer was designed to solve the problem of contact force estimation when only joint position measurements are available. The designed observer has some advantages over the previously reported such as easy implementation/tunning and simultaneous estimation of velocity and force.
- The force observer was successfully applied to estimate the velocity and one chamber pressure of a differential pneumatic piston. The proposed approach had better performance than the existing ones in an experimental comparison as reported in Arteaga-Pérez et al. [2015].
- The GPI observer methodology was adapted to the robust hybrid force/position control of robot manipulators with good results as reported in Gutierrez-Giles et al. [2016].
- It was shown that the GPI observer can be improved for the robust control of mechanical systems by exploiting the well–known passivity properties of these systems. A formal proof of this claim as well as a set of experimental results were reported in Arteaga-Pérez and Gutiérrez-Giles [2014].
- It was solved for the first time, to the best of the author's knowledge, the problem of direct force control over a rigid surface without force nor velocity measurements and unknown geometry of the constraint surface.
- The open problem of master–slave teleoperation for the delay–free scenario without force/velocity measurements and under geometric uncertainty of the rigid remote surface was also solved. A formal proof that guarantees ultimate boundedness of all signals and approximate, but arbitrarily close, estimation of velocity and force as well as position/force tracking was developed.

1.5 Thesis Structure

The document is organized as follows. In Chapter 2 a mathematical model of the teleoperation system is presented as well as some of its properties. There are also included some useful facts regarding the kinematic constraints and the decomposition of the task space. The main result of this work is exposed in Chapter 3, *i.e.*, the design of observer and controller algorithms and the corresponding analysis of the closed loop dynamics. Later in the same chapter, two theorems are stated and formally proven, that guarantee local ultimate boundedness of the closed loop system state. In Chapter 4, both simulation and experimental results are presented to validate the approach. Finally, some conclusions and directions for future work are given in Chapter 5.

Chapter 2

Dynamic Modeling and Properties

In this chapter, the mathematical model of a master–slave teleoperation system is first introduced in which the slave is constrained to be in contact with a rigid surface. This model will be thereafter employed in the design of a controller for both master and slave robots, and in the design of an observer to estimate the contact force and the joint velocities of the slave manipulator. Later, some useful properties of the model are introduced as well as the orthogonal decomposition of the task space, which will be utilized for the dynamical analysis of the teleoperation system in closed loop with the proposed controller and the observer.

2.1 Modelling

Consider a master–slave teleoperation system and let the sub–indexes m and s denote the master and slave manipulators, respectively. For $i = \mathrm{m}, \mathrm{s}$, let $\boldsymbol{q}_i \in \mathbb{R}^n$ be the vector of generalized coordinates. Suppose that there are not delays in the communication channel and that the slave robot is constrained to be in contact with a rigid surface defined as a mapping $\boldsymbol{\varphi}_\mathrm{s} : \mathbb{R}^n \to \mathbb{R}^m$, which satisfies

$$\boldsymbol{\varphi}_\mathrm{s}(\boldsymbol{q}_\mathrm{s}) = \mathbf{0}\,. \tag{2.1}$$

Then the teleoperation system dynamics is given by [Rodríguez-Angeles et al., 2015]

$$\boldsymbol{H}_\mathrm{m}(\boldsymbol{q}_\mathrm{m})\ddot{\boldsymbol{q}}_\mathrm{m} + \boldsymbol{C}_\mathrm{m}(\boldsymbol{q}_\mathrm{m}, \dot{\boldsymbol{q}}_\mathrm{m})\dot{\boldsymbol{q}}_\mathrm{m} + \boldsymbol{D}_\mathrm{m}\dot{\boldsymbol{q}}_\mathrm{m} + \boldsymbol{g}_\mathrm{m}(\boldsymbol{q}_\mathrm{m}) = \boldsymbol{\tau}_\mathrm{m} - \boldsymbol{\tau}_\mathrm{h} \tag{2.2}$$

$$\boldsymbol{H}_\mathrm{s}(\boldsymbol{q}_\mathrm{s})\ddot{\boldsymbol{q}}_\mathrm{s} + \boldsymbol{C}_\mathrm{s}(\boldsymbol{q}_\mathrm{s}, \dot{\boldsymbol{q}}_\mathrm{s})\dot{\boldsymbol{q}}_\mathrm{s} + \boldsymbol{D}_\mathrm{s}\dot{\boldsymbol{q}}_\mathrm{s} + \boldsymbol{g}_\mathrm{s}(\boldsymbol{q}_\mathrm{s}) = \boldsymbol{\tau}_\mathrm{s} + \boldsymbol{J}_{\varphi\mathrm{s}}^{\mathrm{T}}(\boldsymbol{q}_\mathrm{s})\boldsymbol{\lambda}_\mathrm{s}\,, \tag{2.3}$$

where, for $i = \mathrm{m,s}$, $\boldsymbol{H}_i(\boldsymbol{q}_i) \in \mathbb{R}^{n\times n}$ is the inertia matrix, $\boldsymbol{C}_i(\boldsymbol{q}_i, \dot{\boldsymbol{q}}_i)\dot{\boldsymbol{q}}_i \in \mathbb{R}^n$ is the vector of Coriolis and centripetal forces, $\boldsymbol{D}_i \in \mathbb{R}^{n\times n}$ is a diagonal matrix of viscous friction coefficients, $\boldsymbol{g}_i(\boldsymbol{q}_i) \in \mathbb{R}^n$ is the vector of gravitational torques, $\boldsymbol{\tau}_i \in \mathbb{R}^n$ is the vector of generalized inputs, $\boldsymbol{\tau}_\mathrm{h} \in \mathbb{R}^n$ is the torque applied by the human operator over the master robot, $\boldsymbol{\lambda}_\mathrm{s} \in \mathbb{R}^m$ is a vector of Lagrange multipliers that physically represents the contact force over the rigid surface, and

$$\boldsymbol{J}_{\varphi\mathrm{s}}(\boldsymbol{q}_\mathrm{s}) = \nabla\boldsymbol{\varphi}_\mathrm{s}(\boldsymbol{q}_\mathrm{s}) \in \mathbb{R}^{m\times n}, \tag{2.4}$$

is the gradient of the remote surface described by (2.1). This constraint can also be expressed in the slave manipulator Cartesian coordinates as

$$\boldsymbol{\varphi}_\mathrm{s}(\boldsymbol{x}_\mathrm{s}) = \boldsymbol{0}, \tag{2.5}$$

where $\boldsymbol{x}_\mathrm{s} \in \mathbb{R}^n$ is the vector of end–effector coordinates.

It is always possible to carry out a suitable normalization for the gradient of this last constraint,

$$\boldsymbol{J}_{\varphi\mathrm{xs}}(\boldsymbol{x}_\mathrm{s}) = \nabla\boldsymbol{\varphi}_\mathrm{s}(\boldsymbol{x}_\mathrm{s}) \in \mathbb{R}^{m\times n}, \tag{2.6}$$

to be an unitary vector. In this work it is assumed that it is the case. These two gradients are related by

$$\boldsymbol{J}_{\varphi\mathrm{s}}(\boldsymbol{q}_\mathrm{s}) = \boldsymbol{J}_{\varphi\mathrm{xs}}(\boldsymbol{x}_\mathrm{s})\boldsymbol{J}_\mathrm{s}(\boldsymbol{q}_\mathrm{s}), \tag{2.7}$$

where $\boldsymbol{J}_\mathrm{s}(\boldsymbol{q}_\mathrm{s})$ is the geometric Jacobian of the slave manipulator.

2.2 Some Useful Properties

First, the following assumption is introduced, which must be taken into account at the trajectory planning stage.

Assumption 2.1. *None of the manipulators reach any singularity, so that* $\boldsymbol{J}_i(\boldsymbol{q}_i)$, $i = \mathrm{m,s}$ *are always invertible* . □

An *orthogonal decomposition* [Arimoto et al., 1993] of the task space will be carried out as follows. Let $\boldsymbol{J}^+_{\varphi\mathrm{s}} \triangleq \boldsymbol{J}^\mathrm{T}_{\varphi\mathrm{s}}\left(\boldsymbol{J}_{\varphi\mathrm{s}}\boldsymbol{J}^\mathrm{T}_{\varphi\mathrm{s}}\right)^{-1}$, $\boldsymbol{P}_\mathrm{s}(\boldsymbol{q}_\mathrm{s}) = \boldsymbol{J}^+_{\varphi\mathrm{s}}\boldsymbol{J}_{\varphi\mathrm{s}}$, and $\boldsymbol{Q}_\mathrm{s}(\boldsymbol{q}_\mathrm{s}) = \boldsymbol{I}_{n\times n} - \boldsymbol{P}_\mathrm{s}(\boldsymbol{q}_\mathrm{s})$. Notice that since $\boldsymbol{J}_{\varphi\mathrm{xs}}$ is full–rank everywhere and after Assumption 2.1, $\left(\boldsymbol{J}_{\varphi\mathrm{s}}\boldsymbol{J}^\mathrm{T}_{\varphi\mathrm{s}}\right)^{-1}$ always exists. Furthermore, $\boldsymbol{P}_\mathrm{s}$ and $\boldsymbol{Q}_\mathrm{s}$ are projection matrices, *i.e.,* $\boldsymbol{Q}_\mathrm{s}\boldsymbol{P}_\mathrm{s} = \boldsymbol{O}$, $\boldsymbol{Q}_\mathrm{s}\boldsymbol{J}^\mathrm{T}_{\varphi\mathrm{s}} = \boldsymbol{O}$, and $\boldsymbol{J}_{\varphi\mathrm{s}}\boldsymbol{Q}_\mathrm{s} = \boldsymbol{O}$. Moreover,

$\boldsymbol{Q}_\mathrm{s}\boldsymbol{Q}_\mathrm{s} = \boldsymbol{Q}_\mathrm{s}$ and $\boldsymbol{P}_\mathrm{s}\boldsymbol{P}_\mathrm{s} = \boldsymbol{P}_\mathrm{s}$. Then, the following property can be stated [Martínez-Rosas et al., 2006].

Property 2.1. The joint velocity vector $\dot{\boldsymbol{q}}_\mathrm{s}$ satisfies

$$\dot{\boldsymbol{q}}_\mathrm{s} = \boldsymbol{Q}_\mathrm{s}(\boldsymbol{q}_\mathrm{s})\dot{\boldsymbol{q}}_\mathrm{s} + \boldsymbol{P}_\mathrm{s}(\boldsymbol{q}_\mathrm{s})\dot{\boldsymbol{q}}_\mathrm{s} = \boldsymbol{Q}_\mathrm{s}(\boldsymbol{q}_\mathrm{s})\dot{\boldsymbol{q}}_\mathrm{s}\,. \tag{2.8}$$

□

For simplicity, consider that the manipulators have only revolute joints. Thereupon, each one satisfies the following standard properties [Arteaga, 1998].

Property 2.2. The inertia matrix $\boldsymbol{H}_i(\boldsymbol{q}_i)$ is symmetric positive definite and $\forall\, \boldsymbol{q}_i, \boldsymbol{y} \in \mathbb{R}^n$ it holds $\lambda_{\mathrm{h}i}\|\boldsymbol{y}\|^2 \leq \boldsymbol{y}^\mathrm{T}\boldsymbol{H}_i(\boldsymbol{q}_i)\boldsymbol{y} \leq \lambda_{\mathrm{H}i}\|\boldsymbol{y}\|^2$, with $0 < \lambda_{\mathrm{h}i} \leq \lambda_{\mathrm{H}i} < \infty$. □

Property 2.3. With a proper definition of $\boldsymbol{C}_i(\boldsymbol{q}_i, \dot{\boldsymbol{q}}_i)$, the matrix $\dot{\boldsymbol{H}}_i(\boldsymbol{q}_i) - 2\boldsymbol{C}_i(\boldsymbol{q}_i, \dot{\boldsymbol{q}}_i)$ is skew symmetric. □

Property 2.4. The vector $\boldsymbol{C}_i(\boldsymbol{q}_i, \boldsymbol{x}_i)\boldsymbol{y}_i$ satisfies $\boldsymbol{C}_i(\boldsymbol{q}_i, \boldsymbol{x})\boldsymbol{y} = \boldsymbol{C}_i(\boldsymbol{q}_i, \boldsymbol{y})\boldsymbol{x}$, $\forall\, \boldsymbol{x}, \boldsymbol{y} \in \mathbb{R}^n$. □

Finally, it is enunciated the following useful fact taken from Rivera-Dueñas and Arteaga-Pérez [2013].

Fact 2.1. Assume that $\boldsymbol{q}_\mathrm{sd}(t)$ satisfies $\boldsymbol{\varphi}(\boldsymbol{q}_\mathrm{sd}) = \boldsymbol{0}$. Whenever the manipulator is restricted to fulfill (2.1) and the tracking error is small enough, the following approximation can be made

$$\boldsymbol{e}_\mathrm{s} = \boldsymbol{Q}_\mathrm{s}(\boldsymbol{q}_\mathrm{s})\boldsymbol{e}_\mathrm{s}\,, \tag{2.9}$$

because the error tends to be contained in the tangent space at the point $\boldsymbol{q}_\mathrm{s}$, projected by $\boldsymbol{Q}_\mathrm{s}(\boldsymbol{q}_\mathrm{s})$. Furthermore, from Property 2.1 it follows

$$\dot{\boldsymbol{q}}_\mathrm{sd} \approx \boldsymbol{Q}_\mathrm{s}(\boldsymbol{q}_\mathrm{s})\dot{\boldsymbol{q}}_\mathrm{sd} \implies \dot{\boldsymbol{e}}_\mathrm{s} = \boldsymbol{Q}_\mathrm{s}(\boldsymbol{q}_\mathrm{s})\left(\dot{\boldsymbol{q}}_\mathrm{s} - \dot{\boldsymbol{q}}_\mathrm{sd}\right) \approx \boldsymbol{Q}_\mathrm{s}(\boldsymbol{q}_\mathrm{s})\dot{\boldsymbol{e}}_\mathrm{s}\,. \tag{2.10}$$

□

An illustration of Fact 2.1 in Cartesian coordinates is shown in Figure 2.1.

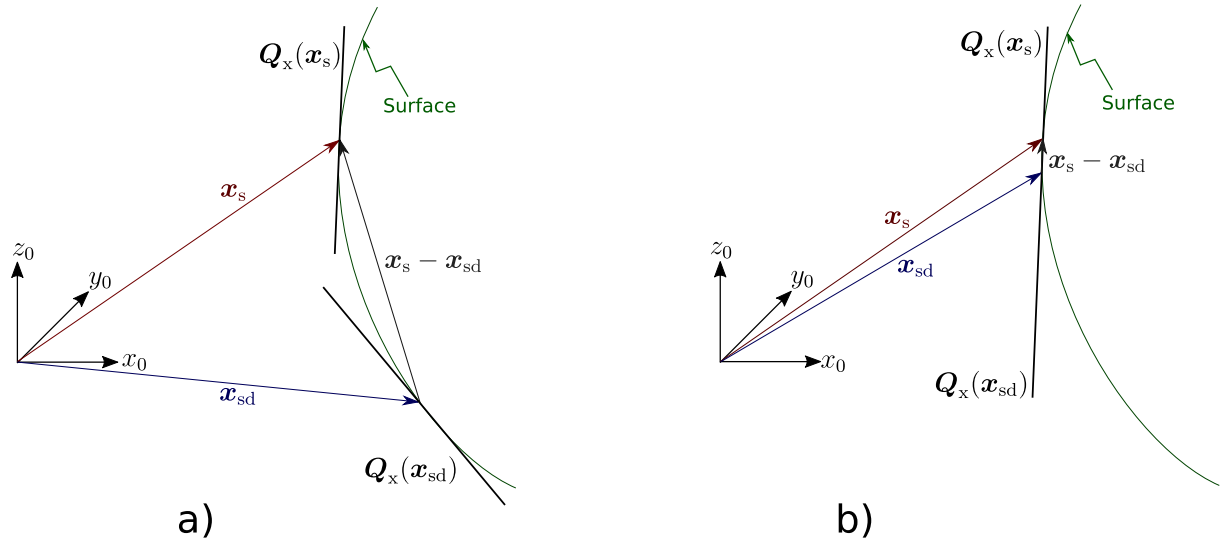

Figure 2.1: a) Position error is not contained in the plane projected by $\boldsymbol{Q}_{\mathrm{x}}$, b) Position error is contained in the plane projected by $\boldsymbol{Q}_{\mathrm{x}}$.

Chapter 3

Transparent Teleoperation

This work considers the case of one–dimensional constraints ($\boldsymbol{\varphi}_\mathrm{s} : \mathbb{R}^n \to \mathbb{R}$), so that $\boldsymbol{\lambda}_\mathrm{s} = \lambda_\mathrm{s} \in \mathbb{R}$ in (2.3) represents the contact force of the slave manipulator over the remote surface. To achieve trajectory tracking of both position and force and *transparency* of the teleoperator, it will be followed the *virtual surfaces* approach introduced in Rodríguez-Angeles et al. [2015]. A diagram of the proposed scheme is shown in Figure 3.1.

3.1 Controller and Observer Design

First, consider a state–space representation of the slave manipulator model (2.3)

$$\dot{\boldsymbol{q}}_\mathrm{s} = \boldsymbol{q}_{2\mathrm{s}} \tag{3.1}$$

$$\dot{\boldsymbol{q}}_{2\mathrm{s}} = \boldsymbol{H}_\mathrm{s}^{-1}(\boldsymbol{q}_\mathrm{s})\left(\boldsymbol{\tau}_\mathrm{s} - \boldsymbol{N}_\mathrm{s}(\boldsymbol{q}_\mathrm{s}, \boldsymbol{q}_{2\mathrm{s}})\right) + \boldsymbol{z}_1\,, \tag{3.2}$$

where $\boldsymbol{N}_\mathrm{s}(\boldsymbol{q}_\mathrm{s}, \boldsymbol{q}_{2\mathrm{s}}) = \boldsymbol{C}_\mathrm{s}(\boldsymbol{q}_\mathrm{s}, \boldsymbol{q}_{2\mathrm{s}})\boldsymbol{q}_{2\mathrm{s}} + \boldsymbol{D}_\mathrm{s}\boldsymbol{q}_{2\mathrm{s}} + \boldsymbol{g}_\mathrm{s}(\boldsymbol{q}_\mathrm{s})$ and

$$\boldsymbol{z}_1 = \boldsymbol{H}_\mathrm{s}^{-1}(\boldsymbol{q}_\mathrm{s})\boldsymbol{J}_{\varphi\mathrm{s}}^{\mathrm{T}}(\boldsymbol{q}_\mathrm{s})\lambda_\mathrm{s}\,. \tag{3.3}$$

The goal is to design an observer to estimate *in an approximate way* the force λ_s and the state $\dot{\boldsymbol{q}}_\mathrm{s} = \boldsymbol{q}_{2\mathrm{s}}$. For this purpose, a generic time–polynomial vector is proposed as an internal representation for $\boldsymbol{z}_1$, which is considered an unknown signal to be estimated via a linear observer of the Luenberger type. This will be possible as long as the following assumptions hold [Sira-Ramírez et al., 2010].

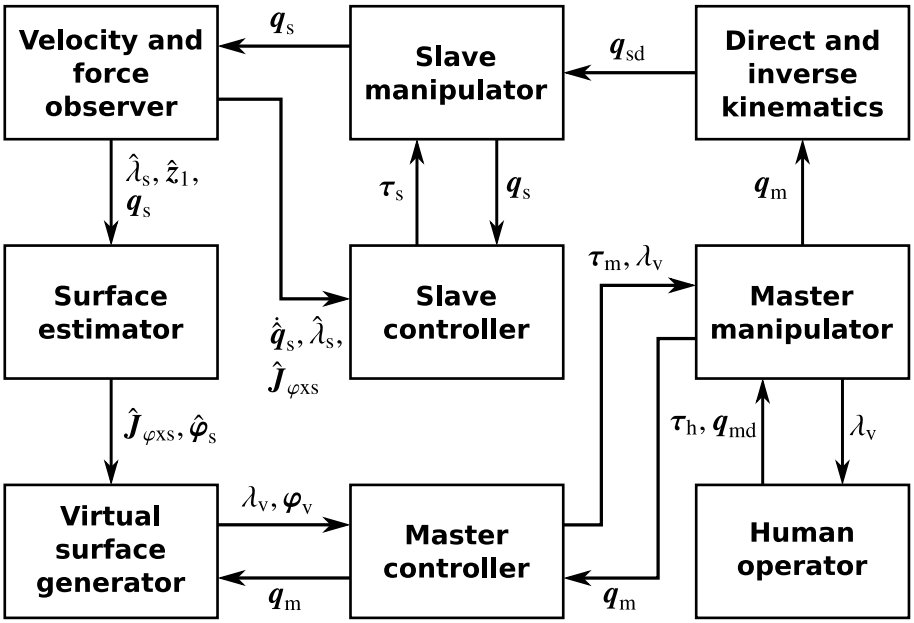

Figure 3.1: Block diagram of the proposed scheme.

Assumption 3.1. *The vector $\boldsymbol{z}_1(t)$ can be written as:*

$$\boldsymbol{z}_1(t) = \sum_{i=0}^{p-1} \boldsymbol{a}_i t^i + \boldsymbol{r}(t), \tag{3.4}$$

where each $\boldsymbol{a}_i$ is a n–vector of constant coefficients and $\boldsymbol{r}(t)$ represents a residual term. □

Assumption 3.2. *At least the first p time derivatives of $\boldsymbol{z}_1(t)$ exist.* □

Under these assumptions $\boldsymbol{z}_1$ can be described by the dynamic internal model

$$\dot{\boldsymbol{z}}_1 = \boldsymbol{z}_2 \tag{3.5}$$

$$\vdots$$

$$\dot{\boldsymbol{z}}_{p-1} = \boldsymbol{z}_p \tag{3.6}$$

$$\dot{\boldsymbol{z}}_p = \boldsymbol{r}^{(p)}(t). \tag{3.7}$$

3.1.1 State observer and estimation

Since the information about the contact force and the direction of the gradient of the constraint (2.1) is contained in the $\boldsymbol{z}_1$ variable, the state space model (3.1)–(3.2), along with the dynamic extension (3.5)–(3.7) will be used as a basis for the observer design.

Force and velocity observer

The following extended–state high–gain linear observer is proposed to reconstruct the velocity and force at the remote side of the teleoperation system

$$\dot{\hat{\boldsymbol{q}}}_{\mathrm{s}} = \hat{\boldsymbol{q}}_{2\mathrm{s}} + \boldsymbol{\lambda}_{p+1}\tilde{\boldsymbol{q}}_{\mathrm{s}} \tag{3.8}$$

$$\dot{\hat{\boldsymbol{q}}}_{2\mathrm{s}} = \boldsymbol{H}_{\mathrm{s}}^{-1}(\boldsymbol{q}_{\mathrm{s}})\left(\boldsymbol{\tau}_{\mathrm{s}} - \boldsymbol{N}_{\mathrm{s}}(\boldsymbol{q}_{\mathrm{s}}, \hat{\boldsymbol{q}}_{2\mathrm{s}})\right) + \hat{\boldsymbol{z}}_1 + \boldsymbol{\lambda}_p\tilde{\boldsymbol{q}}_{\mathrm{s}} \tag{3.9}$$

$$\dot{\hat{\boldsymbol{z}}}_1 = \hat{\boldsymbol{z}}_2 + \boldsymbol{\lambda}_{p-1}\tilde{\boldsymbol{q}}_{\mathrm{s}} \tag{3.10}$$

$$\vdots$$

$$\dot{\hat{\boldsymbol{z}}}_{p-1} = \hat{\boldsymbol{z}}_p + \boldsymbol{\lambda}_1\tilde{\boldsymbol{q}}_{\mathrm{s}} \tag{3.11}$$

$$\dot{\hat{\boldsymbol{z}}}_p = \boldsymbol{\lambda}_0\tilde{\boldsymbol{q}}_{\mathrm{s}}\,, \tag{3.12}$$

where $\tilde{\boldsymbol{q}}_{\mathrm{s}} \triangleq \boldsymbol{q}_{\mathrm{s}} - \hat{\boldsymbol{q}}_{\mathrm{s}}$ and $\boldsymbol{N}_{\mathrm{s}}(\boldsymbol{q}_{\mathrm{s}}, \hat{\boldsymbol{q}}_{2\mathrm{s}}) \triangleq \boldsymbol{C}_{\mathrm{s}}(\boldsymbol{q}_{\mathrm{s}}, \hat{\boldsymbol{q}}_{2\mathrm{s}})\hat{\boldsymbol{q}}_{2\mathrm{s}} + \boldsymbol{D}_{\mathrm{s}}\hat{\boldsymbol{q}}_{2\mathrm{s}} + \boldsymbol{g}_{\mathrm{s}}(\boldsymbol{q}_{\mathrm{s}})$ and $\boldsymbol{\lambda}_0, \boldsymbol{\lambda}_1, \ldots, \boldsymbol{\lambda}_{p+1} \in \mathbb{R}^{n\times n}$, are constant matrices of gains chosen in such a way that the non–zero components of the $n \times n$ complex–valued diagonal matrix

$$\boldsymbol{\rho}(s) = s^{p+2}\boldsymbol{I} + s^{p+1}\boldsymbol{\lambda}_{p+1} + \cdots + s\boldsymbol{\lambda}_1 + \boldsymbol{\lambda}_0\,, \tag{3.13}$$

are Hurwitz polynomials of degree $p+2$.

An estimation of the joint velocity is obtained directly by $\hat{\boldsymbol{q}}_{2\mathrm{s}}$. As for the contact force, consider that after (2.7) and (3.3) it can be obtained

$$\boldsymbol{J}_{\varphi\mathrm{x}}^{\mathrm{T}}(\boldsymbol{x}_{\mathrm{s}})\hat{\lambda}_{\mathrm{s}} = \boldsymbol{J}_{\mathrm{s}}^{-\mathrm{T}}(\boldsymbol{q}_{\mathrm{s}})\boldsymbol{H}_{\mathrm{s}}(\boldsymbol{q}_{\mathrm{s}})\hat{\boldsymbol{z}}_1\,. \tag{3.14}$$

Since $\boldsymbol{J}_{\varphi\mathrm{x}}$ is an unitary vector, by taking the norm on both sides of (3.14), the contact force can be estimated by

$$\hat{\lambda}_{\mathrm{s}} = \|\boldsymbol{J}_{\mathrm{s}}^{-\mathrm{T}}(\boldsymbol{q}_{\mathrm{s}})\boldsymbol{H}_{\mathrm{s}}(\boldsymbol{q}_{\mathrm{s}})\hat{\boldsymbol{z}}_1\|\,. \tag{3.15}$$

Note that neither the state observer (3.8)–(3.12) nor the force estimator (3.15) depend on other signals than the input torques vector $\boldsymbol{\tau}_{\mathrm{s}}$ and the joint positions $\boldsymbol{q}_{\mathrm{s}}$.

Estimation of the surface gradient

Recall that it is supposed that there is no available information about the geometry of the surface. Nevertheless, the following assumption is made in order to design an estimator and to carry out the corresponding stability analysis.

Assumption 3.3. *The remote surface described by (2.5) is smooth, i.e., its partial derivatives of any order with respect to its arguments exist and are continuous [Isidori, 1995, p. 471].* □

Accordingly, an online estimator of the remote surface gradient in end–effector coordinates is proposed as

$$\dot{\hat{\boldsymbol{J}}}_{\varphi\mathrm{xs}}^{\mathrm{T}} = \left(\frac{\gamma}{\hat{\lambda}_{\mathrm{s}} + \epsilon}\right) \hat{\boldsymbol{Q}}_{\mathrm{xs}} \boldsymbol{J}_{\mathrm{s}}^{-\mathrm{T}}(\boldsymbol{q}_{\mathrm{s}}) \boldsymbol{H}_{\mathrm{s}}(\boldsymbol{q}_{\mathrm{s}}) \hat{\boldsymbol{z}}_1 \,, \tag{3.16}$$

where $\gamma > 0$ is the estimation gain, $\epsilon > 0$ is an arbitrary small positive constant to avoid division by zero, and $\hat{\boldsymbol{Q}}_{\mathrm{xs}} \triangleq \boldsymbol{I}_{n\times n} - \hat{\boldsymbol{P}}_{\mathrm{xs}}$, with $\hat{\boldsymbol{P}}_{\mathrm{xs}} \triangleq \hat{\boldsymbol{J}}_{\varphi\mathrm{xs}}^{+} \hat{\boldsymbol{J}}_{\varphi\mathrm{xs}}$, and $\hat{\boldsymbol{J}}_{\varphi\mathrm{xs}}^{+} = \hat{\boldsymbol{J}}_{\varphi\mathrm{xs}}^{\mathrm{T}} (\hat{\boldsymbol{J}}_{\varphi\mathrm{xs}} \hat{\boldsymbol{J}}_{\varphi\mathrm{xs}}^{\mathrm{T}})^{-1}$.

By proposing the surface gradient estimator as in (3.16) it is guaranteed that the norm of the estimated vector will remain constant, *i.e.*, $\|\hat{\boldsymbol{J}}_{\varphi\mathrm{xs}}(t)\| = \|\hat{\boldsymbol{J}}_{\varphi\mathrm{xs}}(t_0))\|, \forall\, t \geq t_0$. To see this, compute

$$\frac{\mathrm{d}}{\mathrm{d}t}\|\hat{\boldsymbol{J}}_{\varphi\mathrm{xs}}\|^2 = 2\hat{\boldsymbol{J}}_{\varphi\mathrm{xs}} \dot{\hat{\boldsymbol{J}}}_{\varphi\mathrm{xs}}^{\mathrm{T}} = 2\left(\frac{\gamma}{\hat{\lambda}_{\mathrm{s}} + \epsilon}\right) \hat{\boldsymbol{J}}_{\varphi\mathrm{xs}} \hat{\boldsymbol{Q}}_{\mathrm{xs}} \boldsymbol{J}_{\mathrm{s}}^{-\mathrm{T}}(\boldsymbol{q}_{\mathrm{s}}) \boldsymbol{H}_{\mathrm{s}}(\boldsymbol{q}_{\mathrm{s}}) \hat{\boldsymbol{z}}_1 = 0 \,, \tag{3.17}$$

since $\hat{\boldsymbol{J}}_{\varphi\mathrm{xs}} \hat{\boldsymbol{Q}}_{\mathrm{xs}} = 0$. Therefore, it is appropriate to set the initial condition of the estimator to satisfy $\|\hat{\boldsymbol{J}}_{\varphi\mathrm{xs}}(t_0))\| = 1$.

Note that (3.17) is valid regardless how accurate the surface reconstruction could be. The matrices $\hat{\boldsymbol{P}}_{\mathrm{s}}$ and $\hat{\boldsymbol{Q}}_{\mathrm{s}}$, and the vector $\hat{\boldsymbol{J}}_{\varphi\mathrm{s}}^{+}$ can be expressed in joint coordinates by defining

$$\hat{\boldsymbol{J}}_{\varphi\mathrm{s}} \triangleq \hat{\boldsymbol{J}}_{\varphi\mathrm{xs}} \boldsymbol{J}_{\mathrm{s}} \,, \tag{3.18}$$

with $\hat{\boldsymbol{P}}_{\mathrm{s}}$, $\hat{\boldsymbol{Q}}_{\mathrm{s}}$, and $\hat{\boldsymbol{J}}_{\varphi\mathrm{s}}^{+}$ determined analogously to $\hat{\boldsymbol{P}}_{\mathrm{xs}}$, $\hat{\boldsymbol{Q}}_{\mathrm{xs}}$, and $\hat{\boldsymbol{J}}_{\varphi\mathrm{xs}}^{+}$.

3.1.2 Master and slave controllers

In this section, the estimated variables of the previous section are utilized in a controller design for the teleoperation system. The design is intended to obtain the best possible degree of transparency while guaranteeing stability of the closed loop system.

Assume that a desired force $\lambda_{\mathrm{sd}} > 0$ is commanded by the human operator. Define the position tracking error in joint coordinates at the slave side as

$$\boldsymbol{e}_{\mathrm{s}} \triangleq \boldsymbol{q}_{\mathrm{s}} - \boldsymbol{q}_{\mathrm{sd}}\,, \tag{3.19}$$

where $\boldsymbol{q}_{\mathrm{sd}} \in \mathbb{R}^n$ is obtained by solving the inverse kinematics of the slave robot with the pose of the master manipulator as the desired one. Taking this into account, the control law proposed for the slave manipulator is

$$\boldsymbol{\tau}_{\mathrm{s}} = -\boldsymbol{K}_{\mathrm{ps}}\boldsymbol{e}_{\mathrm{s}} - \boldsymbol{K}_{\mathrm{vs}}(\hat{\boldsymbol{q}}_{\mathrm{s2}} - \dot{\boldsymbol{q}}_{\mathrm{sd}}) - \hat{\boldsymbol{Q}}_{\mathrm{s}}\boldsymbol{K}_{\mathrm{is}}\int_{t_0}^{t}\boldsymbol{e}_{\mathrm{s}}\,\mathrm{d}\vartheta - \hat{\boldsymbol{J}}_{\varphi s}^{\mathrm{T}}\lambda_{\mathrm{sd}} + \hat{\boldsymbol{J}}_{\varphi s}^{+}k_{\mathrm{Fis}}\Delta\bar{F}_{\mathrm{s}}\,, \tag{3.20}$$

where $\boldsymbol{K}_{\mathrm{ps}}, \boldsymbol{K}_{\mathrm{vs}}, \boldsymbol{K}_{\mathrm{is}} \in \mathbb{R}^{n\times n}$ are diagonal positive definite matrices of constant gains, $k_{\mathrm{Fis}} > 0$ is the integral force control gain and

$$\Delta\bar{\lambda}_{\mathrm{s}} \triangleq \hat{\lambda}_{\mathrm{s}} - \lambda_{\mathrm{sd}} \tag{3.21}$$

$$\Delta\bar{F}_{\mathrm{s}} \triangleq \int_{t_0}^{t}\Delta\bar{\lambda}_{\mathrm{s}}\,\mathrm{d}\vartheta\,. \tag{3.22}$$

Since the geometry of the remote environment is unknown, a *virtual surface* cannot be created directly as in Rodríguez-Angeles et al. [2015], but the information of the estimator (3.16) must be employed. To overcome this situation, a local approximation of constraint (2.5) is considered as described in Pliego-Jiménez and Arteaga-Pérez [2015], as follows.

It is assumed that the human operator is responsible for the desired trajectory by moving the master manipulator. Then, the desired trajectory in task space coordinates for the slave manipulator is given by $\boldsymbol{x}_{\mathrm{sd}} = \boldsymbol{x}_{\mathrm{m}}$ (with a possible scale factor), and the approximation for the virtual surface constraint is thus proposed as

$$\hat{\boldsymbol{\varphi}}_{\mathrm{v}} = \hat{\boldsymbol{J}}_{\varphi\mathrm{xs}}(\boldsymbol{x}_{\mathrm{sd}} - \boldsymbol{x}_{\mathrm{sa}})\,, \tag{3.23}$$

where $\boldsymbol{x}_{\mathrm{sa}}$ is the output of the first order filter

$$\dot{\boldsymbol{x}}_{\mathrm{sa}} = -\eta\boldsymbol{x}_{\mathrm{sa}} + \eta\hat{\boldsymbol{x}}_{\mathrm{s}}(\hat{\boldsymbol{q}}_{\mathrm{s}})\,, \tag{3.24}$$

where $\eta > 0$ and $\hat{\boldsymbol{x}}_{\mathrm{s}}(\hat{\boldsymbol{q}}_{\mathrm{s}})$ is the slave robot direct kinematics with $\hat{\boldsymbol{q}}_{\mathrm{s}}$ as argument instead $\boldsymbol{q}_{\mathrm{s}}$.

Remark 3.1. The justification behind the introduction of the filter (3.24) is the following. The remote surface is locally approximated by a plane and then the difference between the desired

position at time t and the measured position an instant before, *i.e.*, at $t-\Delta t$, must be orthogonal to $\hat{\boldsymbol{J}}_{\varphi\mathrm{xs}}$. In this context, the unitary–gain filter (3.24) acts as a continuous approximation of the required time–delay (see Figure 3.2).

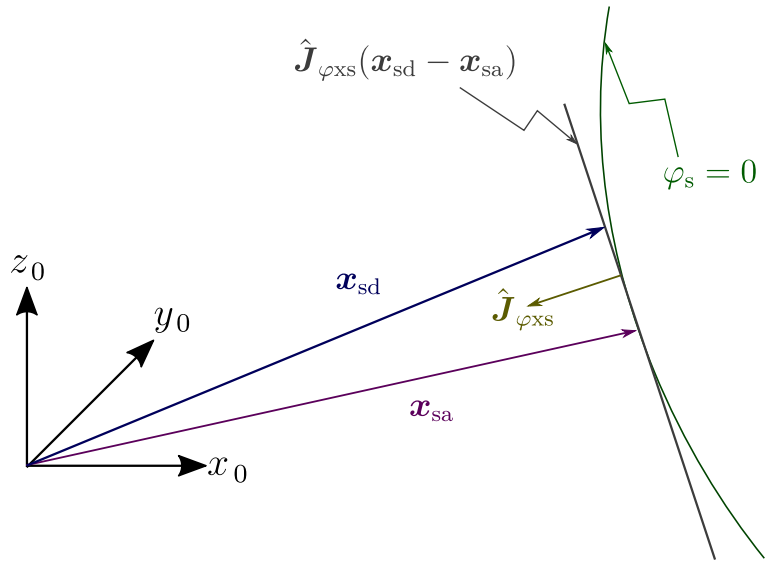

Figure 3.2: Local surface estimation.

Since the estimated surface is locally approximated by a plane, its first and second time derivatives can be in turn approximated by

$$\hat{\dot{\boldsymbol{\varphi}}}_{\mathrm{v}} = \hat{\boldsymbol{J}}_{\varphi\mathrm{xs}}(\dot{\boldsymbol{x}}_{\mathrm{sd}}-\dot{\boldsymbol{x}}_{\mathrm{sa}}) \tag{3.25}$$

$$\hat{\ddot{\boldsymbol{\varphi}}}_{\mathrm{v}} = \hat{\boldsymbol{J}}_{\varphi\mathrm{xs}}(\ddot{\boldsymbol{x}}_{\mathrm{sd}}-\ddot{\boldsymbol{x}}_{\mathrm{sa}})\,. \tag{3.26}$$

To reflect the contact force to the operator, a Lagrange multiplier can be iteratively computed as in Bayo and Avello [1994]. This algorithm is intended for simulation purposes and the authors have found that it converges in less than four iterations. However, for real time implementation no more than one iteration can be done in a sampling period, which corresponds to the *Generic Penalty Method* introduced in Bayo et al. [1988]. Therefore, the Lagrange multiplier accounting for the virtual force can be estimated by

$$\lambda_{\mathrm{v}} = \alpha_{\mathrm{v}}\left(\hat{\ddot{\boldsymbol{\varphi}}}_{\mathrm{v}} + 2\xi\omega_{\mathrm{n}}\hat{\dot{\boldsymbol{\varphi}}}_{\mathrm{v}} + \omega_{\mathrm{n}}^2\hat{\boldsymbol{\varphi}}_{\mathrm{v}}\right), \tag{3.27}$$

where $\alpha_{\mathrm{v}}, \xi, \omega > 0$.

To achieve the desired transparency of the teleoperation system, an online cancellation of the master manipulator dynamics is carried out. On the other hand, the contact force must be reflected to the human operator through the master manipulator. Consequently, the control law for the master robot is proposed as

$$\boldsymbol{\tau}_{\mathrm{m}} = \boldsymbol{H}(\boldsymbol{q}_{\mathrm{m}})\ddot{\boldsymbol{q}}_{\mathrm{m}} + \boldsymbol{C}_{\mathrm{m}}(\boldsymbol{q}_{\mathrm{m}}, \dot{\boldsymbol{q}}_{\mathrm{m}})\dot{\boldsymbol{q}}_{\mathrm{m}} + \boldsymbol{D}_{\mathrm{m}}\dot{\boldsymbol{q}}_{\mathrm{m}} + \boldsymbol{g}_{\mathrm{m}}(\boldsymbol{q}_{\mathrm{m}}) - \hat{\boldsymbol{J}}_{\varphi\mathrm{v}}^{\mathrm{T}}(k_{\mathrm{Fv}}\Delta\lambda_{\mathrm{vs}} + k_{\mathrm{Fiv}}\Delta F_{\mathrm{vs}}) \,, \tag{3.28}$$

where $k_{\mathrm{Fv}}, k_{\mathrm{Fiv}} > 0$ are constant gains, $\hat{\boldsymbol{J}}_{\varphi\mathrm{v}} \triangleq \hat{\boldsymbol{J}}_{\varphi\mathrm{s}}$ (with a possible scale factor), and

$$\Delta\lambda_{\mathrm{vs}} \triangleq \lambda_{\mathrm{v}} - \hat{\lambda}_{\mathrm{s}} \tag{3.29}$$

$$\Delta F_{\mathrm{vs}} \triangleq \int_{t_0}^{t} \Delta\lambda_{\mathrm{vs}}\, \mathrm{d}\vartheta \,. \tag{3.30}$$

Remark 3.2. For the master manipulator it is assumed, for simplicity's sake, that joint velocities and accelerations are available from measurements. Nevertheless, it can also be employed an observer similar to (3.8)–(3.12) to obtain the required signals with the corresponding complication of the stability analysis. □

3.1.3 Human behavior

Now, an assumption related to the human operator behavior is introduced both to carry out the stability analysis and for simulation purposes. Let $\boldsymbol{q}_{\mathrm{d}}(t) \in \mathbb{R}^n$ be the desired trajectory for the master manipulator in joint coordinates as wished by the human and $\boldsymbol{e}_{\mathrm{m}} \triangleq \boldsymbol{q}_{\mathrm{m}} - \boldsymbol{q}_{\mathrm{d}}$ the corresponding tracking error.

Assumption 3.4. *The human operator imposes the torque $\boldsymbol{\tau}_{\mathrm{h}}$ over the master manipulator according with the following dynamic behavior*

$$\boldsymbol{\tau}_{\mathrm{h}} = \hat{\boldsymbol{Q}}_{\mathrm{v}} \left\{ \boldsymbol{K}_{\mathrm{ph}}\boldsymbol{e}_{\mathrm{m}} + \boldsymbol{K}_{\mathrm{vh}}\dot{\boldsymbol{e}}_{\mathrm{m}} + \boldsymbol{K}_{\mathrm{ih}} \int_{t_0}^{t} \boldsymbol{e}_{\mathrm{m}}\, \mathrm{d}\vartheta \right\} + \hat{\boldsymbol{J}}_{\varphi\mathrm{v}}^{\mathrm{T}} \{ k_{\mathrm{Fh}}\Delta\lambda_{\mathrm{vd}} + k_{\mathrm{Fih}}\Delta F_{\mathrm{vd}} \} \,, \tag{3.31}$$

where $\hat{\boldsymbol{Q}}_{\mathrm{v}} \triangleq \boldsymbol{I}_{n\times n} - \hat{\boldsymbol{J}}_{\varphi\mathrm{v}}^{+}\hat{\boldsymbol{J}}_{\varphi\mathrm{v}}$, with $\hat{\boldsymbol{J}}_{\varphi\mathrm{v}}^{+} = \hat{\boldsymbol{J}}_{\varphi\mathrm{v}}^{\mathrm{T}}(\hat{\boldsymbol{J}}_{\varphi\mathrm{v}}\hat{\boldsymbol{J}}_{\varphi\mathrm{v}}^{\mathrm{T}})^{-1}$, $\boldsymbol{K}_{\mathrm{ph}}, \boldsymbol{K}_{\mathrm{vh}}, \boldsymbol{K}_{\mathrm{ih}} \in \mathbb{R}^{n\times n}$ are symmetric positive definite matrices, $k_{\mathrm{Fh}}, k_{\mathrm{Fih}} > 0$, and

$$\Delta\lambda_{\mathrm{vd}} \triangleq \lambda_{\mathrm{v}} - \lambda_{\mathrm{sd}} \tag{3.32}$$

$$\Delta F_{\mathrm{vd}} \triangleq \int_{t_0}^{t} \Delta\lambda_{\mathrm{vd}}\, \mathrm{d}\vartheta \,. \tag{3.33}$$

□

Remark 3.3. To accurately model the human behavior, time delays arising from the arm reflexes latency should be taken into account [Kurtzer et al., 2008]. In contrast, in Tee et al. [2004] a simple *PD* plus a feed–forward term was proposed, based on previously reported physiological findings. By adding the integral action and omitting the feed–forward term, which depends on the specific task learning, one obtains the position *PID* and force *PI* model given in (3.31). Although this is a very restrictive model for the human behavior, its simplicity is advantageous for simulation and stability analysis. Moreover, the validity of its inclusion in a teleoperation scheme was experimentally tested in Rodríguez-Angeles et al. [2015]. The only difference in this work with the model employed in Rodríguez-Angeles et al. [2015] is that the directions of the constrained and unconstrained motions are in terms of the estimated virtual surface, which in turn emerges from the remote surface estimation. Notice that even if the estimation is not accurate, the master robot would generate a resistance to motion in the $\hat{\boldsymbol{J}}_{\varphi \mathrm{v}}$ direction. As a result, the operator feels natural to plan the position trajectory over the plane projected by $\hat{\boldsymbol{Q}}_{\mathrm{v}}$. In fact, the operator should be able to plan the trajectory over the virtual surface blindly, only with the reflected force sensation. Nevertheless, visual feedback could be beneficial for the trajectory planning task. □

3.2 Closed Loop Dynamics

Let the state estimation errors be

$$\tilde{\boldsymbol{q}}_{\mathrm{s}2} \triangleq \boldsymbol{q}_{\mathrm{s}2} - \hat{\boldsymbol{q}}_{s2} \tag{3.34}$$

and

$$\tilde{\boldsymbol{z}}_i \triangleq \boldsymbol{z}_i - \hat{\boldsymbol{z}}_i, i = 1, \ldots, p\,. \tag{3.35}$$

The slave manipulator dynamics (3.1)–(3.2) and (3.5)–(3.7) in closed loop with the observer (3.8)–(3.12) results in the estimation error dynamics

$$\dot{\tilde{\boldsymbol{q}}}_{\mathrm{s}} = \tilde{\boldsymbol{q}}_{\mathrm{s}2} - \boldsymbol{\lambda}_{p+1}\tilde{\boldsymbol{q}}_{\mathrm{s}} \tag{3.36}$$

$$\dot{\tilde{\boldsymbol{q}}}_{\mathrm{s}2} = -\boldsymbol{H}_{\mathrm{s}}^{-1}(\boldsymbol{q}_{\mathrm{s}})\left(\boldsymbol{N}_{\mathrm{s}}(\boldsymbol{q}_{\mathrm{s}},\boldsymbol{q}_{\mathrm{s}2}) - \boldsymbol{N}_{\mathrm{s}}(\boldsymbol{q}_{\mathrm{s}},\hat{\boldsymbol{q}}_{\mathrm{s}2})\right) + \tilde{\boldsymbol{z}}_1 - \boldsymbol{\lambda}_p\tilde{\boldsymbol{q}}_{\mathrm{s}} \tag{3.37}$$

$$\dot{\tilde{\boldsymbol{z}}}_1 = \tilde{\boldsymbol{z}}_2 - \boldsymbol{\lambda}_{p-1}\tilde{\boldsymbol{q}}_{\mathrm{s}} \tag{3.38}$$

$$\vdots$$

$$\dot{\tilde{\boldsymbol{z}}}_{p-1} = \tilde{\boldsymbol{z}}_p - \boldsymbol{\lambda}_1\tilde{\boldsymbol{q}}_{\mathrm{s}} \tag{3.39}$$

$$\dot{\tilde{\boldsymbol{z}}}_p = \boldsymbol{r}^{(p)}(t) - \boldsymbol{\lambda}_0\tilde{\boldsymbol{q}}_{\mathrm{s}}\,. \tag{3.40}$$

By taking the time derivative of (3.36) and substituting (3.37) one obtains

$$\ddot{\tilde{\boldsymbol{q}}}_{\mathrm{s}} + \boldsymbol{\lambda}_{p+1}\dot{\tilde{\boldsymbol{q}}}_{\mathrm{s}} + \boldsymbol{\lambda}_p\tilde{\boldsymbol{q}}_{\mathrm{s}} = \tilde{\boldsymbol{z}}_1 + \boldsymbol{f}_{\mathrm{s}}(t)\,, \tag{3.41}$$

where

$$\begin{aligned}\boldsymbol{f}_{\mathrm{s}}(t) &= -\boldsymbol{H}_{\mathrm{s}}^{-1}(\boldsymbol{q}_{\mathrm{s}})\left(\boldsymbol{N}_{\mathrm{s}}(\boldsymbol{q}_{\mathrm{s}},\boldsymbol{q}_{\mathrm{s}2}) - \boldsymbol{N}_{\mathrm{s}}(\boldsymbol{q}_{\mathrm{s}},\hat{\boldsymbol{q}}_{\mathrm{s}2})\right)\\ &= -\boldsymbol{H}_{\mathrm{s}}^{-1}(\boldsymbol{q}_{\mathrm{s}})\left(\boldsymbol{C}_{\mathrm{s}}(\boldsymbol{q}_{\mathrm{s}},\boldsymbol{q}_{\mathrm{s}2})\boldsymbol{q}_{\mathrm{s}2} - \boldsymbol{C}_{\mathrm{s}}(\boldsymbol{q}_{\mathrm{s}},\hat{\boldsymbol{q}}_{\mathrm{s}2})\hat{\boldsymbol{q}}_{\mathrm{s}2} + \boldsymbol{D}_{\mathrm{s}}\tilde{\boldsymbol{q}}_{\mathrm{s}2}\right).\end{aligned} \tag{3.42}$$

After (3.19), (3.36), and (3.37), and by recurrently applying Property 2.4 yields

$$\begin{aligned}\boldsymbol{C}_{\mathrm{s}}(\boldsymbol{q}_{\mathrm{s}},\boldsymbol{q}_{\mathrm{s}2})\boldsymbol{q}_{\mathrm{s}2} - \boldsymbol{C}_{\mathrm{s}}(\boldsymbol{q}_{\mathrm{s}},\hat{\boldsymbol{q}}_{\mathrm{s}2})\hat{\boldsymbol{q}}_{\mathrm{s}2} &= \boldsymbol{C}_{\mathrm{s}}(\boldsymbol{q}_{\mathrm{s}},\dot{\boldsymbol{e}}_{\mathrm{s}} + \dot{\boldsymbol{q}}_{\mathrm{sd}})\left(\tilde{\boldsymbol{q}}_{\mathrm{s}2} + \hat{\boldsymbol{q}}_{\mathrm{s}2}\right) - \boldsymbol{C}_{\mathrm{s}}(\boldsymbol{q}_{\mathrm{s}},\hat{\boldsymbol{q}}_{\mathrm{s}2})\left(\boldsymbol{q}_{\mathrm{s}2} - \tilde{\boldsymbol{q}}_{\mathrm{s}2}\right)\\
&= \boldsymbol{C}_{\mathrm{s}}(\boldsymbol{q}_{\mathrm{s}},\dot{\boldsymbol{e}}_{\mathrm{s}} + \dot{\boldsymbol{q}}_{\mathrm{sd}})\tilde{\boldsymbol{q}}_{\mathrm{s}2} + \boldsymbol{C}_{\mathrm{s}}(\boldsymbol{q}_{\mathrm{s}},\dot{\boldsymbol{e}}_{\mathrm{s}} + \dot{\boldsymbol{q}}_{\mathrm{sd}})\hat{\boldsymbol{q}}_{\mathrm{s}2}\\
&\quad - \boldsymbol{C}_{\mathrm{s}}(\boldsymbol{q}_{\mathrm{s}},\hat{\boldsymbol{q}}_{\mathrm{s}2})\boldsymbol{q}_{\mathrm{s}2} + \boldsymbol{C}_{\mathrm{s}}(\boldsymbol{q}_{\mathrm{s}},\hat{\boldsymbol{q}}_{\mathrm{s}2})\tilde{\boldsymbol{q}}_{\mathrm{s}2}\\
&= \boldsymbol{C}_{\mathrm{s}}(\boldsymbol{q}_{\mathrm{s}},\dot{\boldsymbol{e}}_{\mathrm{s}} + \dot{\boldsymbol{q}}_{\mathrm{sd}})\tilde{\boldsymbol{q}}_{\mathrm{s}2} + \boldsymbol{C}_{\mathrm{s}}(\boldsymbol{q}_{\mathrm{s}},\dot{\boldsymbol{e}}_{\mathrm{s}} + \dot{\boldsymbol{q}}_{\mathrm{sd}})\hat{\boldsymbol{q}}_{\mathrm{s}2}\\
&\quad - \boldsymbol{C}_{\mathrm{s}}(\boldsymbol{q}_{\mathrm{s}},\dot{\boldsymbol{e}}_{\mathrm{s}} + \dot{\boldsymbol{q}}_{\mathrm{sd}})\hat{\boldsymbol{q}}_{\mathrm{s}2} + \boldsymbol{C}_{\mathrm{s}}(\boldsymbol{q}_{\mathrm{s}},\tilde{\boldsymbol{q}}_{\mathrm{s}2})\hat{\boldsymbol{q}}_{\mathrm{s}2}\\
&= \boldsymbol{C}_{\mathrm{s}}(\boldsymbol{q}_{\mathrm{s}},\dot{\boldsymbol{e}}_{\mathrm{s}} + \dot{\boldsymbol{q}}_{\mathrm{sd}})\left(\dot{\tilde{\boldsymbol{q}}}_{\mathrm{s}} + \boldsymbol{\lambda}_{p+1}\tilde{\boldsymbol{q}}_{\mathrm{s}}\right) + \boldsymbol{C}_{\mathrm{s}}(\boldsymbol{q}_{\mathrm{s}},\tilde{\boldsymbol{q}}_{\mathrm{s}2})\left(\boldsymbol{q}_{\mathrm{s}2} - \tilde{\boldsymbol{q}}_{\mathrm{s}2}\right)\\
&= \boldsymbol{C}_{\mathrm{s}}(\boldsymbol{q}_{\mathrm{s}},\dot{\boldsymbol{e}}_{\mathrm{s}} + \dot{\boldsymbol{q}}_{\mathrm{sd}})\left(\dot{\tilde{\boldsymbol{q}}}_{\mathrm{s}} + \boldsymbol{\lambda}_{p+1}\tilde{\boldsymbol{q}}_{\mathrm{s}}\right) + \boldsymbol{C}_{\mathrm{s}}(\boldsymbol{q}_{\mathrm{s}},\dot{\boldsymbol{e}}_{\mathrm{s}} + \dot{\boldsymbol{q}}_{\mathrm{sd}})\tilde{\boldsymbol{q}}_{\mathrm{s}2}\\
&\quad - \boldsymbol{C}_{\mathrm{s}}(\boldsymbol{q}_{\mathrm{s}},\tilde{\boldsymbol{q}}_{\mathrm{s}2})\tilde{\boldsymbol{q}}_{\mathrm{s}2}\\
&= 2\boldsymbol{C}_{\mathrm{s}}(\boldsymbol{q}_{\mathrm{s}},\dot{\boldsymbol{e}}_{\mathrm{s}} + \dot{\boldsymbol{q}}_{\mathrm{sd}})(\dot{\tilde{\boldsymbol{q}}}_{\mathrm{s}} + \boldsymbol{\lambda}_{p+1}\tilde{\boldsymbol{q}}_{\mathrm{s}})\\
&\quad - \boldsymbol{C}_{\mathrm{s}}(\boldsymbol{q}_{\mathrm{s}},\dot{\tilde{\boldsymbol{q}}}_{\mathrm{s}} + \boldsymbol{\lambda}_{p+1}\tilde{\boldsymbol{q}}_{\mathrm{s}})(\dot{\tilde{\boldsymbol{q}}}_{\mathrm{s}} + \boldsymbol{\lambda}_{p+1}\tilde{\boldsymbol{q}}_{\mathrm{s}})\,,\end{aligned} \tag{3.43}$$

so that (3.42) can be written as

$$\begin{aligned}\boldsymbol{f}_{\mathrm{s}}(t) = -\boldsymbol{H}_{\mathrm{s}}^{-1}(\boldsymbol{q}_{\mathrm{s}}) \big[& 2\boldsymbol{C}_{\mathrm{s}}(\boldsymbol{q}_{\mathrm{s}}, \dot{\boldsymbol{e}}_{\mathrm{s}} + \dot{\boldsymbol{q}}_{\mathrm{sd}})(\dot{\tilde{\boldsymbol{q}}}_{\mathrm{s}} + \boldsymbol{\lambda}_{p+1}\tilde{\boldsymbol{q}}_{\mathrm{s}}) \\ & -\boldsymbol{C}_{\mathrm{s}}(\boldsymbol{q}_{\mathrm{s}}, \dot{\tilde{\boldsymbol{q}}}_{\mathrm{s}} + \boldsymbol{\lambda}_{p+1}\tilde{\boldsymbol{q}}_{\mathrm{s}})(\dot{\tilde{\boldsymbol{q}}}_{\mathrm{s}} + \boldsymbol{\lambda}_{p+1}\tilde{\boldsymbol{q}}_{\mathrm{s}}) + \boldsymbol{D}_{\mathrm{s}}(\dot{\tilde{\boldsymbol{q}}}_{\mathrm{s}} + \boldsymbol{\lambda}_{p+1}\tilde{\boldsymbol{q}}_{\mathrm{s}}) \big] . \end{aligned} \tag{3.44}$$

By taking p time derivatives of (3.41) and after (3.38)–(3.40) one has

$$\tilde{\boldsymbol{q}}_{\mathrm{s}}^{(p+2)} + \boldsymbol{\lambda}_{p+1}\tilde{\boldsymbol{q}}_{\mathrm{s}}^{(p+1)} + \cdots + \boldsymbol{\lambda}_0\tilde{\boldsymbol{q}}_{\mathrm{s}} = \boldsymbol{r}^{(p)}(t) + \boldsymbol{f}_{\mathrm{s}}^{(p)}(t) . \tag{3.45}$$

This last equation can be rewritten in state space form as

$$\dot{\boldsymbol{x}}_{\mathrm{o}} = \boldsymbol{A}\boldsymbol{x}_{\mathrm{o}} + \boldsymbol{B}\boldsymbol{r}_{\mathrm{f}} , \tag{3.46}$$

where $\boldsymbol{r}_{\mathrm{f}} = \boldsymbol{r}^{(p)}(t) + \boldsymbol{f}_{\mathrm{s}}^{(p)}(t)$ and

$$\boldsymbol{x}_{\mathrm{o}} \triangleq \begin{bmatrix} \tilde{\boldsymbol{q}}_{\mathrm{s}} & \cdots & \tilde{\boldsymbol{q}}_{\mathrm{s}}^{(p+1)} \end{bmatrix}^{\mathrm{T}} \tag{3.47}$$

$$\boldsymbol{A} = \begin{bmatrix} \boldsymbol{O} & \boldsymbol{I} & \cdots & \boldsymbol{O} \\ \vdots & \vdots & \ddots & \vdots \\ \boldsymbol{O} & \boldsymbol{O} & \cdots & \boldsymbol{I} \\ -\boldsymbol{\lambda}_0 & -\boldsymbol{\lambda}_1 & \cdots & -\boldsymbol{\lambda}_{p+1} \end{bmatrix} \tag{3.48}$$

$$\boldsymbol{B} = \begin{bmatrix} \boldsymbol{O} & \cdots & \boldsymbol{O} & \boldsymbol{I} \end{bmatrix}^{\mathrm{T}} . \tag{3.49}$$

In order to obtain the closed loop dynamics for the slave manipulator, first the control law (3.20) is rewritten as

$$\begin{aligned}\boldsymbol{\tau}_{\mathrm{s}} = & -\boldsymbol{K}_{\mathrm{vs}}\dot{\boldsymbol{e}}_{\mathrm{s}} - \boldsymbol{K}_{\mathrm{ps}}\boldsymbol{e}_{\mathrm{s}} - \boldsymbol{K}_{\mathrm{is}}\boldsymbol{Q}_{\mathrm{s}}\int_0^t \boldsymbol{e}_{\mathrm{s}}\,\mathrm{d}\vartheta - \boldsymbol{J}_{\varphi\mathrm{s}}^{\mathrm{T}}\lambda_{\mathrm{sd}} + k_{\mathrm{Fis}}\boldsymbol{J}_{\varphi\mathrm{s}}^{+}\Delta\bar{F}_{\mathrm{s}} \\ & + \boldsymbol{K}_{\mathrm{vs}}(\dot{\tilde{\boldsymbol{q}}}_{\mathrm{s}} + \boldsymbol{\lambda}_{p+1}\tilde{\boldsymbol{q}}_{\mathrm{s}}) + \boldsymbol{K}_{\mathrm{is}}\tilde{\boldsymbol{Q}}_{\mathrm{s}}\int_0^t \boldsymbol{e}_{\mathrm{s}}\,\mathrm{d}\vartheta + \tilde{\boldsymbol{J}}_{\varphi s}^{\mathrm{T}}\lambda_{\mathrm{sd}} - k_{\mathrm{Fis}}\tilde{\boldsymbol{J}}_{\varphi s}^{+}\Delta\bar{F}_{\mathrm{s}} , \end{aligned} \tag{3.50}$$

where $\tilde{\boldsymbol{Q}}_{\mathrm{s}} \triangleq \boldsymbol{Q}_{\mathrm{s}} - \hat{\boldsymbol{Q}}_{\mathrm{s}}$, $\tilde{\boldsymbol{J}}_{\varphi s} \triangleq \boldsymbol{J}_{\varphi s} - \hat{\boldsymbol{J}}_{\varphi s}$, and $\tilde{\boldsymbol{J}}_{\varphi s}^{+} \triangleq \boldsymbol{J}_{\varphi s}^{+} - \hat{\boldsymbol{J}}_{\varphi s}^{+}$.

Define

$$\frac{\mathrm{d}}{\mathrm{d}t}\boldsymbol{\sigma} \triangleq \dot{\boldsymbol{e}}_{\mathrm{s}} + \boldsymbol{\Lambda}\boldsymbol{e}_{\mathrm{s}} , \tag{3.51}$$

where $\boldsymbol{\Lambda} \in \mathbb{R}^{n\times n}$ is a diagonal positive definite matrix. It is always possible to find $\boldsymbol{K}_{\mathrm{vs}} \in \mathbb{R}^{n\times n}$ and $\bar{\boldsymbol{K}}_{\mathrm{is}} \in \mathbb{R}^{n\times n}$ such that

$$\boldsymbol{K}_{\mathrm{ps}} = \boldsymbol{K}_{\mathrm{vs}}\boldsymbol{\Lambda} + \bar{\boldsymbol{K}}_{\mathrm{is}} \tag{3.52}$$

$$\boldsymbol{K}_{\mathrm{is}} = \bar{\boldsymbol{K}}_{\mathrm{is}}\boldsymbol{\Lambda}\,. \tag{3.53}$$

Therefore, the control law (3.50) is equivalent to

$$\begin{aligned}\boldsymbol{\tau}_{\mathrm{s}} = &-\boldsymbol{K}_{\mathrm{vs}}\frac{\mathrm{d}}{\mathrm{d}t}\boldsymbol{\sigma} - \bar{\boldsymbol{K}}_{\mathrm{is}}\boldsymbol{Q}_{\mathrm{s}}\boldsymbol{\sigma} - \boldsymbol{J}_{\varphi\mathrm{s}}^{\mathrm{T}}\lambda_{\mathrm{sd}} + k_{\mathrm{Fis}}\boldsymbol{J}_{\varphi\mathrm{s}}^{+}\Delta\bar{F}_{\mathrm{s}} + \boldsymbol{K}_{\mathrm{vs}}(\dot{\tilde{\boldsymbol{q}}}_{\mathrm{s}} + \boldsymbol{\lambda}_{p+1}\tilde{\boldsymbol{q}}_{\mathrm{s}}) \\ &+ \boldsymbol{K}_{\mathrm{is}}\tilde{\boldsymbol{Q}}_{\mathrm{s}}\int_0^t \boldsymbol{e}_{\mathrm{s}}\,\mathrm{d}\vartheta + \tilde{\boldsymbol{J}}_{\varphi s}^{\mathrm{T}}\lambda_{\mathrm{sd}} - k_{\mathrm{Fis}}\tilde{\boldsymbol{J}}_{\varphi s}^{+}\Delta\bar{F}_{\mathrm{s}}\,,\end{aligned} \tag{3.54}$$

as long as $\boldsymbol{Q}_{\mathrm{s}}\boldsymbol{\Lambda} = \boldsymbol{\Lambda}\boldsymbol{Q}_{\mathrm{s}}$ holds, what can always be achieved for instance by setting $\boldsymbol{\Lambda} = k_\lambda \boldsymbol{I}$.

Now, define

$$\dot{\boldsymbol{q}}_{\mathrm{r}} \triangleq \dot{\boldsymbol{q}}_{\mathrm{sd}} - \boldsymbol{\Lambda}\boldsymbol{e}_{\mathrm{s}} - \boldsymbol{K}_{\mathrm{vs}}^{-1}\bar{\boldsymbol{K}}_{\mathrm{is}}\boldsymbol{Q}_{\mathrm{s}}\boldsymbol{\sigma} + \frac{1}{2}\boldsymbol{K}_{\mathrm{vs}}^{-1}\boldsymbol{J}_{\varphi s}^{\mathrm{T}}\Delta\lambda_{\mathrm{s}} + \frac{1}{2}k_{\mathrm{Fis}}\boldsymbol{K}_{\mathrm{vs}}^{-1}\boldsymbol{J}_{\varphi s}^{+}\Delta\bar{F}_{\mathrm{s}} \tag{3.55}$$

$$\begin{aligned}\boldsymbol{s} &\triangleq \dot{\boldsymbol{q}}_{\mathrm{s}} - \dot{\boldsymbol{q}}_{\mathrm{r}} = \left(\frac{\mathrm{d}}{\mathrm{d}t}\boldsymbol{\sigma} + \boldsymbol{K}_{\mathrm{vs}}^{-1}\bar{\boldsymbol{K}}_{\mathrm{is}}\boldsymbol{Q}_{\mathrm{s}}\boldsymbol{\sigma}\right) + \left(-\frac{1}{2}\boldsymbol{K}_{\mathrm{vs}}^{-1}\boldsymbol{J}_{\varphi s}^{\mathrm{T}}\Delta\lambda_{\mathrm{s}} - \frac{1}{2}k_{\mathrm{Fis}}\boldsymbol{K}_{\mathrm{vs}}^{-1}\boldsymbol{J}_{\varphi s}^{+}\Delta\bar{F}_{\mathrm{s}}\right) \\ &\triangleq \boldsymbol{s}_{\mathrm{p}} + \boldsymbol{s}_{\mathrm{F}}\,,\end{aligned} \tag{3.56}$$

where $\Delta\lambda_{\mathrm{s}} = \lambda_{\mathrm{s}} - \lambda_{\mathrm{sd}}$ is the force tracking error.

Thus the closed loop dynamics of the slave manipulator is described by

$$\boldsymbol{H}_{\mathrm{s}}\dot{\boldsymbol{s}} + \boldsymbol{C}_{\mathrm{s}}\boldsymbol{s} + \boldsymbol{K}_{\mathrm{Dvs}}\boldsymbol{s} = \frac{1}{2}\boldsymbol{J}_{\varphi s}^{\mathrm{T}}\Delta\lambda_{\mathrm{s}} + \frac{1}{2}k_{\mathrm{Fis}}\boldsymbol{J}_{\varphi s}^{+}\Delta\bar{F}_{\mathrm{s}} + \boldsymbol{y}_{\mathrm{a}}\,, \tag{3.57}$$

where $\boldsymbol{K}_{\mathrm{Dvs}} = \boldsymbol{K}_{\mathrm{vs}} + \boldsymbol{D}_{\mathrm{s}}$, and

$$\begin{aligned}\boldsymbol{y}_{\mathrm{a}} = &\boldsymbol{K}_{\mathrm{vs}}(\dot{\tilde{\boldsymbol{q}}}_{\mathrm{s}} + \boldsymbol{\lambda}_{p+1}\tilde{\boldsymbol{q}}_{\mathrm{s}}) + \boldsymbol{K}_{\mathrm{is}}\tilde{\boldsymbol{Q}}_{\mathrm{s}}\int_0^t \boldsymbol{e}_{\mathrm{s}}\,\mathrm{d}\vartheta + \tilde{\boldsymbol{J}}_{\varphi s}^{\mathrm{T}}\lambda_{\mathrm{sd}} - k_{\mathrm{Fis}}\tilde{\boldsymbol{J}}_{\varphi s}^{+}\Delta\bar{F}_{\mathrm{s}} \\ &- \left(\boldsymbol{H}_{\mathrm{s}}(\boldsymbol{q}_{\mathrm{s}})\ddot{\boldsymbol{q}}_{\mathrm{r}} + \boldsymbol{C}_{\mathrm{s}}(\boldsymbol{q}_{\mathrm{s}}, \boldsymbol{q}_{\mathrm{s2}})\dot{\boldsymbol{q}}_{\mathrm{r}} + \boldsymbol{D}_{\mathrm{s}}\dot{\boldsymbol{q}}_{\mathrm{r}} + \boldsymbol{g}(\boldsymbol{q}_{\mathrm{s}})\right)\,.\end{aligned} \tag{3.58}$$

To obtain the dynamics of the surface estimation error, let

$$\tilde{\boldsymbol{J}}_{\varphi\mathrm{xs}} \triangleq \boldsymbol{J}_{\varphi\mathrm{xs}} - \hat{\boldsymbol{J}}_{\varphi\mathrm{xs}}\,. \tag{3.59}$$

By taking into account (3.16) leads to

$$\dot{\tilde{\boldsymbol{J}}}^{\mathrm{T}}_{\varphi \mathrm{xs}} = \dot{\boldsymbol{J}}^{\mathrm{T}}_{\varphi \mathrm{xs}} - \dot{\hat{\boldsymbol{J}}}^{\mathrm{T}}_{\varphi \mathrm{xs}} = \dot{\boldsymbol{J}}^{\mathrm{T}}_{\varphi \mathrm{xs}} - \left(\frac{\gamma}{\hat{\lambda}_{\mathrm{s}} + \epsilon}\right) \hat{\boldsymbol{Q}}_{\mathrm{xs}} \boldsymbol{J}_{\mathrm{s}}^{-\mathrm{T}}(\boldsymbol{q}_{\mathrm{s}}) \boldsymbol{H}_{\mathrm{s}}(\boldsymbol{q}_{\mathrm{s}}) \hat{\boldsymbol{z}}_1 \,. \tag{3.60}$$

Finally, for the master robot, from (2.2), (3.28), and (3.31) one obtains

$$\begin{aligned} \hat{\boldsymbol{J}}^{\mathrm{T}}_{\varphi \mathrm{v}} \{ k_{\mathrm{Fv}} \Delta\lambda_{\mathrm{vs}} + k_{\mathrm{Fiv}} \Delta F_{\mathrm{vs}} + k_{\mathrm{Fh}} \Delta\lambda_{\mathrm{vd}} + k_{\mathrm{Fih}} \Delta F_{\mathrm{vd}} \} \\ + \hat{\boldsymbol{Q}}_{\mathrm{v}} \left\{ \boldsymbol{K}_{\mathrm{ph}} \boldsymbol{e}_{\mathrm{m}} + \boldsymbol{K}_{\mathrm{vh}} \dot{\boldsymbol{e}}_{\mathrm{m}} + \boldsymbol{K}_{\mathrm{ih}} \int_0^t \boldsymbol{e}_{\mathrm{m}} \, \mathrm{d}\vartheta \right\} = \boldsymbol{0} \,. \end{aligned} \tag{3.61}$$

From (3.21)–(3.22), (3.29)–(3.30), and (3.32)–(3.33) it is easy to get

$$\Delta\lambda_{\mathrm{vs}} = \Delta\lambda_{\mathrm{vd}} - \Delta\bar{\lambda}_{\mathrm{s}} \tag{3.62}$$

$$\Delta F_{\mathrm{vs}} = \Delta F_{\mathrm{vd}} - \Delta\bar{F}_{\mathrm{s}} \,, \tag{3.63}$$

so that (3.61) can be rewritten as

$$\begin{aligned} \hat{\boldsymbol{J}}^{\mathrm{T}}_{\varphi \mathrm{v}} \{ (k_{\mathrm{Fv}} + k_{\mathrm{Fh}}) \Delta\lambda_{\mathrm{vd}} + (k_{\mathrm{Fiv}} + k_{\mathrm{Fih}}) \Delta F_{\mathrm{vd}} \} \\ + \hat{\boldsymbol{Q}}_{\mathrm{v}} \left\{ \boldsymbol{K}_{\mathrm{ph}} \boldsymbol{e}_{\mathrm{m}} + \boldsymbol{K}_{\mathrm{vh}} \dot{\boldsymbol{e}}_{\mathrm{m}} + \boldsymbol{K}_{\mathrm{ih}} \int_0^t \boldsymbol{e}_{\mathrm{m}} \, \mathrm{d}\vartheta \right\} = \hat{\boldsymbol{J}}^{\mathrm{T}}_{\varphi \mathrm{v}} \left\{ k_{\mathrm{Fv}} \Delta\bar{\lambda}_{\mathrm{s}} + k_{\mathrm{Fiv}} \Delta\bar{F}_{\mathrm{s}} \right\} . \end{aligned} \tag{3.64}$$

Notice that (3.64) describes two dynamics evolving in orthogonal subspaces. By taking advantage of the fact that $\hat{\boldsymbol{J}}_{\varphi \mathrm{v}}$ is full rank, they can be analyzed separately as

$$(k_{\mathrm{Fv}} + k_{\mathrm{Fh}}) \Delta\lambda_{\mathrm{vd}} + (k_{\mathrm{Fiv}} + k_{\mathrm{Fih}}) \Delta F_{\mathrm{vd}} = k_{\mathrm{Fv}} \Delta\bar{\lambda}_{\mathrm{s}} + k_{\mathrm{Fiv}} \Delta\bar{F}_{\mathrm{s}} \tag{3.65}$$

$$\hat{\boldsymbol{Q}}_{\mathrm{v}} \left(\boldsymbol{K}_{\mathrm{vh}} \dot{\boldsymbol{e}}_{\mathrm{m}} + \boldsymbol{K}_{\mathrm{ph}} \boldsymbol{e}_{\mathrm{m}} + \boldsymbol{K}_{\mathrm{ih}} \int_0^t \boldsymbol{e}_{\mathrm{m}} \, \mathrm{d}\vartheta \right) = \boldsymbol{0} \,. \tag{3.66}$$

3.3 Stability Analysis

Before stating the main result on the master–slave teleoperation system, an auxiliary result is presented, which only takes into account the slave manipulator in closed loop with the force and velocity observer, and the surface estimator.

Theorem 3.1. *Consider the slave manipulator in contact with a rigid surface described by (2.1) and (2.3) in closed loop with the observer (3.8)–(3.12) and (3.15), the controller (3.20), and the*

surface estimator (3.16), whose complete closed loop dynamics is given by (3.21)–(3.22), (3.46), (3.57), and (3.60). Suppose that the desired slave position $\boldsymbol{q}_{\mathrm{sd}}(t)$ *is smooth. Let*

$$\boldsymbol{y}_{\mathrm{s}} \triangleq \begin{bmatrix} \boldsymbol{x}_{\mathrm{o}} & \boldsymbol{s} & \Delta\bar{F}_{\mathrm{s}} & \tilde{\boldsymbol{J}}_{\varphi\mathrm{xs}} \end{bmatrix}^{\mathrm{T}}, \tag{3.67}$$

and define a region $\mathscr{D}_{\mathrm{s}} \triangleq \{\boldsymbol{y}_{\mathrm{s}} \in \mathbb{R}^{(p+2)n+4} | \, \|\boldsymbol{y}_{\mathrm{s}}\| \leq y_{\max}\}$ *where* $y_{\max}$ *is a positive constant small enough for Fact 2.1 to hold, i.e.,*

$$\boldsymbol{e}_{\mathrm{s}} = \boldsymbol{Q}_{\mathrm{s}}\boldsymbol{e}_{\mathrm{s}} \quad \texttt{and} \quad \dot{\boldsymbol{e}}_{\mathrm{s}} = \boldsymbol{Q}_{\mathrm{s}}\dot{\boldsymbol{e}}_{\mathrm{s}}\,. \tag{3.68}$$

Assume that the manipulator never losses contact with the environment. Then, a set of controller gains $\boldsymbol{K}_{\mathrm{ps}}$, $\boldsymbol{K}_{\mathrm{vs}}$, $\boldsymbol{K}_{\mathrm{is}}$ *and* k_{Fis} *in (3.20),* γ *in (3.16), and a set of observer gains* $\boldsymbol{\lambda}_0, \ldots, \boldsymbol{\lambda}_{p+1}$ *in (3.48) can always be found to achieve uniform ultimate boundedness of* $\boldsymbol{y}_{\mathrm{s}}$ *provided the initial condition* $\boldsymbol{y}_{\mathrm{s}}(t_0)$ *is small enough such that* $\boldsymbol{y}_{\mathrm{s}}$ *does never leave* $\mathscr{D}_{\mathrm{s}}$ *during the transient response. Furthermore, the tracking errors* $\boldsymbol{e}_{\mathrm{s}}$, $\dot{\boldsymbol{e}}_{\mathrm{s}}$, *and* $\Delta\lambda_{\mathrm{s}}$, *and the estimation errors* $\boldsymbol{x}_{\mathrm{o}}$ *and* $\tilde{\boldsymbol{J}}_{\varphi\mathrm{xs}}$ *can be made arbitrarily small as well.* □

The proof is developed in four steps. In step a) is shown that whenever the state $\boldsymbol{y}_{\mathrm{s}}$ is inside the region $\mathscr{D}_{\mathrm{s}}$, all signals of interest remain bounded. Next, in part b) is proved that, in particular, the norm of the observation error $\boldsymbol{x}_{\mathrm{o}}$ defined in (3.47) can be made arbitrarily small *independently* of all other states by selecting the poles of $\boldsymbol{A}$ in (3.48) far away in the left half of the complex plane. In the next step c), Lyapunov–like arguments are given to show that the state $\boldsymbol{y}_{\mathrm{s}}$ can be forced to remain in $\mathscr{D}_{\mathrm{s}}$ by an appropriate selection of the controller and estimator gains. Finally, in step d) is shown that estimation of joint–velocities and contact force are achieved in an approximate but arbitrarily close manner and that position and force tracking is also achieved.

Proof. Theorem 3.1 states a local stability result, valid only in a region of interest $\mathscr{D}_{\mathrm{s}}$, where Fact 2.1 holds. Therefore, it must be shown that any signal of interest is bounded whenever $\boldsymbol{y}_{\mathrm{s}} \in \mathscr{D}_{\mathrm{s}}$ and that, with a proper choice of gains, $\boldsymbol{y}_{\mathrm{s}}$ will stay in $\mathscr{D}_{\mathrm{s}}$ for all time and will tend to an arbitrary small region around the origin. Consider the next steps:

a) First, we show that whenever the state $\boldsymbol{y}_{\mathrm{s}} \in \mathscr{D}_{\mathrm{s}}$, then every signal of interest is also bounded. From (3.56) it is

$$\frac{\mathrm{d}}{\mathrm{d}t}\boldsymbol{\sigma} = -\boldsymbol{K}_{\mathrm{vs}}^{-1}\bar{\boldsymbol{K}}_{\mathrm{is}}\boldsymbol{Q}_{\mathrm{s}}\boldsymbol{\sigma} + \boldsymbol{s}_{\mathrm{p}}\,, \tag{3.69}$$

where $\boldsymbol{s}_\mathrm{p}$ is bounded in $\mathscr{D}_\mathrm{s}$, because due to Fact 2.1 $\boldsymbol{s}_\mathrm{p}$ and $\boldsymbol{s}_\mathrm{F}$ are orthogonal. For the sake of simplicity, consider $\boldsymbol{K}_\mathrm{vs} = k_\mathrm{vs}\boldsymbol{I}$ and $\bar{\boldsymbol{K}}_\mathrm{is} = \bar{k}_\mathrm{is}\boldsymbol{I}$. Then it can be shown that $\boldsymbol{\sigma}$ and $\frac{\mathrm{d}}{\mathrm{d}t}\boldsymbol{\sigma}$ are bounded and $\|\boldsymbol{Q}_\mathrm{s}\boldsymbol{\sigma}\|$ and $\|\frac{\mathrm{d}}{\mathrm{d}t}\boldsymbol{\sigma}\|$ can be made arbitrarily small by setting $\bar{k}_\mathrm{i}$ large enough. As a result, from (3.51) $\dot{\boldsymbol{e}}_\mathrm{s}$, $\boldsymbol{e}_\mathrm{s}$, and $\int_0^t \boldsymbol{e}_\mathrm{s}\,\mathrm{d}\vartheta$ are bounded. Since $\dot{\boldsymbol{q}}_\mathrm{sd}$ and $\boldsymbol{q}_\mathrm{sd}$ are bounded by assumption, then $\dot{\boldsymbol{q}}_\mathrm{s} = \boldsymbol{q}_\mathrm{s2}$ and $\boldsymbol{q}_\mathrm{s}$ must be bounded. Furthermore, $\hat{\boldsymbol{q}}_\mathrm{s}$, $\dot{\hat{\boldsymbol{q}}}_\mathrm{s}$, and $\hat{\boldsymbol{q}}_\mathrm{s2}$ are also bounded after (3.36) and because $\boldsymbol{x}_\mathrm{o}$ is bounded in $\mathscr{D}_\mathrm{s}$. From (3.59) it follows that $\hat{\boldsymbol{J}}_{\varphi\mathrm{xs}}$, $\hat{\boldsymbol{J}}_{\varphi\mathrm{s}}$, $\hat{\boldsymbol{Q}}_\mathrm{xs}$, and $\hat{\boldsymbol{Q}}_\mathrm{s}$ are bounded after Assumption 3.3 and because $\bar{\boldsymbol{J}}_{\varphi\mathrm{xs}}$ is bounded in $\mathscr{D}_\mathrm{s}$. This implies after (3.20) that $\boldsymbol{\tau}_\mathrm{s}$ is bounded.

Now, consider [Murray et al., 1994]

$$\begin{aligned}\lambda_\mathrm{s} = &\left(\boldsymbol{J}_{\varphi\mathrm{s}}(\boldsymbol{q}_\mathrm{s})\boldsymbol{H}_\mathrm{s}^{-1}(\boldsymbol{q}_\mathrm{s})\boldsymbol{J}_{\varphi\mathrm{s}}^\mathrm{T}(\boldsymbol{q}_\mathrm{s})\right)^{-1}\left\{\boldsymbol{J}_{\varphi\mathrm{s}}(\boldsymbol{q}_\mathrm{s})\boldsymbol{H}_\mathrm{s}^{-1}(\boldsymbol{q}_\mathrm{s})\left(\boldsymbol{\tau}_\mathrm{s} - \boldsymbol{N}_\mathrm{s}(\boldsymbol{q}_\mathrm{s},\boldsymbol{q}_\mathrm{s2})\right)\right.\\ &\left.+\,\boldsymbol{J}_{\varphi\mathrm{s}}(\boldsymbol{q}_\mathrm{s},\boldsymbol{q}_\mathrm{s2})\boldsymbol{q}_\mathrm{s2}\right\}.\end{aligned} \tag{3.70}$$

Since $\boldsymbol{H}_\mathrm{s}(\boldsymbol{q}_\mathrm{s})$ is bounded and positive definite, then $\boldsymbol{\lambda}_\mathrm{s}$ is bounded, which in turn means that $\boldsymbol{z}_1$ in (3.3) is bounded too. By taking into account Assumptions 2.1 and 3.3, the partial derivatives $\partial\varphi_\mathrm{s}(\boldsymbol{q}_\mathrm{s})/\partial\boldsymbol{q}_\mathrm{s}, \partial^2\varphi_\mathrm{s}(\boldsymbol{q}_\mathrm{s})/\partial\boldsymbol{q}_\mathrm{s}^2, \ldots, \partial^{p+1}\varphi_\mathrm{s}(\boldsymbol{q}_\mathrm{s})/\partial\boldsymbol{q}_\mathrm{s}^{p+1}$ are bounded. Therefore, $\dot{\boldsymbol{J}}_{\varphi\mathrm{s}}(\boldsymbol{q}_\mathrm{s}) = \left(\partial\boldsymbol{J}_{\varphi\mathrm{s}}(\boldsymbol{q}_\mathrm{s})/\partial\boldsymbol{q}_\mathrm{s}\right)\dot{\boldsymbol{q}}_\mathrm{s}$ must be bounded as well as $\boldsymbol{f}_\mathrm{s}(t)$ in (3.44) and $\dot{\boldsymbol{q}}_\mathrm{r}$ in (3.55). From (3.41) one can conclude that $\tilde{\boldsymbol{z}}_1$ is bounded and, as a consequence, $\hat{\boldsymbol{z}}_1$ and $\hat{\lambda}_\mathrm{s}$ in (3.15), and $\Delta\bar{\lambda}_\mathrm{s}$ in (3.21) must be bounded. After (3.16) and (3.60), $\dot{\hat{\boldsymbol{J}}}_{\varphi\mathrm{s}}$ and $\dot{\bar{\boldsymbol{J}}}_{\varphi\mathrm{s}}$ are bounded as well.

Taking into account (3.70) and the slave manipulator model (3.1)–(3.3), one can write the joint acceleration as a function of only $(\boldsymbol{q}_\mathrm{s}, \boldsymbol{q}_\mathrm{s2}, \boldsymbol{\tau}_\mathrm{s})$, *i.e.*,

$$\dot{\boldsymbol{q}}_\mathrm{s2} = \ddot{\boldsymbol{q}}_\mathrm{s} = \boldsymbol{f}_\mathrm{q}(\boldsymbol{q}_\mathrm{s}, \dot{\boldsymbol{q}}_\mathrm{s}, \boldsymbol{\tau}_\mathrm{s}), \tag{3.71}$$

which clearly shows that $\dot{\boldsymbol{q}}_\mathrm{s2}$ is bounded. Since $\ddot{\boldsymbol{q}}_\mathrm{sd}$ is bounded and $\dddot{\boldsymbol{q}}_\mathrm{s}$ is then bounded from (3.41), $\ddot{\boldsymbol{e}}_\mathrm{s}$, $\dddot{\tilde{\boldsymbol{q}}}_\mathrm{s}$, and $\dot{\tilde{\boldsymbol{q}}}_\mathrm{s2}$ must be bounded after (3.36). Now, by similar arguments, $\boldsymbol{\tau}_\mathrm{s}$ in (3.20) can be written as a function of bounded variables, *i.e.*,

$$\boldsymbol{\tau}_\mathrm{s} = \boldsymbol{f}_\tau\left(\dot{\boldsymbol{q}}_\mathrm{sd}, \int_0^t \boldsymbol{e}_\mathrm{s}\,\mathrm{d}\vartheta, \boldsymbol{e}_\mathrm{s}, \tilde{\boldsymbol{q}}_\mathrm{s}, \dot{\tilde{\boldsymbol{q}}}_\mathrm{s}, \hat{\boldsymbol{J}}_{\varphi\mathrm{s}}, \lambda_\mathrm{sd}, \Delta\bar{F}_\mathrm{s}\right). \tag{3.72}$$

Therefore, its time derivative must be a function of the form

$$\dot{\boldsymbol{\tau}}_\mathrm{s} = \dot{\boldsymbol{f}}_\tau\left(\dot{\boldsymbol{q}}_\mathrm{sd}, \ddot{\boldsymbol{q}}_\mathrm{sd}, \int_0^t \boldsymbol{e}_\mathrm{s}\,\mathrm{d}\vartheta, \boldsymbol{e}_\mathrm{s}, \dot{\boldsymbol{e}}_\mathrm{s}, \tilde{\boldsymbol{q}}_\mathrm{s}, \dot{\tilde{\boldsymbol{q}}}_\mathrm{s}, \ddot{\tilde{\boldsymbol{q}}}_\mathrm{s}, \hat{\boldsymbol{J}}_{\varphi\mathrm{s}}, \dot{\hat{\boldsymbol{J}}}_{\varphi\mathrm{s}}, \lambda_\mathrm{sd}, \dot{\lambda}_\mathrm{sd}, \Delta\bar{F}_\mathrm{s}, \Delta\bar{\lambda}_\mathrm{s}\right), \tag{3.73}$$

which is bounded since it depends on variables we have already proven to be bounded.

On the other hand, the time derivative of $\dot{\boldsymbol{q}}_\mathrm{r}$ in (3.55) is given by

$$\begin{aligned}\ddot{\boldsymbol{q}}_\mathrm{r} = \ddot{\boldsymbol{q}}_\mathrm{sd} - \boldsymbol{\Lambda}\dot{\boldsymbol{e}}_\mathrm{s} - \boldsymbol{K}_\mathrm{vs}^{-1}\bar{\boldsymbol{K}}_\mathrm{is}\dot{\boldsymbol{Q}}_\mathrm{s}\boldsymbol{\sigma} - \boldsymbol{K}_\mathrm{vs}^{-1}\bar{\boldsymbol{K}}_\mathrm{is}\boldsymbol{Q}_\mathrm{s}\frac{\mathrm{d}}{\mathrm{d}t}\boldsymbol{\sigma} + \frac{1}{2}\boldsymbol{K}_\mathrm{vs}^{-1}\dot{\boldsymbol{J}}_{\varphi s}^\mathrm{T}\Delta\lambda_\mathrm{s} \\ + \frac{1}{2}\boldsymbol{K}_\mathrm{vs}^{-1}\boldsymbol{J}_{\varphi s}^\mathrm{T}\frac{\mathrm{d}}{\mathrm{d}t}(\Delta\lambda_\mathrm{s}) + \frac{1}{2}k_\mathrm{Fis}\boldsymbol{K}_\mathrm{vs}^{-1}\dot{\boldsymbol{J}}_{\varphi s}^{+}\Delta\bar{F}_\mathrm{s} + \frac{1}{2}k_\mathrm{Fis}\boldsymbol{K}_\mathrm{vs}^{-1}\boldsymbol{J}_{\varphi s}^{+}\Delta\bar{\lambda}_\mathrm{s}\,, \end{aligned} \tag{3.74}$$

which again turns out to be bounded since from (3.70), $\frac{\mathrm{d}}{\mathrm{d}t}(\Delta\lambda_\mathrm{s})$ is a function only of $(\boldsymbol{q}_\mathrm{s}, \dot{\boldsymbol{q}}_\mathrm{s}, \ddot{\boldsymbol{q}}_\mathrm{s}, \boldsymbol{\tau}_\mathrm{s}, \dot{\boldsymbol{\tau}}_\mathrm{s})$. Then, there must exist a positive constant c_a such that $\boldsymbol{y}_\mathrm{a}$ in (3.58) fulfills $\|\boldsymbol{y}_\mathrm{a}\| \leq c_\mathrm{a}$, whenever $\boldsymbol{y}_\mathrm{s} \in \mathscr{D}_\mathrm{s}$. As a direct consequence, $\dot{\boldsymbol{s}}$ in (3.57) is bounded.

By differentiating (3.56) one obtains

$$\begin{aligned}\dot{\boldsymbol{s}} = \ddot{\boldsymbol{\sigma}} + \boldsymbol{K}_\mathrm{vs}^{-1}\bar{\boldsymbol{K}}_\mathrm{is}\dot{\boldsymbol{Q}}_\mathrm{s}\boldsymbol{\sigma} + \boldsymbol{K}_\mathrm{vs}^{-1}\bar{\boldsymbol{K}}_\mathrm{is}\boldsymbol{Q}_\mathrm{s}\frac{\mathrm{d}}{\mathrm{d}t}\boldsymbol{\sigma} - \frac{1}{2}\boldsymbol{K}_\mathrm{vs}^{-1}\dot{\boldsymbol{J}}_{\varphi s}^\mathrm{T}\Delta\lambda_\mathrm{s} - \frac{1}{2}\boldsymbol{K}_\mathrm{vs}^{-1}\boldsymbol{J}_{\varphi s}^\mathrm{T}\frac{\mathrm{d}}{\mathrm{d}t}(\Delta\lambda_\mathrm{s}) \\ - \frac{1}{2}k_\mathrm{Fis}\boldsymbol{K}_\mathrm{vs}^{-1}\dot{\boldsymbol{J}}_{\varphi s}^{+}\Delta\bar{F}_\mathrm{s} - \frac{1}{2}k_\mathrm{Fis}\boldsymbol{K}_\mathrm{vs}^{-1}\boldsymbol{J}_{\varphi s}^{+}\Delta\bar{\lambda}_\mathrm{s}\,, \end{aligned} \tag{3.75}$$

so that $\ddot{\boldsymbol{\sigma}}$ must be bounded.

At this point, an iterative argument is carried out. First, by computing the time derivative of (3.71) it is

$$\boldsymbol{q}_\mathrm{s}^{(3)} = \dot{\boldsymbol{f}}_\mathrm{q}(\boldsymbol{q}_\mathrm{s}, \dot{\boldsymbol{q}}_\mathrm{s}, \ddot{\boldsymbol{q}}_\mathrm{s}, \boldsymbol{\tau}_\mathrm{s}, \dot{\boldsymbol{\tau}}_\mathrm{s})\,, \tag{3.76}$$

which shows that $\boldsymbol{q}_\mathrm{s}^{(3)}$, $\boldsymbol{e}_\mathrm{s}^{(3)}$ and $\hat{\boldsymbol{q}}_\mathrm{s}^{(3)}$ are bounded. Combining (3.8) and (3.9), it can be written

$$\hat{\boldsymbol{z}}_1 = \boldsymbol{f}_{\hat{z}_1}(\boldsymbol{q}_\mathrm{s}, \dddot{\tilde{\boldsymbol{q}}}_\mathrm{s}, \ddot{\tilde{\boldsymbol{q}}}_\mathrm{s}, \dot{\tilde{\boldsymbol{q}}}_\mathrm{s}, \hat{\boldsymbol{q}}_\mathrm{s2}, \boldsymbol{\tau}_\mathrm{s})\,. \tag{3.77}$$

This implies that

$$\dot{\hat{\boldsymbol{z}}}_1 = \dot{\boldsymbol{f}}_{\hat{z}_1}\left(\boldsymbol{q}_\mathrm{s}, \dot{\boldsymbol{q}}_\mathrm{s}, \ddot{\tilde{\boldsymbol{q}}}_\mathrm{s}, \hat{\boldsymbol{q}}_\mathrm{s}^{(3)}, \tilde{\boldsymbol{q}}_\mathrm{s}, \dot{\tilde{\boldsymbol{q}}}_\mathrm{s}, \ddot{\tilde{\boldsymbol{q}}}_\mathrm{s}, \hat{\boldsymbol{q}}_\mathrm{s2}, \dot{\hat{\boldsymbol{q}}}_\mathrm{s2}, \boldsymbol{\tau}_\mathrm{s}, \dot{\boldsymbol{\tau}}_\mathrm{s}\right) \tag{3.78}$$

is bounded and so are $\dot{\hat{\lambda}}_\mathrm{s}$ and $\frac{\mathrm{d}}{\mathrm{d}t}(\Delta\bar{\lambda}_\mathrm{s})$ as a consequence. From (3.16) it follows

$$\dot{\hat{\boldsymbol{J}}}_{\varphi\mathrm{xs}} = \dot{\boldsymbol{f}}_{\hat{\mathrm{J}}_{\varphi\mathrm{xs}}}(\boldsymbol{q}_\mathrm{s}, \hat{\boldsymbol{z}}_1)\,, \tag{3.79}$$

where (3.15) has been taken into account. Then, after (3.18) it means

$$\dot{\hat{\boldsymbol{J}}}_{\varphi \mathrm{s}} = \dot{\boldsymbol{f}}_{\hat{\mathrm{J}}_{\varphi \mathrm{s}}}(\boldsymbol{q}_{\mathrm{s}}, \dot{\boldsymbol{q}}_{\mathrm{s}}, \hat{\boldsymbol{z}}_1) \tag{3.80}$$

$$\ddot{\hat{\boldsymbol{J}}}_{\varphi \mathrm{s}} = \ddot{\boldsymbol{f}}_{\hat{\mathrm{J}}_{\varphi \mathrm{s}}}(\boldsymbol{q}_{\mathrm{s}}, \dot{\boldsymbol{q}}_{\mathrm{s}}, \ddot{\boldsymbol{q}}_{\mathrm{s}}, \hat{\boldsymbol{z}}_1, \dot{\hat{\boldsymbol{z}}}_1), \tag{3.81}$$

which implies that $\ddot{\hat{\boldsymbol{Q}}}_{\mathrm{s}}$ is bounded. On the other hand

$$\ddot{\boldsymbol{J}}_{\varphi \mathrm{s}} = \boldsymbol{f}_{\mathrm{J}_{\varphi \mathrm{s}}}(\boldsymbol{q}_{\mathrm{s}}, \dot{\boldsymbol{q}}_{\mathrm{s}}, \ddot{\boldsymbol{q}}_{\mathrm{s}}) \tag{3.82}$$

must be bounded from Assumption 3.3 and because $\dot{\boldsymbol{q}}_{\mathrm{s}}$ and $\dot{\boldsymbol{q}}_{\mathrm{s2}}$ are bounded, which along with (3.81) means that $\dddot{\boldsymbol{J}}_{\varphi \mathrm{s}}$ is bounded. Now, from (3.73) it is

$$\ddot{\boldsymbol{\tau}}_{\mathrm{s}} = \ddot{\boldsymbol{f}}_{\tau}\left(\dot{\boldsymbol{q}}_{\mathrm{sd}}, \ldots, \boldsymbol{q}_{\mathrm{sd}}^{(3)}, \int_0^t \boldsymbol{e}_{\mathrm{s}}\, \mathrm{d}\vartheta, \boldsymbol{e}_{\mathrm{s}}, \ldots, \ddot{\boldsymbol{e}}_{\mathrm{s}}, \tilde{\boldsymbol{q}}_{\mathrm{s}}, \ldots, \tilde{\boldsymbol{q}}_{\mathrm{s}}^{(3)}, \hat{\boldsymbol{J}}_{\varphi \mathrm{s}}, \ldots, \ddot{\hat{\boldsymbol{J}}}_{\varphi \mathrm{s}}, \lambda_{\mathrm{sd}}, \ldots, \ddot{\lambda}_{\mathrm{sd}}, \Delta\bar{F}_{\mathrm{s}}, \Delta\bar{\lambda}_{\mathrm{s}}, \frac{\mathrm{d}}{\mathrm{d}t}(\Delta\bar{\lambda}_{\mathrm{s}})\right), \tag{3.83}$$

which is bounded based on the same arguments as those in the previous discussion. By the definition of $\boldsymbol{f}_{\mathrm{s}}$ in (3.44) it can be written

$$\boldsymbol{f}_{\mathrm{s}} = \boldsymbol{f}_{\mathrm{s}}(\boldsymbol{q}_{\mathrm{s}}, \dot{\boldsymbol{q}}_{\mathrm{s}}, \dot{\boldsymbol{q}}_{\mathrm{sd}}, \tilde{\boldsymbol{q}}_{\mathrm{s}}, \dot{\tilde{\boldsymbol{q}}}_{\mathrm{s}}) \tag{3.84}$$

$$\dot{\boldsymbol{f}}_{\mathrm{s}} = \dot{\boldsymbol{f}}_{\mathrm{s}}(\boldsymbol{q}_{\mathrm{s}}, \dot{\boldsymbol{q}}_{\mathrm{s}}, \ddot{\boldsymbol{q}}_{\mathrm{s}}, \dot{\boldsymbol{q}}_{\mathrm{sd}}, \ddot{\boldsymbol{q}}_{\mathrm{sd}}, \tilde{\boldsymbol{q}}_{\mathrm{s}}, \dot{\tilde{\boldsymbol{q}}}_{\mathrm{s}}, \ddot{\tilde{\boldsymbol{q}}}_{\mathrm{s}}). \tag{3.85}$$

As a result, from (3.41) one can conclude that $\dot{\tilde{\boldsymbol{z}}}_1$ is bounded, and so is $\dot{\boldsymbol{z}}_1$. Following this procedure iteratively, leads to

$$\boldsymbol{q}_{\mathrm{s}}^{(p+1)} = \boldsymbol{f}_{\mathrm{q}}^{(p-1)}\left(\boldsymbol{q}_{\mathrm{s}}, \ldots, \boldsymbol{q}_{\mathrm{s}}^{(p)}, \boldsymbol{\tau}_{\mathrm{s}}, \ldots, \boldsymbol{\tau}_{\mathrm{s}}^{(p-1)}\right), \tag{3.86}$$

which means that $\boldsymbol{q}_{\mathrm{s}}^{(p+1)}$ and $\hat{\boldsymbol{q}}_{\mathrm{s}}^{(p+1)}$ (and all their previous derivatives) are bounded. From (3.78) it follows

$$\hat{\boldsymbol{z}}_1^{(p-1)} = \boldsymbol{f}_{\hat{\mathrm{z}}_1}^{(p-1)}\left(\boldsymbol{q}_{\mathrm{s}}, \ldots, \boldsymbol{q}_{\mathrm{s}}^{(p-1)}, \hat{\boldsymbol{q}}_{\mathrm{s}}, \ldots, \hat{\boldsymbol{q}}_{\mathrm{s}}^{(p+1)}, \tilde{\boldsymbol{q}}_{\mathrm{s}}, \ldots, \tilde{\boldsymbol{q}}_{\mathrm{s}}^{(p)}, \dot{\tilde{\boldsymbol{q}}}_{\mathrm{s2}}, \ldots \hat{\boldsymbol{q}}_{\mathrm{s2}}^{(p-1)}, \boldsymbol{\tau}_{\mathrm{s}}, \ldots, \boldsymbol{\tau}_{\mathrm{s}}^{(p-1)}\right), \tag{3.87}$$

which must be bounded as well as all its previous time derivatives. It also implies that $\ddot{\bar{\lambda}}_{\mathrm{s}},\ldots,\hat{\lambda}_{\mathrm{s}}^{(p-1)}$ and $\mathrm{d}^2(\Delta\bar{\lambda}_{\mathrm{s}})/\mathrm{d}t^2,\ldots,\mathrm{d}^{p-1}(\Delta\bar{\lambda}_{\mathrm{s}})/\mathrm{d}t^{p-1}$ are bounded. In the same manner, from (3.81) it follows

$$\hat{\boldsymbol{J}}_{\varphi\mathrm{s}}^{(p)} = \boldsymbol{f}_{\hat{\mathrm{J}}_{\varphi\mathrm{s}}}^{(p)}\left(\boldsymbol{q}_{\mathrm{s}},\ldots,\boldsymbol{q}_{\mathrm{s}}^{(p)},\hat{\boldsymbol{z}}_1,\ldots,\hat{\boldsymbol{z}}_1^{(p-1)}\right). \tag{3.88}$$

Also, from (3.83) it is obtained

$$\boldsymbol{\tau}_{\mathrm{s}}^{(p)} = \boldsymbol{f}_{\tau}^{(p)}\left(\dot{\boldsymbol{q}}_{\mathrm{sd}},\ldots,\boldsymbol{q}_{\mathrm{sd}}^{(p+1)},\int_0^t \boldsymbol{e}_{\mathrm{s}}\,\mathrm{d}\vartheta,\boldsymbol{e}_{\mathrm{s}},\ldots,\boldsymbol{e}_{\mathrm{s}}^{(p)},\tilde{\boldsymbol{q}}_{\mathrm{s}},\ldots,\tilde{\boldsymbol{q}}_{\mathrm{s}}^{(p+1)},\right.$$
$$\left.\hat{\boldsymbol{J}}_{\varphi\mathrm{s}},\ldots,\hat{\boldsymbol{J}}_{\varphi\mathrm{s}}^{(p)},\lambda_{\mathrm{sd}},\ldots,\lambda_{\mathrm{sd}}^{(p)},\Delta\bar{F}_{\mathrm{s}},\Delta\bar{\lambda}_{\mathrm{s}},\ldots,\mathrm{d}^{(p-1)}(\Delta\bar{\lambda}_{\mathrm{s}})/\mathrm{d}t^{(p-1)}\right),$$

that is bounded, since it is a function of bounded signals. On the other hand, from (3.85) it can be written

$$\boldsymbol{f}_{\mathrm{s}}^{(p)} = \boldsymbol{f}_{\mathrm{s}}^{(p)}\left(\boldsymbol{q}_{\mathrm{s}},\ldots,\boldsymbol{q}_{\mathrm{s}}^{(p+1)},\dot{\boldsymbol{q}}_{\mathrm{sd}},\ldots,\boldsymbol{q}_{\mathrm{sd}}^{(p+1)},\tilde{\boldsymbol{q}}_{\mathrm{s}},\ldots,\tilde{\boldsymbol{q}}_{\mathrm{s}}^{(p+1)}\right), \tag{3.89}$$

which is bounded with all its previous derivatives bounded too. From (3.41) it is computed

$$\tilde{\boldsymbol{q}}_{\mathrm{s}}^{(p+1)} + \boldsymbol{\lambda}_{p+1}\tilde{\boldsymbol{q}}_{\mathrm{s}}^{(p)} + \boldsymbol{\lambda}_p\tilde{\boldsymbol{q}}_{\mathrm{s}}^{(p-1)} = \tilde{\boldsymbol{z}}_1^{(p-1)} + \boldsymbol{f}_{\mathrm{s}}^{(p-1)}, \tag{3.90}$$

which implies that $(\tilde{\boldsymbol{z}}_1,\ldots,\tilde{\boldsymbol{z}}_1^{(p-1)})$ are bounded too. Also, from (3.3) and (3.70) it can be seen that

$$\boldsymbol{z}_1 = \boldsymbol{f}_{\mathrm{z}_1}(\boldsymbol{q}_{\mathrm{s}},\dot{\boldsymbol{q}}_{\mathrm{s}},\boldsymbol{\tau}_{\mathrm{s}}), \tag{3.91}$$

from where it can be stated that all its time derivatives up to

$$\boldsymbol{z}_1^{(p)} = \boldsymbol{f}_{\mathrm{z}_1}^{(p)}\left(\boldsymbol{q}_{\mathrm{s}},\ldots,\boldsymbol{q}_{\mathrm{s}}^{(p+1)},\boldsymbol{\tau}_{\mathrm{s}},\ldots,\boldsymbol{\tau}_{\mathrm{s}}^{(p)}\right) \tag{3.92}$$

must be bounded as well.

From (3.5)–(3.7) it can be concluded that $(\boldsymbol{z}_1,\boldsymbol{z}_2,\ldots,\boldsymbol{z}_p,\dot{\boldsymbol{z}}_1,\dot{\boldsymbol{z}}_2,\ldots,\dot{\boldsymbol{z}}_p)$ and $\boldsymbol{r}^{(p)}$ must be bounded, since $\boldsymbol{z}_p = \boldsymbol{z}_1^{(p)}$. Furthermore, from (3.12), one can see that $\dot{\hat{\boldsymbol{z}}}_p$ is bounded as well. Also, since $(\boldsymbol{z}_1,\ldots,\boldsymbol{z}_1^{(p-1)})$ are bounded, one can easily show that the estimated variables $(\boldsymbol{z}_2,\ldots,\boldsymbol{z}_p,\dot{\boldsymbol{z}}_2,\ldots,\dot{\boldsymbol{z}}_{p-1})$ must be bounded. Moreover, all the related errors must be bounded as well.

b) Consider system (3.46), where the matrix $\boldsymbol{A}$ in (3.48) has been chosen to have all its eigenvalues with real part negative. Since the system is time invariant it must hold [Khalil, 2002, p. 156]

$$\|\boldsymbol{e}^{(t-t_0)\boldsymbol{A}}\| \leq k e^{-\delta(t-t_0)}, \tag{3.93}$$

and the state is bounded by

$$\|\boldsymbol{x}_\mathrm{o}(t)\| \leq k e^{-\delta(t-t_0)}\|\boldsymbol{x}_\mathrm{o}(t_0)\| + \frac{k\|\boldsymbol{B}\|}{\delta} \sup_{t_0\leq\vartheta\leq t} \|\boldsymbol{r}_\mathrm{f}(\vartheta)\|, \tag{3.94}$$

where it has been shown that $\boldsymbol{r}_\mathrm{f}$ is bounded, meaning that $\sup_{t_0\leq\vartheta\leq t} \|\boldsymbol{r}_\mathrm{f}(\vartheta)\|$ can be replaced by a constant value, say r_max. If k/δ can be set arbitrarily small, then the ultimate bound for $\|\boldsymbol{x}_\mathrm{o}(t)\|$ given by

$$\|\boldsymbol{x}_\mathrm{o}(t)\| \leq \frac{k}{\delta}\|\boldsymbol{B}\| r_\mathrm{max} \tag{3.95}$$

can be made arbitrarily small as well. To show that this is possible, suppose for simplicity's sake that the eigenvalues of $\boldsymbol{A}$ are chosen all real and distinct, satisfying

$$\lambda_{n(p+1)} < \lambda_{n(p+1)-1} < \cdots < \lambda_1 < 0. \tag{3.96}$$

Then, the right eigenvectors of $\boldsymbol{A}$, $\boldsymbol{e}_i$, with $i = 1,\ldots,n(p+1)$ satisfies

$$\boldsymbol{A}\boldsymbol{e}_i = \lambda_i \boldsymbol{e}_i, \tag{3.97}$$

while for the corresponding left eigenvector $\boldsymbol{\eta}_i$ with $i = 1,\ldots,n(p+1)$ it holds

$$\boldsymbol{\eta}_i^\mathrm{T}\boldsymbol{A} = \lambda_i \boldsymbol{\eta}_i^\mathrm{T}. \tag{3.98}$$

Note that it is assumed that $\|\boldsymbol{e}_i\| = \|\boldsymbol{\eta}_i\| = 1 \;\forall\; i = 1,\ldots,n(p+1)$ and that it holds [Callier and Desoer, 1991, p. 84]

$$\boldsymbol{\eta}_i^\mathrm{T}\boldsymbol{e}_j = \delta_{ij}, \tag{3.99}$$

for $i, j = 1,\ldots,n(p+1)$, where δ_{ij} is the Kronecker symbol satisfying $\delta_{ij} = 0$ if $i \neq j$ and $\delta_{ii} = 1$. Under these conditions, it can be shown that

$$e^{(t-t_0)\boldsymbol{A}} = \sum_{i=1}^{n(p+1)} e^{\lambda_i(t-t_0)} \boldsymbol{e}_i \boldsymbol{\eta}_i^\mathrm{T}. \tag{3.100}$$

By taking norms one has

$$\|e^{(t-t_0)\boldsymbol{A}}\| \leq \sum_{i=1}^{n(p+1)} e^{\lambda_i(t-t_0)}\|\boldsymbol{e}_i\|\|\boldsymbol{\eta}_i\| = \sum_{i=1}^{n(p+1)} e^{\lambda_i(t-t_0)}, \tag{3.101}$$

and from (3.96) it is

$$\begin{aligned}\|e^{(t-t_0)\boldsymbol{A}}\| &\leq \sum_{i=1}^{n(p+1)} e^{\lambda_1(t-t_0)} \\ &= n(p+1)e^{\lambda_1(t-t_0)} = n(p+1)e^{-\delta(t-t_0)},\end{aligned} \tag{3.102}$$

with

$$\delta \triangleq |\lambda_1| = |\lambda_{\max}\boldsymbol{A}|. \tag{3.103}$$

Setting

$$k = n(p+1) \tag{3.104}$$

one gets (3.93). Since δ can be chosen arbitrarily large, then k/δ can be set arbitrarily small.

Remark 3.4. The above result shows that the observation errors $\boldsymbol{x}_\mathrm{o}$ in (3.95) can be made arbitrarily small *independently* of the rest of the state vector $\boldsymbol{s}$ and $\Delta\bar{\boldsymbol{F}}$ and that the initial condition $\boldsymbol{x}_\mathrm{o}(t_0)$ could be arbitrarily large. The necessity of having a small enough initial condition for $\boldsymbol{x}_\mathrm{o}$ as well lies simply in the fact that otherwise position tracking could not be achieved, as it will be shown later. □

Now, consider the positive definite function

$$V_\mathrm{a} = \boldsymbol{x}_\mathrm{o}^\mathrm{T}\boldsymbol{P}_\mathrm{o}\boldsymbol{x}_\mathrm{o}, \tag{3.105}$$

with $\boldsymbol{x}_\mathrm{o}$ defined in (3.47) and $\boldsymbol{P}_\mathrm{o} = \boldsymbol{P}_\mathrm{o}^\mathrm{T} > \boldsymbol{O}$ given as the solution of

$$\boldsymbol{A}^\mathrm{T}\boldsymbol{P}_\mathrm{o} + \boldsymbol{P}_\mathrm{o}\boldsymbol{A} = -\boldsymbol{Q}_\mathrm{o}, \tag{3.106}$$

where $\boldsymbol{Q}_\mathrm{o}$ is a positive definite matrix and $\boldsymbol{A}$ is given by (3.48). As mentioned before, whenever $\boldsymbol{y}_\mathrm{s} \in \mathscr{D}_\mathrm{s}$, $\boldsymbol{r}_\mathrm{f}$ in (3.46) is bounded by $r_{\max}$.

By taking the time derivative of (3.105) along (3.46) one obtains

$$\begin{aligned}\dot{V}_\mathrm{a} &= \boldsymbol{x}_\mathrm{o}^\mathrm{T}\boldsymbol{P}_\mathrm{o}\left(\boldsymbol{A}\boldsymbol{x}_\mathrm{o}+\boldsymbol{B}\boldsymbol{r}_\mathrm{f}\right)+\left(\boldsymbol{A}\boldsymbol{x}_\mathrm{o}+\boldsymbol{B}\boldsymbol{r}_\mathrm{f}\right)^\mathrm{T}\boldsymbol{P}_\mathrm{o}\boldsymbol{x}_\mathrm{o}\\ &= \boldsymbol{x}_\mathrm{o}^\mathrm{T}\left(\boldsymbol{P}_\mathrm{o}\boldsymbol{A}+\boldsymbol{A}^\mathrm{T}\boldsymbol{P}_\mathrm{o}\right)\boldsymbol{x}_\mathrm{o}+\boldsymbol{x}_\mathrm{o}^\mathrm{T}\boldsymbol{P}_\mathrm{o}\boldsymbol{B}\boldsymbol{r}_\mathrm{f}+\left(\boldsymbol{B}\boldsymbol{r}_\mathrm{f}\right)^\mathrm{T}\boldsymbol{P}_\mathrm{o}\boldsymbol{x}_\mathrm{o}\\ &= -\boldsymbol{x}_\mathrm{o}^\mathrm{T}\boldsymbol{Q}_\mathrm{o}\boldsymbol{x}_\mathrm{o}+2\boldsymbol{x}_\mathrm{o}^\mathrm{T}\boldsymbol{P}_\mathrm{o}\boldsymbol{B}\boldsymbol{r}_\mathrm{f}.\end{aligned} \tag{3.107}$$

Clearly it holds

$$\begin{aligned}\dot{V}_\mathrm{a} &\leq -\lambda_{\min}(\boldsymbol{Q}_\mathrm{o})\|\boldsymbol{x}_\mathrm{o}\|^2+2\lambda_{\max}(\boldsymbol{P}_\mathrm{o})\|\boldsymbol{x}_\mathrm{o}\|\|\boldsymbol{B}\|r_{\max}\\ &= -\|\boldsymbol{x}_\mathrm{o}\|\left(\lambda_{\min}(\boldsymbol{Q}_\mathrm{o})\|\boldsymbol{x}_\mathrm{o}\|-2\lambda_{\max}(\boldsymbol{P}_\mathrm{o})\|\boldsymbol{B}\|r_{\max}\right).\end{aligned} \tag{3.108}$$

Then, it follows

$$\dot{V}_\mathrm{a}\leq 0 \quad \text{if} \quad \|\boldsymbol{x}_\mathrm{o}(t)\|\geq\frac{2\lambda_{\max}(\boldsymbol{P}_\mathrm{o})}{\lambda_{\min}(\boldsymbol{Q}_\mathrm{o})}\|\boldsymbol{B}\|r_{\max}, \tag{3.109}$$

where $\lambda_{\min}(\cdot)$ and $\lambda_{\max}(\cdot)$ denote the minimum and the maximum eigenvalue of their arguments, respectively.

From the previous discussion, after (3.95), (3.103), and (3.104) the ultimate bound for $\boldsymbol{x}_\mathrm{o}$ in (3.93) is given by

$$\|\boldsymbol{x}_\mathrm{o}(t)\|\leq\frac{n(p+1)}{|\lambda_{\max}(\boldsymbol{A})|}\|\boldsymbol{B}\|r_{\max}, \quad \text{as} \quad t\to\infty. \tag{3.110}$$

Since $n(p+1)$ is fixed and $|\lambda_{\max}(\boldsymbol{A})|$ can be chosen arbitrarily large, the ultimate bound of $\boldsymbol{x}_\mathrm{o}$ can be made arbitrarily small. Besides, it can be proved that this bound also fulfills [Khalil, 2002]

$$\|\boldsymbol{x}_\mathrm{o}(t)\|\leq\frac{2\lambda_{\max}(\boldsymbol{P}_\mathrm{o})}{\lambda_{\min}(\boldsymbol{Q}_\mathrm{o})}\sqrt{\frac{\lambda_{\max}(\boldsymbol{P}_\mathrm{o})}{\lambda_{\min}(\boldsymbol{P}_\mathrm{o})}}\|\boldsymbol{B}\|r_{\max}. \tag{3.111}$$

Since $\lambda_{\max}(\boldsymbol{P}_\mathrm{o})/\lambda_{\min}(\boldsymbol{P}_\mathrm{o})\geq 1$ and, after (3.110), the norm $\|\boldsymbol{x}_\mathrm{o}(t)\|$ can be made arbitrarily small, then the term $\lambda_{\max}(\boldsymbol{P}_\mathrm{o})/\lambda_{\min}(\boldsymbol{Q}_\mathrm{o})$ can also be made arbitrarily small. Notice that the pair $(\boldsymbol{P}_\mathrm{o},\boldsymbol{Q}_\mathrm{o})$ in not unique, but there must exist a combination that makes (3.110)–(3.111) equivalent. We assume that this is the case.

c) Till now it has been shown that whenever $\boldsymbol{y}_\mathrm{s}\in\mathscr{D}_\mathrm{s}$, every signal of interest is bounded and furthermore, that the observation errors can be made arbitrarily small independently of the rest of the state error. The next step is to show that whenever $\boldsymbol{y}_\mathrm{s}(t_0)$ is small

enough, then it can be enforced for $\boldsymbol{y}_\mathrm{s}$ to remain in $\mathscr{D}_\mathrm{s}$ and that actually $\|\boldsymbol{y}_\mathrm{s}\|$ can be made arbitrarily small, *i.e.,* $\boldsymbol{y}_\mathrm{s}$ is uniform ultimately bounded with ultimate bound arbitrarily small as depicted in Figure 3.3.

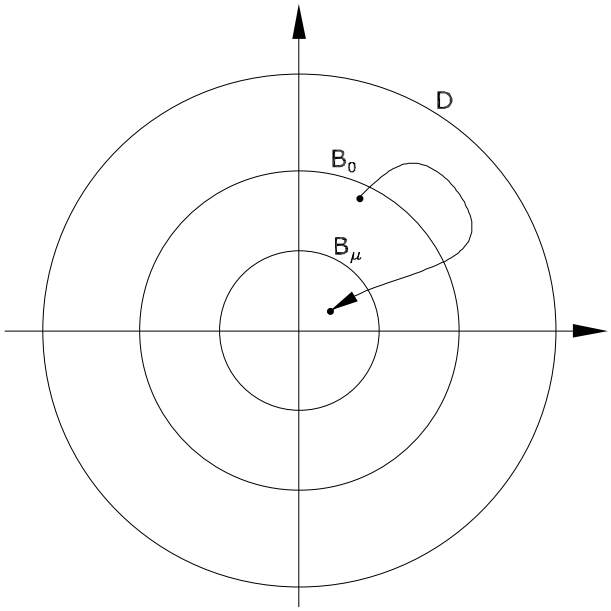

Figure 3.3: Ultimate boundedness of the state $\boldsymbol{y}_\mathrm{s}$.

Let

$$V_\mathrm{s} = \frac{1}{2}\boldsymbol{s}^\mathrm{T}\boldsymbol{H}_\mathrm{s}(\boldsymbol{q})\boldsymbol{s} + \frac{1}{4}\frac{k_\mathrm{Fis}}{k_\mathrm{vs}}(\Delta\bar{F}_\mathrm{s})^2 \tag{3.112}$$

be a positive function of $\boldsymbol{s}$ and $\Delta\bar{F}_\mathrm{s}$. Taking into account Properties 2.1–2.4, (3.51), (3.56), and (3.67), the time derivative of (3.112) along (3.22) and (3.57) is given by

$$\begin{aligned}\dot{V}_\mathrm{s} =& -\boldsymbol{s}^\mathrm{T}\boldsymbol{K}_\mathrm{Dvs}\boldsymbol{s} + \boldsymbol{s}^\mathrm{T}\boldsymbol{y}_\mathrm{a} - \frac{1}{4}k_\mathrm{vs}^{-1}(\Delta\lambda_\mathrm{s})^2\boldsymbol{J}_{\varphi\mathrm{s}}\boldsymbol{J}_{\varphi\mathrm{s}}^\mathrm{T} - \frac{1}{2}\frac{k_\mathrm{Fis}}{k_\mathrm{vs}}\Delta\bar{F}_\mathrm{s}(\boldsymbol{J}_{\varphi\mathrm{s}}^+)^\mathrm{T}\boldsymbol{H}_\mathrm{s}(\boldsymbol{q}_\mathrm{s})\tilde{\boldsymbol{z}}_1 \\ & - \frac{1}{4}\frac{k_\mathrm{Fis}^2}{k_\mathrm{vs}}(\Delta\bar{F}_\mathrm{s})^2(\boldsymbol{J}_{\varphi\mathrm{s}}\boldsymbol{J}_{\varphi\mathrm{s}}^\mathrm{T})^{-1} \\ \leq& -k_\mathrm{vs}\|\boldsymbol{s}\|^2 + c_\mathrm{a}\|\boldsymbol{s}\| + \frac{1}{2}\frac{k_\mathrm{Fis}\lambda_\mathrm{H}c_\varphi^+}{k_\mathrm{vs}}|\Delta\bar{F}_\mathrm{s}|\|\tilde{\boldsymbol{z}}_1\| - \frac{1}{4}\frac{k_\mathrm{Fis}^2c_\varphi^-}{k_\mathrm{vs}}|\Delta\bar{F}_\mathrm{s}|^2,\end{aligned} \tag{3.113}$$

where $c_\varphi^+ \triangleq \|\boldsymbol{J}_{\varphi\mathrm{s}}^+\|_\mathrm{max}$ and $c_\varphi^- \triangleq \inf_{\boldsymbol{q}_\mathrm{s}\in\mathbb{R}^n}\left\{\boldsymbol{J}_{\varphi\mathrm{s}}(\boldsymbol{q}_\mathrm{s})\boldsymbol{J}_{\varphi\mathrm{s}}^\mathrm{T}(\boldsymbol{q}_\mathrm{s})\right\}^{-1}$. Note that, since $\boldsymbol{J}_{\varphi\mathrm{s}}(\boldsymbol{q}_\mathrm{s})$ is full rank for every $\boldsymbol{q}_\mathrm{s}\in\mathbb{R}^n$ and the Jacobian of the manipulator is non–singular and upper bounded, it is $0 < c_\varphi^\pm < \infty$.

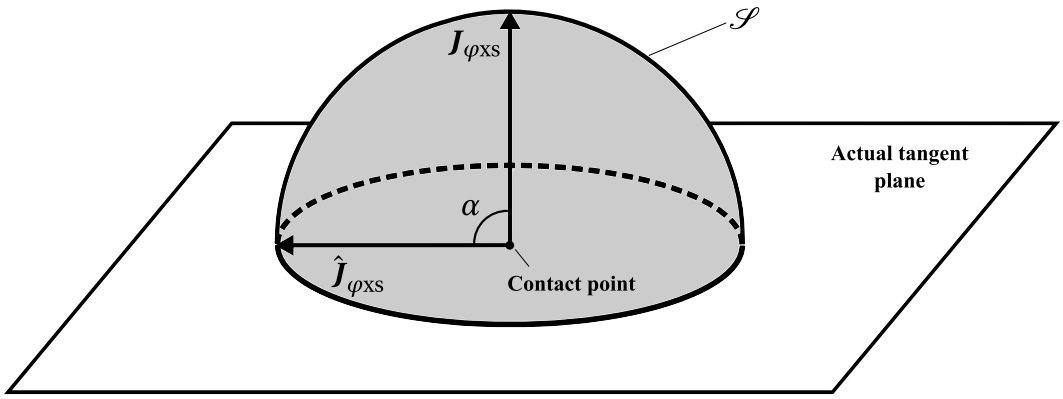

Figure 3.4: Region $\mathscr{S}$

For the surface estimation error dynamics define

$$V_{\varphi \mathrm{xs}} = \frac{1}{2} \tilde{\boldsymbol{J}}_{\varphi \mathrm{xs}} \tilde{\boldsymbol{J}}_{\varphi \mathrm{xs}}^{\mathrm{T}} . \tag{3.114}$$

Its time derivative is given by

$$\dot{V}_{\varphi \mathrm{xs}} = \tilde{\boldsymbol{J}}_{\varphi \mathrm{xs}} \dot{\tilde{\boldsymbol{J}}}_{\varphi \mathrm{xs}}^{\mathrm{T}} = -\tilde{\boldsymbol{J}}_{\varphi \mathrm{xs}} \dot{\hat{\boldsymbol{J}}}_{\varphi \mathrm{xs}}^{\mathrm{T}} + \tilde{\boldsymbol{J}}_{\varphi \mathrm{xs}} \dot{\boldsymbol{J}}_{\varphi \mathrm{xs}}^{\mathrm{T}} . \tag{3.115}$$

After (3.3) and (3.16), and since $\tilde{\boldsymbol{z}}_1 = \boldsymbol{z}_1 - \hat{\boldsymbol{z}}_1$, one obtains

$$\dot{V}_{\varphi \mathrm{xs}} = -\frac{\gamma}{\hat{\lambda}_{\mathrm{s}} + \epsilon} \tilde{\boldsymbol{J}}_{\varphi \mathrm{xs}} \hat{\boldsymbol{Q}}_{\mathrm{xs}} \left(\boldsymbol{J}_{\varphi \mathrm{xs}}^{\mathrm{T}} \lambda_{\mathrm{s}} - \boldsymbol{J}_{\mathrm{s}}^{-\mathrm{T}}(\boldsymbol{q}_{\mathrm{s}}) \boldsymbol{H}_{\mathrm{s}}(\boldsymbol{q}_{\mathrm{s}}) \tilde{\boldsymbol{z}}_1 \right) + \tilde{\boldsymbol{J}}_{\varphi \mathrm{xs}} \dot{\boldsymbol{J}}_{\varphi \mathrm{xs}}^{\mathrm{T}} . \tag{3.116}$$

Hence, because $\hat{\boldsymbol{Q}}_{\mathrm{xs}} \hat{\boldsymbol{J}}_{\varphi \mathrm{xs}}^{\mathrm{T}} = \boldsymbol{O}$ and $\hat{\boldsymbol{Q}}_{\mathrm{xs}} \hat{\boldsymbol{Q}}_{\mathrm{xs}} = \hat{\boldsymbol{Q}}_{\mathrm{xs}} = \hat{\boldsymbol{Q}}_{\mathrm{xs}}^{\mathrm{T}}$, it is

$$\dot{V}_{\varphi \mathrm{xs}} = -\frac{\gamma}{\hat{\lambda}_{\mathrm{s}} + \epsilon} \left(\tilde{\boldsymbol{J}}_{\varphi \mathrm{xs}} \hat{\boldsymbol{Q}}_{\mathrm{xs}}^{\mathrm{T}} \hat{\boldsymbol{Q}}_{\mathrm{xs}} \tilde{\boldsymbol{J}}_{\varphi \mathrm{xs}}^{\mathrm{T}} \lambda_{\mathrm{s}} - \tilde{\boldsymbol{J}}_{\varphi \mathrm{xs}} \hat{\boldsymbol{Q}}_{\mathrm{xs}} \boldsymbol{J}_{\mathrm{s}}^{-\mathrm{T}}(\boldsymbol{q}_{\mathrm{s}}) \boldsymbol{H}_{\mathrm{s}}(\boldsymbol{q}_{\mathrm{s}}) \tilde{\boldsymbol{z}}_1 \right) + \tilde{\boldsymbol{J}}_{\varphi \mathrm{xs}} \dot{\boldsymbol{J}}_{\varphi \mathrm{xs}}^{\mathrm{T}} . \tag{3.117}$$

Since $\boldsymbol{q}_{\mathrm{s}}$ and $\dot{\boldsymbol{q}}_{\mathrm{s}}$ are bounded in $\mathscr{D}_{\mathrm{s}}$ and the surface is assumed to be smooth, there must exist a positive constant, say υ_{x}, such that $\| \dot{\boldsymbol{J}}_{\varphi \mathrm{xs}} \| \leq \upsilon_{\mathrm{x}} < \infty$. Also, consider a closed subset of the workspace of the manipulator centred at $\{ \boldsymbol{x}_{\mathrm{s}} \in \mathbb{R}^n | \tilde{\boldsymbol{J}}_{\varphi \mathrm{xs}}(\boldsymbol{x}_{\mathrm{s}}) = \boldsymbol{0} \}$ and defined by $\mathscr{S} = \{ \boldsymbol{x}_{\mathrm{s}} \in \mathbb{R}^n | \, \| \tilde{\boldsymbol{J}}_{\varphi \mathrm{xs}}(\boldsymbol{x}_{\mathrm{s}}) \| \leq \sqrt{2} \}$, *i.e.,* the region of the workspace where the angle α between the normal to the surface $\boldsymbol{J}_{\varphi \mathrm{xs}}$ and its estimate $\hat{\boldsymbol{J}}_{\varphi \mathrm{xs}}$ is at most 90°, or equivalently $0 \leq \alpha \leq \pi/2$ (see Figure 3.4). Notice that this implies that the region $\mathscr{S}$ must be taken into account at the definition of the region $\mathscr{D}_{\mathrm{s}}$. As can be seen in Figure 3.5, and recalling

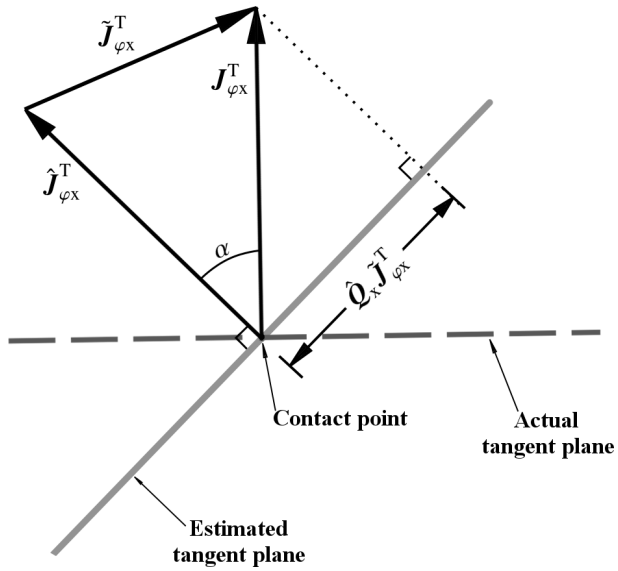

Figure 3.5: Projections

that $\|\hat{\boldsymbol{J}}_{\varphi xs}\| = \|\boldsymbol{J}_{\varphi xs}\| = 1$, from the cosine rule one has (for $\alpha \leq \pi/2$)

$$\|\tilde{\boldsymbol{J}}_{\varphi xs}\|^2 = 2\,(1-\cos(\alpha)) \leq 2\left(1-\cos^2(\alpha)\right) = 2\|\hat{\boldsymbol{Q}}_{xs}\tilde{\boldsymbol{J}}^{T}_{\varphi xs}\|^2\,, \tag{3.118}$$

since from the same figure it can be seen that $\|\hat{\boldsymbol{Q}}_{xs}\tilde{\boldsymbol{J}}^{T}_{\varphi xs}\| = \cos(\pi/2-\alpha) = \sin(\alpha)$. Hence (3.118) implies

$$\|\tilde{\boldsymbol{J}}_{\varphi xs}\| \leq \sqrt{2}\|\hat{\boldsymbol{Q}}_{xs}\tilde{\boldsymbol{J}}^{T}_{\varphi xs}\|\,. \tag{3.119}$$

Moreover, given that the robot always exerts force over the surface, there must exist a constant, say c_λ, such that $\lambda_s \geq c_\lambda > 0, \forall\, t \geq t_0$. Also, since it has been proven that $\hat{\lambda}_s$ is bounded in $\mathscr{D}_s$, after (3.15) there must exist a constant, say $c_{\hat{\lambda}}$, such that $0 \leq \hat{\lambda}_s \leq c_{\hat{\lambda}} < \infty, \forall\, t \geq t_0$. Therefore, (3.117) satisfies

$$\dot{V}_{\varphi xs} \leq -\frac{\gamma c_\lambda}{\hat{\lambda}_s+\epsilon}\|\hat{\boldsymbol{Q}}_{xs}\tilde{\boldsymbol{J}}^{T}_{\varphi xs}\|\left(\|\hat{\boldsymbol{Q}}_{xs}\tilde{\boldsymbol{J}}^{T}_{\varphi xs}\| - \frac{\lambda_H}{c_\lambda}\|\boldsymbol{J}_s^{-T}(\boldsymbol{q}_s)\|\|\tilde{\boldsymbol{z}}_1\| - \frac{c_{\hat{\lambda}}+\epsilon}{\gamma c_\lambda}\sqrt{2}\upsilon_x\right), \tag{3.120}$$

where υ_x is a bound for $\dot{\boldsymbol{J}}_{\varphi xs}$.

In part b) it was stated that by choosing the eigenvalues of $\boldsymbol{A}$ in (3.48) far away on the left in the complex plane, one guarantees that $(\tilde{\boldsymbol{q}}_s,\ldots,\tilde{\boldsymbol{q}}_s^{(p+2)})$ can be made arbitrarily small independently of the values of k_{vs} and k_{Fis} (see Remark 3.4). This implies after (3.44)

that $\boldsymbol{f}_{\mathrm{s}}(t)$, and hence $\tilde{\boldsymbol{z}}_1$ in (3.41), can also be made arbitrarily small, which in turn implies that $(\lambda_{\mathrm{H}}/c_\lambda)\|\boldsymbol{J}_{\mathrm{s}}^{-\mathrm{T}}(\boldsymbol{q}_{\mathrm{s}})\|\|\tilde{\boldsymbol{z}}_1\|$ can be made arbitrarily small as well, since after Assumption 2.1 $\boldsymbol{J}_{\mathrm{s}}^{-1}(\boldsymbol{q}_{\mathrm{s}})$ always exists. Finally, the term $(c_{\hat{\lambda}}+\epsilon)\sqrt{2}v_{\mathrm{x}}/\gamma c_\lambda$ can be made arbitrarily small by setting γ sufficiently large. By defining

$$c_{\mathrm{Q}} \triangleq \frac{\lambda_{\mathrm{H}}}{c_\lambda}\|\boldsymbol{J}_{\mathrm{s}}^{-\mathrm{T}}(\boldsymbol{q}_{\mathrm{s}})\|\|\tilde{\boldsymbol{z}}_1\| + \frac{c_{\hat{\lambda}}+\epsilon}{\gamma c_\lambda}\sqrt{2}v_{\mathrm{x}}, \tag{3.121}$$

one has

$$\|\hat{\boldsymbol{Q}}_{\mathrm{xs}}\tilde{\boldsymbol{J}}_{\varphi\mathrm{xs}}^{\mathrm{T}}\| \geq c_{\mathrm{Q}} \implies \dot{V}_{\varphi\mathrm{xs}} \leq 0\,. \tag{3.122}$$

After (3.114), it can be stated

$$\frac{1}{2}\|\tilde{\boldsymbol{J}}_{\varphi\mathrm{xs}}\|^2 \leq V_{\varphi\mathrm{xs}} \leq \frac{1}{2}\|\tilde{\boldsymbol{J}}_{\varphi\mathrm{xs}}\|^2, \tag{3.123}$$

which means that for $\dot{V}_{\varphi\mathrm{xs}} \leq 0$

$$\|\tilde{\boldsymbol{J}}_{\varphi\mathrm{xs}}(t)\| \leq \|\tilde{\boldsymbol{J}}_{\varphi\mathrm{xs}}(t_0)\|, \quad \forall\, t \geq t_0\,. \tag{3.124}$$

In the extreme case that $\|\hat{\boldsymbol{Q}}_{\mathrm{xs}}\tilde{\boldsymbol{J}}_{\varphi\mathrm{xs}}\| \equiv c_{\mathrm{Q}}$, after (3.119), the ultimate bound for $\|\tilde{\boldsymbol{J}}_{\varphi\mathrm{xs}}\|$ is given by

$$\|\tilde{\boldsymbol{J}}_{\varphi\mathrm{xs}}\| \leq \sqrt{2}c_{\mathrm{Q}}\,. \tag{3.125}$$

Furthermore, the smaller $\|\hat{\boldsymbol{Q}}_{\mathrm{xs}}\tilde{\boldsymbol{J}}_{\varphi\mathrm{xs}}^{\mathrm{T}}\|$, the smaller $\|\tilde{\boldsymbol{J}}_{\varphi\mathrm{xs}}\|$.

By adding the functions defined in (3.105), (3.112) and (3.114) it is obtained the positive definite function

$$\begin{aligned} V = V_{\mathrm{a}} + V_{\mathrm{s}} + V_{\varphi\mathrm{xs}} &= \boldsymbol{x}_{\mathrm{o}}^{\mathrm{T}}\boldsymbol{P}_{\mathrm{o}}\boldsymbol{x}_{\mathrm{o}} + \frac{1}{2}\boldsymbol{s}^{\mathrm{T}}\boldsymbol{H}_{\mathrm{s}}(\boldsymbol{q})\boldsymbol{s} + \frac{1}{4}\frac{k_{\mathrm{Fis}}}{k_{\mathrm{vs}}}(\Delta\bar{F}_{\mathrm{s}})^2 + \frac{1}{2}\tilde{\boldsymbol{J}}_{\varphi\mathrm{xs}}\tilde{\boldsymbol{J}}_{\varphi\mathrm{xs}}^{\mathrm{T}} \\ &= \boldsymbol{y}_{\mathrm{s}}^{\mathrm{T}}\begin{bmatrix} \boldsymbol{P}_{\mathrm{o}} & \boldsymbol{O} & \boldsymbol{O} & \boldsymbol{O} \\ \boldsymbol{O} & \frac{1}{2}\boldsymbol{H}_{\mathrm{s}}(\boldsymbol{q}_{\mathrm{s}}) & \boldsymbol{O} & \boldsymbol{O} \\ \boldsymbol{O} & \boldsymbol{O} & \frac{1}{4}k_{\mathrm{Fis}}/k_{\mathrm{vs}} & \boldsymbol{O} \\ \boldsymbol{O} & \boldsymbol{O} & \boldsymbol{O} & \frac{1}{2}\boldsymbol{I} \end{bmatrix}\boldsymbol{y}_{\mathrm{s}} = \boldsymbol{y}_{\mathrm{s}}^{\mathrm{T}}\boldsymbol{M}_{\mathrm{s}}(\boldsymbol{q}_{\mathrm{s}})\boldsymbol{y}_{\mathrm{s}}\,, \end{aligned} \tag{3.126}$$

where each $\boldsymbol{O}$ is a matrix or vector of zeros of appropriate dimensions. Given Property 2.2, we can find two positive constants, λ_{m} and λ_{M}, such that

$$\lambda_{\mathrm{m}}\|\boldsymbol{y}_{\mathrm{s}}\|^2 \leq V(\boldsymbol{y}_{\mathrm{s}}) \leq \lambda_{\mathrm{M}}\|\boldsymbol{y}_{\mathrm{s}}\|^2\,. \tag{3.127}$$

After (3.108), (3.113) and (3.120), the time derivative of (3.126) along the trajectories of the system fulfills

$$\begin{aligned}\dot{V} \leq & -\lambda_{\min}(\boldsymbol{Q}_{\mathrm{o}})\|\boldsymbol{x}_{\mathrm{o}}\|\left(\|\boldsymbol{x}_{\mathrm{o}}\|-\frac{2\lambda_{\max}(\boldsymbol{P}_{\mathrm{o}})\|\boldsymbol{B}\|r_{\max}}{\lambda_{\min}(\boldsymbol{Q}_{\mathrm{o}})}\right)-k_{\mathrm{vs}}\|\boldsymbol{s}\|\left(\|\boldsymbol{s}\|-\frac{c_{\mathrm{a}}}{k_{\mathrm{vs}}}\right)\\ & -\frac{1}{4}\frac{k_{\mathrm{Fis}}^2 c_{\varphi}^{-}}{k_{\mathrm{vs}}}|\Delta\bar{F}_{\mathrm{s}}|\left(|\Delta\bar{F}_{\mathrm{s}}|-\frac{2\lambda_{\mathrm{H}}c_{\varphi}^{+}}{k_{\mathrm{Fis}}c_{\varphi}^{-}}\|\tilde{\boldsymbol{z}}_1\|\right)\\ & -\frac{\gamma c_{\lambda}}{\hat{\lambda}_{\mathrm{s}}+\epsilon}\|\hat{\boldsymbol{Q}}_{\mathrm{xs}}\tilde{\boldsymbol{J}}_{\varphi\mathrm{xs}}^{\mathrm{T}}\|\left(\|\hat{\boldsymbol{Q}}_{\mathrm{xs}}\tilde{\boldsymbol{J}}_{\varphi\mathrm{xs}}^{\mathrm{T}}\|-\frac{\lambda_{\mathrm{H}}}{c_{\lambda}}\|\boldsymbol{J}_{\mathrm{s}}^{-\mathrm{T}}(\boldsymbol{q}_{\mathrm{s}})\|\|\tilde{\boldsymbol{z}}_1\|-\frac{c_{\hat{\lambda}}+\epsilon}{\gamma c_{\lambda}}\sqrt{2}v_{\mathrm{x}}\right).\end{aligned} \tag{3.128}$$

According to the previous discussion, the terms

$$\frac{2\lambda_{\max}(\boldsymbol{P}_{\mathrm{o}})\|\boldsymbol{B}\|r_{\max}}{\lambda_{\min}(\boldsymbol{Q}_{\mathrm{o}})},\ \frac{c_{\mathrm{a}}}{k_{\mathrm{vs}}},\ \frac{2\lambda_{\mathrm{H}}c_{\varphi}^{+}}{k_{\mathrm{Fis}}c_{\varphi}^{-}}\|\tilde{\boldsymbol{z}}_1\|,\ \frac{\lambda_{\mathrm{H}}}{c_{\lambda}}\|\boldsymbol{J}_{\mathrm{s}}^{-\mathrm{T}}(\boldsymbol{q}_{\mathrm{s}})\|\|\tilde{\boldsymbol{z}}_1\|,\ \text{and}\ \frac{c_{\hat{\lambda}}+\epsilon}{\gamma c_{\lambda}}\sqrt{2}v_{\mathrm{x}}$$

can be made arbitrarily small in $\mathscr{D}_{\mathrm{s}}$ by choosing the eigenvalues of $\boldsymbol{A}$ in (3.48) far away on the left in the complex plane and the gains k_{vs}, k_{Fis}, and γ large enough.

Overall, we can always find a positive arbitrarily small constant μ such that

$$\dot{V} \leq 0 \quad \text{if} \quad \|\boldsymbol{y}_{\mathrm{s}}\| \geq \mu. \tag{3.129}$$

Once $\|\boldsymbol{y}_{\mathrm{s}}\| = \mu$, from (3.127) the maximum value that $\|\boldsymbol{y}_{\mathrm{s}}\|$ can take is given by

$$\lambda_{\mathrm{m}}\|\boldsymbol{y}_{\mathrm{s}}\|^2 \leq V(\boldsymbol{y}_{\mathrm{s}}) \leq \lambda_{\mathrm{M}}\mu^2 \implies \|\boldsymbol{y}_{\mathrm{s}}\| \leq \sqrt{\frac{\lambda_{\mathrm{M}}}{\lambda_{\mathrm{m}}}}\mu \triangleq b, \tag{3.130}$$

where b is the ultimate bound of the state $\boldsymbol{y}_{\mathrm{s}}$. Recall that it must be guaranteed that $\|\boldsymbol{y}_{\mathrm{s}}\| \leq y_{\max}$, $\forall\, t \geq t_0$. This can be done by setting gains large enough to satisfy

$$\mu < \sqrt{\frac{\lambda_{\mathrm{m}}}{\lambda_{\mathrm{M}}}}y_{\max}. \tag{3.131}$$

Also, the initial condition must satisfy

$$\|\boldsymbol{y}_{\mathrm{s}}(t_0)\| < \sqrt{\frac{\lambda_{\mathrm{m}}}{\lambda_{\mathrm{M}}}}y_{\max} \tag{3.132}$$

to guarantee that $\boldsymbol{y}_{\mathrm{s}}$ never leaves the region $\mathscr{D}_{\mathrm{s}}$.

d) Finally, since b can be made arbitrarily small, then $\|\boldsymbol{y}_{\mathrm{s}}\|$ can be made arbitrarily close to zero. This implies the that observation errors $\tilde{\boldsymbol{q}}_{\mathrm{s}},\ldots,\tilde{\boldsymbol{q}}_{\mathrm{s}}^{(p+2)}$ are made approximately zero. Therefore, after (3.36), $\tilde{\boldsymbol{q}}_{\mathrm{s}2}\approx\boldsymbol{0}\implies\boldsymbol{q}_{\mathrm{s}2}\approx\hat{\boldsymbol{q}}_{\mathrm{s}2}$, *i.e.,* $\hat{\boldsymbol{q}}_{\mathrm{s}2}$ is an arbitrarily close estimation of the vector of joint velocities $\boldsymbol{q}_{\mathrm{s}2}$. Also, we have proved that $\tilde{\boldsymbol{z}}_1\approx\boldsymbol{0}$, which after (3.3) and (3.15) means that $\lambda_{\mathrm{s}}-\hat{\lambda}_{\mathrm{s}}\approx 0\implies\hat{\lambda}_{\mathrm{s}}\approx\lambda_{\mathrm{s}}$ for $\lambda_{\mathrm{s}}>0$, which implies arbitrary close estimation of the contact force. Since the ultimate bound of $\|\boldsymbol{y}_{\mathrm{s}}\|$, and therefore of $\|\boldsymbol{s}\|$ and $\|\Delta\bar{F}_{\mathrm{s}}\|$, can be made arbitrarily small, from (3.56) one can see that the ultimate bound of $\Delta\lambda_{\mathrm{s}}$ must be arbitrarily small as well, implying that force tracking is achieved.

□

Now, the main result of this work is presented, which is focused on the ultimate boundedness of the state and the transparency of the teleoperation system.

Theorem 3.2. *Let the master–slave teleoperation system described by (2.2)–(2.3) be in closed loop with the force and velocity observers (3.8)–(3.12) and (3.15), the surface estimator (3.16), and let the behavior of the human operator be described as in Assumption 3.4. Then, the system error dynamics is completely characterized by (3.21)–(3.22), (3.32)–(3.33), (3.46), (3.57), (3.60), and (3.64). Let*

$$\boldsymbol{y}\triangleq\begin{bmatrix}\boldsymbol{x}_{\mathrm{o}} & \boldsymbol{s} & \Delta\bar{F}_{\mathrm{s}} & \tilde{\boldsymbol{J}}_{\varphi\mathrm{xs}} & \Delta F_{\mathrm{vd}}\end{bmatrix}^{\mathrm{T}}, \tag{3.133}$$

and define a region $\mathscr{D}\triangleq\{\boldsymbol{y}\in\mathbb{R}^{(p+2)n+5}\,|\,\|\boldsymbol{y}\|\leq y_{\max}\}$ *where* $y_{\max}$ *is a positive constant small enough for Fact 2.1 to hold, i.e.,*

$$\boldsymbol{e}_{\mathrm{s}}=\boldsymbol{Q}_{\mathrm{s}}\boldsymbol{e}_{\mathrm{s}}\quad\texttt{and}\quad\dot{\boldsymbol{e}}_{\mathrm{s}}=\boldsymbol{Q}_{\mathrm{s}}\dot{\boldsymbol{e}}_{\mathrm{s}}\,. \tag{3.134}$$

Assume that the slave manipulator never losses contact with the environment. Furthermore, assume that the desired position for the master manipulator $\boldsymbol{q}_{\mathrm{md}}(t)$*, planned by the operator, is such that the approximations (analogous to Fact 2.1)*

$$\hat{\boldsymbol{Q}}_{\mathrm{v}}\boldsymbol{e}_{\mathrm{m}}\approx\boldsymbol{e}_{\mathrm{m}} \tag{3.135}$$

$$\hat{\boldsymbol{Q}}_{\mathrm{v}}\dot{\boldsymbol{e}}_{\mathrm{m}}\approx\dot{\boldsymbol{e}}_{\mathrm{m}} \tag{3.136}$$

hold. Then, a set of controller gains $\boldsymbol{K}_{\mathrm{ps}}$*,* $\boldsymbol{K}_{\mathrm{vs}}$*,* $\boldsymbol{K}_{\mathrm{is}}$ *and* k_{Fis} *in (3.20),* k_{Fv} *and* k_{Fiv} *in (3.28),* γ *in (3.16), and a set of observer gains* $\boldsymbol{\lambda}_0,\ldots,\boldsymbol{\lambda}_{p+1}$ *in (3.48) can be found to achieve:* (i) *position and velocity tracking at the master side,* (ii) *ultimate boundedness of* $\boldsymbol{y}$*, with arbitrary small ultimate bound, and* (iii) *transparency of the teleoperation system.* □

Proof. (i) For simplicity's sake let $\boldsymbol{K}_{\text{vh}} = k_{\text{vh}}\boldsymbol{I}_{n\times n}$ and $\boldsymbol{K}_{\text{ih}} = k_{\text{ih}}\boldsymbol{I}_{n\times n}$. Define $\boldsymbol{e}_{\text{Im}} \triangleq \int_{t_0}^{t} \boldsymbol{e}_{\text{m}}\,\mathrm{d}\vartheta$ and let

$$V_{\text{m}} = \frac{1}{2}k_{\text{vh}}\boldsymbol{e}_{\text{m}}^{\text{T}}\boldsymbol{e}_{\text{m}} + \frac{1}{2}k_{\text{ih}}\boldsymbol{e}_{\text{Im}}^{\text{T}}\boldsymbol{e}_{\text{Im}}\,. \tag{3.137}$$

By taking into account (3.135)–(3.136), the time derivative of (3.137) along (3.66) is given by

$$\dot{V}_{\text{m}} = -\boldsymbol{e}_{\text{m}}^{\text{T}}\boldsymbol{K}_{\text{ph}}\boldsymbol{e}_{\text{m}} \leq 0\,. \tag{3.138}$$

From LaSalle's theorem if $\dot{V}_{\text{m}} \equiv 0 \implies \boldsymbol{e}_{\text{m}} \equiv \boldsymbol{0} \implies \dot{\boldsymbol{e}}_{\text{m}} \equiv \boldsymbol{0}$ then the trajectories of (3.66) tend asymptotically to the set $(\dot{\boldsymbol{e}}_{\text{m}}, \boldsymbol{e}_{\text{m}}, \hat{\boldsymbol{Q}}_{\text{v}}\boldsymbol{e}_{\text{Im}}) = (\boldsymbol{0}, \boldsymbol{0}, \boldsymbol{0})$

Remark 3.5. It is important to point out that the dynamics described in (3.66) is actually independent of the rest of the system, because whether the estimate of $\hat{\boldsymbol{Q}}_{\text{v}}$ is accurate or not, the master controller will create that surface and reflect it to the operator. □

(ii) Notice that all the premises of Theorem 3.1 are satisfied, since $\boldsymbol{y}_{\text{s}}$ in (3.67) is a subset of $\boldsymbol{y}$ in (3.133) and then it must be bounded in $\mathscr{D}$. Nevertheless, some slight modifications must be done to extend the proof of Theorem 3.1 for the state $\boldsymbol{y}$ defined in (3.133).

First, in part a) of the proof of Theorem 3.1 it is shown that all signals of interest are bounded in $\mathscr{D}$. Trivially ΔF_{vd} is bounded in $\mathscr{D}$ and, under the arguments of the original proof, $\Delta\bar{\lambda}_{\text{s}}$ and $\Delta\bar{F}_{\text{s}}$ are also bounded, so that after (3.65), $\Delta\lambda_{\text{vd}}$ must be bounded as well. Second, in part c) of the proof of Theorem 3.1 it is proposed the positive definite function

$$V = \boldsymbol{x}_{\text{o}}^{\text{T}}\boldsymbol{P}_{\text{o}}\boldsymbol{x}_{\text{o}} + \frac{1}{2}\boldsymbol{s}^{\text{T}}\boldsymbol{H}_{\text{s}}(\boldsymbol{q})\boldsymbol{s} + \frac{1}{4}\frac{k_{\text{Fis}}}{k_{\text{vs}}}(\Delta\bar{F}_{\text{s}})^2 + \frac{1}{2}\tilde{\boldsymbol{J}}_{\varphi\text{xs}}\tilde{\boldsymbol{J}}_{\varphi\text{xs}}^{\text{T}}\,, \tag{3.139}$$

with $\boldsymbol{P}_{\text{o}} = \boldsymbol{P}_{\text{o}}^{\text{T}} > \boldsymbol{O}$ the solution of

$$\boldsymbol{A}^{\text{T}}\boldsymbol{P}_{\text{o}} + \boldsymbol{P}_{\text{o}}\boldsymbol{A} = -\boldsymbol{Q}_{\text{o}}\,, \tag{3.140}$$

and where $\boldsymbol{Q}_{\text{o}}$ is a positive definite matrix and $\boldsymbol{A}$ is given by (3.48). To include the state ΔF_{vd}, it is proposed

$$V_{\text{F}} = \frac{1}{2}\frac{k_{\text{Fv}} + k_{\text{Fh}}}{k_{\text{Fiv}} + k_{\text{Fih}}}(\Delta F_{\text{vd}})^2\,, \tag{3.141}$$

whose time derivative along (3.65) is given by

$$\dot{V}_{\mathrm{F}} = -\left(\Delta F_{\mathrm{vd}}\right)^2 + \left(\Delta F_{\mathrm{vd}}\right) \frac{k_{\mathrm{Fv}} \Delta \bar{\lambda}_{\mathrm{s}} + k_{\mathrm{Fiv}} \Delta \bar{F}_{\mathrm{s}}}{k_{\mathrm{Fiv}} + k_{\mathrm{Fih}}} \tag{3.142}$$

$$\leq -|\Delta F_{\mathrm{vd}}| \left(|\Delta F_{\mathrm{vd}}| - \frac{|k_{\mathrm{Fv}} \Delta \bar{\lambda}_{\mathrm{s}} + k_{\mathrm{Fiv}} \Delta \bar{F}_{\mathrm{s}}|}{k_{\mathrm{Fiv}} + k_{\mathrm{Fih}}} \right). \tag{3.143}$$

By setting k_{Fiv} sufficiently large, the term $(|k_{\mathrm{Fv}} \Delta \bar{\lambda}_{\mathrm{s}} + k_{\mathrm{Fiv}} \Delta \bar{F}_{\mathrm{s}}|)/(k_{\mathrm{Fiv}} + k_{\mathrm{Fih}})$ in (3.143) can be made arbitrarily small in $\mathscr{D}$. On the other hand, by adding the functions (3.139) and (3.141) one obtains

$$V_{\mathrm{T}} = V + V_{\mathrm{F}} = \boldsymbol{y}^{\mathrm{T}} \begin{bmatrix} \boldsymbol{P}_{\mathrm{o}} & \boldsymbol{O} & \boldsymbol{O} & \boldsymbol{O} & \boldsymbol{O} \\ \boldsymbol{O} & \frac{1}{2}\boldsymbol{H}_{\mathrm{s}}(\boldsymbol{q}_{\mathrm{s}}) & \boldsymbol{O} & \boldsymbol{O} & \boldsymbol{O} \\ \boldsymbol{O} & \boldsymbol{O} & \frac{1}{4} k_{\mathrm{Fis}} / k_{\mathrm{vs}} & \boldsymbol{O} & \boldsymbol{O} \\ \boldsymbol{O} & \boldsymbol{O} & \boldsymbol{O} & \frac{1}{2}\boldsymbol{I} & \boldsymbol{O} \\ \boldsymbol{O} & \boldsymbol{O} & \boldsymbol{O} & \boldsymbol{O} & \frac{1}{2} k_{\mathrm{FT}} \end{bmatrix} \boldsymbol{y} = \boldsymbol{y}^{\mathrm{T}} \boldsymbol{M}(\boldsymbol{q}_{\mathrm{s}}) \boldsymbol{y}, \tag{3.144}$$

where $k_{\mathrm{FT}} = (k_{\mathrm{Fv}} + k_{\mathrm{Fh}})/(k_{\mathrm{Fiv}} + k_{\mathrm{Fih}})$. After Property 2.2, one can find two positive constants, λ_{mT} and λ_{MT}, such that

$$\lambda_{\mathrm{mT}} \|\boldsymbol{y}\|^2 \leq V_{\mathrm{T}}(\boldsymbol{y}) \leq \lambda_{\mathrm{MT}} \|\boldsymbol{y}\|^2. \tag{3.145}$$

Accordingly with the above discussion and from the proof of Theorem 3.1, an arbitrarily small positive constant μ_{T} can always be found, such that

$$\dot{V}_{\mathrm{T}} \leq 0 \quad \text{if} \quad \|\boldsymbol{y}\| \geq \mu_{\mathrm{T}}. \tag{3.146}$$

Once $\|\boldsymbol{y}\| = \mu_{\mathrm{T}}$, from (3.145) the maximum value that $\|\boldsymbol{y}\|$ can take is given by

$$\lambda_{\mathrm{m_T}} \|\boldsymbol{y}\|^2 \leq V_{\mathrm{T}}(\boldsymbol{y}) \leq \lambda_{\mathrm{M_T}} \mu_{\mathrm{T}}^2 \implies \|\boldsymbol{y}\| \leq \sqrt{\frac{\lambda_{\mathrm{M_T}}}{\lambda_{\mathrm{m_T}}}} \mu_{\mathrm{T}} \triangleq b_{\mathrm{T}}, \tag{3.147}$$

where $\lambda_{\mathrm{m_T}}, \lambda_{\mathrm{M_T}} > 0$ and b_{T} is the ultimate bound of the state $\boldsymbol{y}$, that can be made arbitrarily small by an appropriate selection of the controller and observer gains. Recall that it must be guaranteed that $\|\boldsymbol{y}\| \leq y_{\max}$, $\forall t \geq t_0$. This can be done by setting gains large enough to satisfy

$$\mu_{\mathrm{T}} < \sqrt{\frac{\lambda_{\mathrm{m_T}}}{\lambda_{\mathrm{M_T}}}} y_{\max}. \tag{3.148}$$

Also, the initial condition must satisfy

$$\|\boldsymbol{y}(t_0)\| < \sqrt{\frac{\lambda_{\mathrm{m_T}}}{\lambda_{\mathrm{M_T}}}}\, y_{\max} \tag{3.149}$$

to guarantee that $\boldsymbol{y}$ never leaves the region $\mathscr{D}$.

(iii) For simplicity's sake assume that there is no escalation in the force reflected to the operator. In this case, the transparency is achieved if $\lambda_{\mathrm{v}} = \lambda_{\mathrm{s}}$. Notice that after (3.32)–(3.33) and the above discussion, (3.65) represents a stable filter with an arbitrarily small input. This implies, after (3.62)–(3.63) that

$$(\Delta\bar{\lambda}_{\mathrm{s}}, \Delta\bar{F}_{\mathrm{s}}) \approx (0,0) \implies (\Delta\lambda_{\mathrm{vd}}, \Delta F_{\mathrm{vd}}) \approx 0 \implies \lambda_{\mathrm{sd}} \approx \lambda_{\mathrm{v}} \approx \lambda_{\mathrm{s}} \approx \hat{\lambda}_{\mathrm{s}}, \text{ as } t \to \infty, \tag{3.150}$$

which establishes the convergence of the observer, the force tracking, and the transparency of the teleoperation system. □

Chapter 4

Simulations and Experimental Results

In this chapter, a validation of the controller–observer scheme presented in Chapter 3 is carried out through numerical simulations and experiments. The simulation results are presented to illustrate basically two points in contrast with the experiments. The first point is the convergence of the force estimation to the measured signal. Due to hardware limitations, it was not possible to measure the real force in the experimental bed, so the validation of the convergence of the observer is validated only in the simulations. The second point is to illustrate the performance of the approach in an ideal scenario, in contrast with the experimental results where disturbances, modeling uncertainties, and unmodeled dynamics are unavoidable.

4.1 Simulation Results

A numerical simulation consisting in two full–actuated revolute manipulators with two joints in planar movement was carried out. The parameters for both robots are: mass of the links $m_1 = 3.9473[\text{Kg}]$, $m_2 = 0.6232[\text{Kg}]$, length of the links $l_1 = l_2 = 0.38[\text{m}]$, and viscous friction coefficients $d_1 = d_2 = 1.2[\text{Kg}\cdot\text{m/sec}]$. The (assumed unknown) surface is a segment of a circle described by

$$\varphi_{\text{s}}(\boldsymbol{x}_{\text{s}}) = (x-h)^2 + (y-k)^2 - r^2 = 0\,, \tag{4.1}$$

where (x, y) stands for the slave task–space coordinates, *i.e.*, $\boldsymbol{x}_{\text{s}} = \begin{bmatrix} x & y \end{bmatrix}^{\text{T}}$, $r = 0.1[\text{m}]$ is the radius, and $(h, k) = (0.4, 0)[\text{m}]$ are the coordinates of the centre of the circle. At the beginning of the task the tip of the slave manipulator is in contact with the surface and the Cartesian position of both manipulators coincide, but the initial condition for the gradient estimator (3.16) is set with an initial error (see Figure 4.8).

The task consisted in following a trajectory from the point $(x, y) = (0.32, 0.06)$[m] to the point $(x, y) = (0.48, 0.06)$[m] over the surface in a time $t_f = 10$[sec], while simultaneously it is desired to track a force signal given by

$$\lambda_{sd}(t) = \begin{cases} 20 + 40\,(\cos(0.8\pi\, t/\, t_f)\sin(1.6\pi\, t/\, t_f))\ [\mathrm{N}] & \text{if } t \le t_f \\ 20 + 40\,(\cos(0.8\pi)\sin(1.6\pi))\ [\mathrm{N}] & \text{if } t > t_f. \end{cases} \tag{4.2}$$

The controller gains for the slave control law (3.20) are $\boldsymbol{K}_{ps} = \mathrm{diag}(2000, 2000)$, $\boldsymbol{K}_{vs} = \mathrm{diag}(10, 10)$, $\boldsymbol{K}_{is} = \mathrm{diag}(1000, 1000)$, and $k_{Fis} = 0.5$. For the master control law (3.28) the gains are $k_{Fv} = 0.1$ and $k_{Fiv} = 0.1$. The proposed gains for the human behaviour given by Assumption 3.4 are $\boldsymbol{K}_{ph} = \mathrm{diag}(100, 100)$, $\boldsymbol{K}_{vh} = \mathrm{diag}(1, 1)$, $\boldsymbol{K}_{ih} = \mathrm{diag}(0.1, 0.1)$, $k_{Fh} = 0.01$, and $k_{Fih} = 0.1$. For the observer (3.8)–(3.12) it was set $p = 2$, with observer gains $\lambda_0 = 2.56 \times 10^6 \boldsymbol{I}$, $\lambda_1 = 2.56 \times 10^5 \boldsymbol{I}$, $\lambda_2 = 9600\boldsymbol{I}$, and $\lambda_0 = 160\boldsymbol{I}$, *i.e.,* the observer poles were located at $p_{o1} = p_{o2} = p_{o3} = p_{o4} = -40$. For the surface estimator (3.16) there were chosen $\gamma = 10$ and $\epsilon = 0.0001$. Also, it was set $\eta = 500$ in (3.24). Finally, for the Lagrange multiplier computation in (3.27) there were set $\alpha_v = 1$, $\xi = 0.1$, and $\omega_n = 200$.

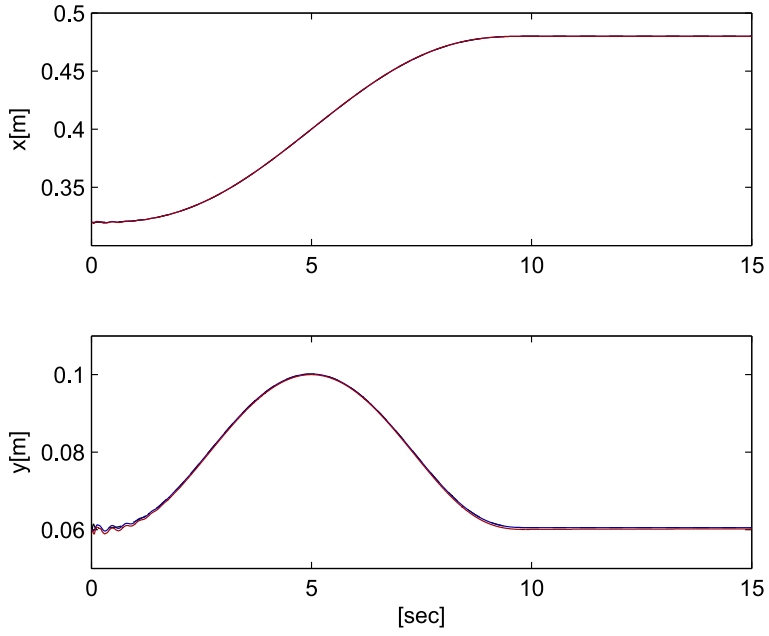

Figure 4.1: Simulation, position tracking in Cartesian coordinates: desired (- - -), master (—), slave (—).

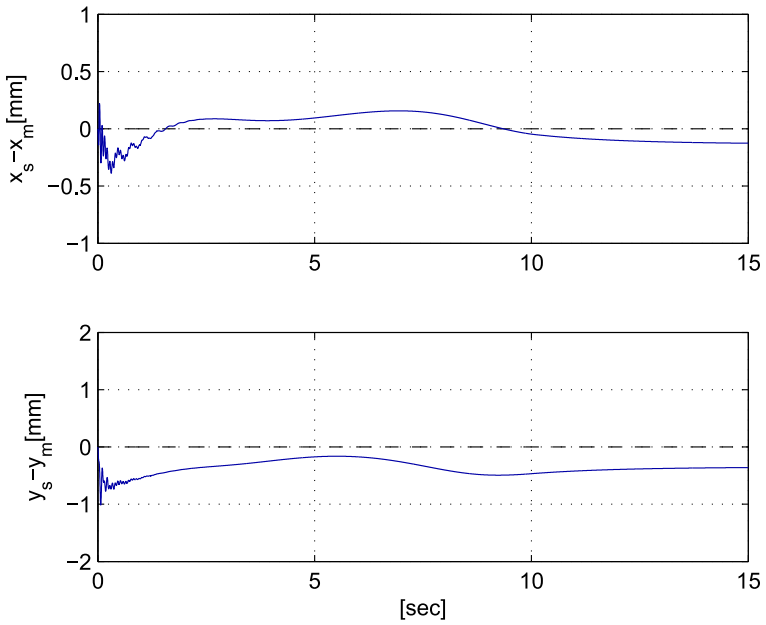

Figure 4.2: Simulation, position tracking error.

Figure 4.1 shows the position tracking in Cartesian coordinates, while in Figure 4.2 the tracking error, $\boldsymbol{x}_{\mathrm{s}} - \boldsymbol{x}_{\mathrm{m}}$, is presented. In these figures the ultimate boundedness of the position error, guaranteed by the proposed scheme, can be appreciated. In Figure 4.3 it is shown the position tracking in the xy plane.

The force tracking of the signal (4.2) is presented in Figure 4.4, while the force tracking error and the force estimation error are shown in Figures 4.5 and 4.6, respectively. In these figures, it can be noticed the convergence of all force signals after the transient response.

Figure 4.7 shows the estimation of the components of the surface gradient vector, while a zoom in the axis time of the first second is presented in Figure 4.8. Finally, the estimated joint velocity and the real one are shown in Figure 4.9.

The simulation results clearly show that there is an ultimate bounded error for both position and force tracking of the teleoperation scheme. The ultimate bound can be made arbitrarily small by using high–gain. Nevertheless, the observer and controller gains are limited by the bandwidth of the system and the measurement noise. In this particular case, the main limitation is the sample period for the implemented control loop, which was considered to be $T = 2$[msec]. Another inconvenience of using high–gain is the so called *peaking* phenomena, which can be appreciated at the beginning of the transient response.

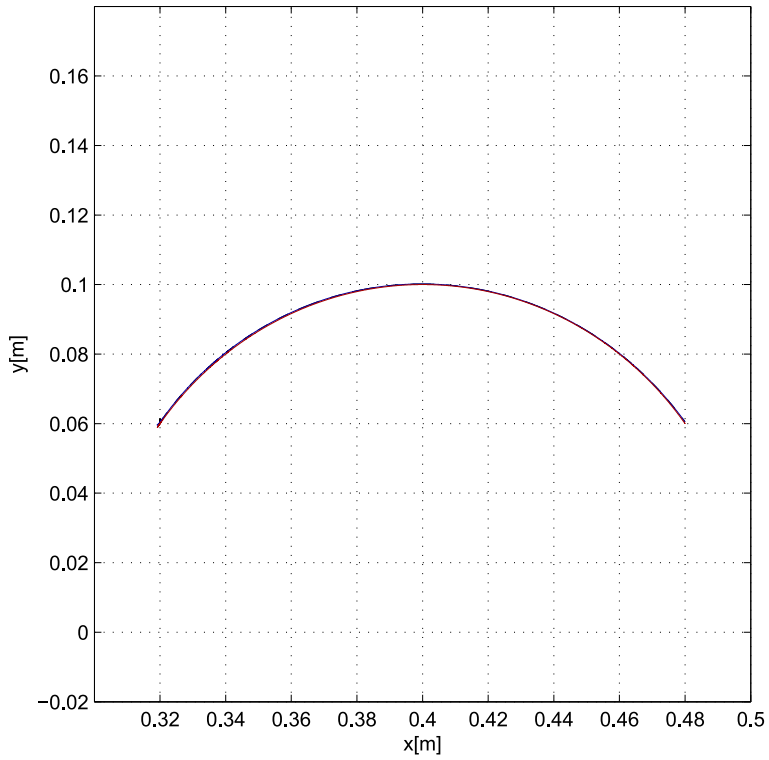

Figure 4.3: Simulation, position tracking in the xy plane.

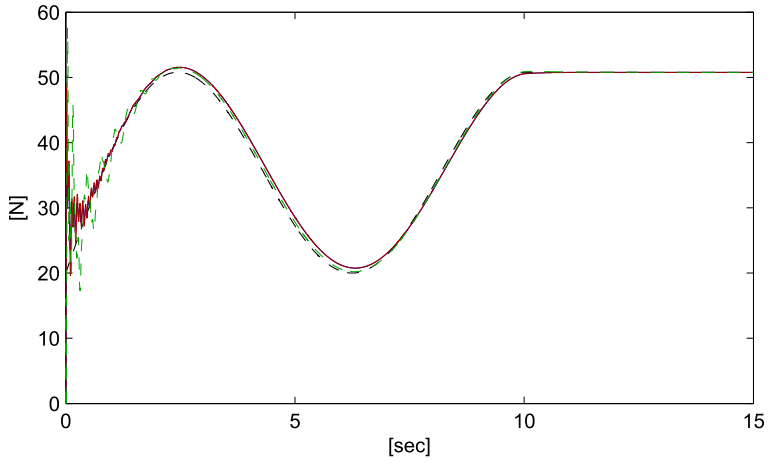

Figure 4.4: Simulation, force tracking and estimation: desired (- - -), real(—), estimated(—), virtual(- - -).

On the other hand, in Figure 4.4 it can be seen that $\lambda_s \approx \lambda_v \approx \lambda_{sd}$, what shows the transparency of the system. Furthermore, in Figures 4.7 and 4.8 it is shown that the gradient of the surface can be online estimated without force nor velocity measurements at the slave side.

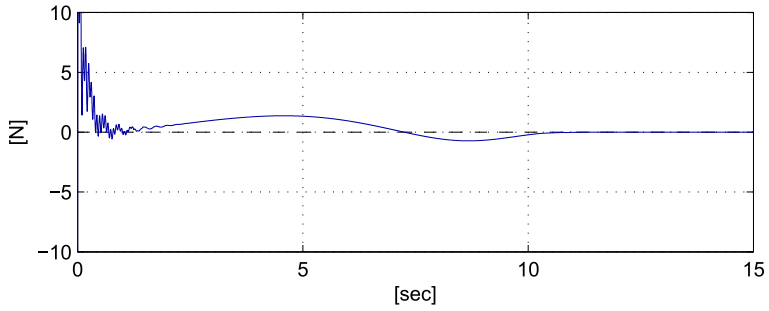

Figure 4.5: Simulation, force tracking error.

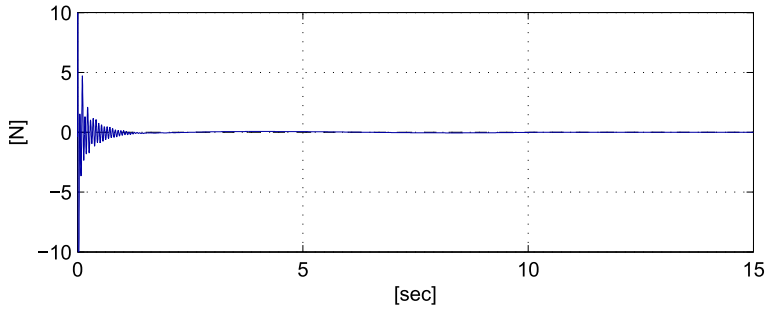

Figure 4.6: Simulation, force estimation error.

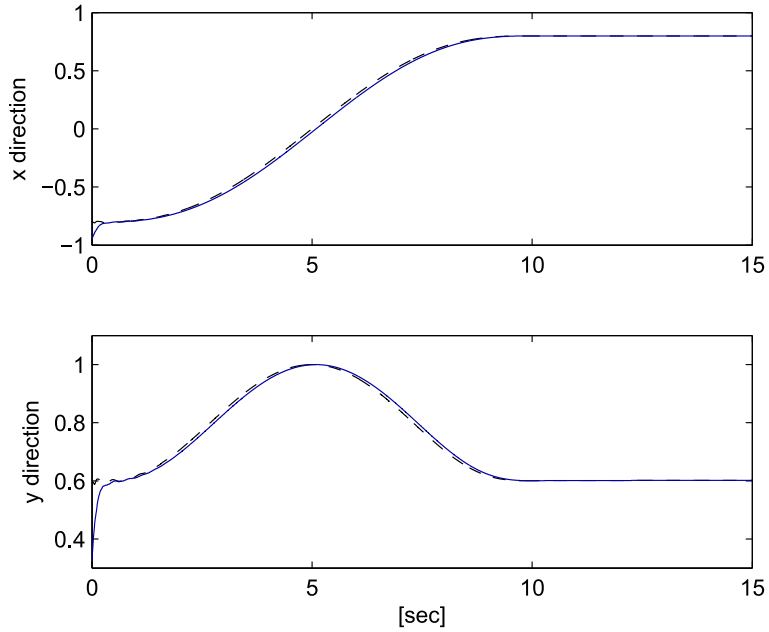

Figure 4.7: Simulation, estimation of the surface gradient: $\boldsymbol{J}_{\varphi \mathrm{xs}}$ (- - -), $\hat{\boldsymbol{J}}_{\varphi \mathrm{xs}}$ (—).

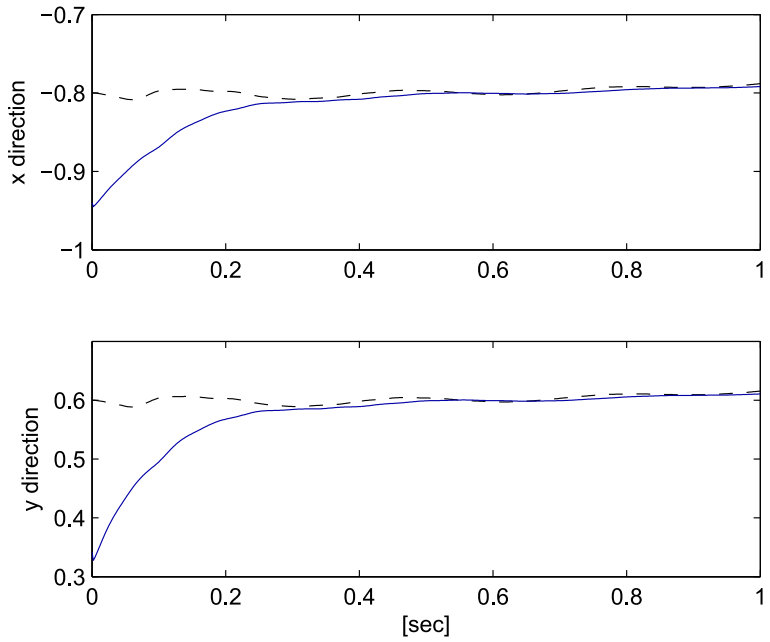

Figure 4.8: Simulation, zoom of Figure 4.7: $\boldsymbol{J}_{\varphi \mathrm{xs}}$ (- - -), $\hat{\boldsymbol{J}}_{\varphi \mathrm{xs}}$ (—).

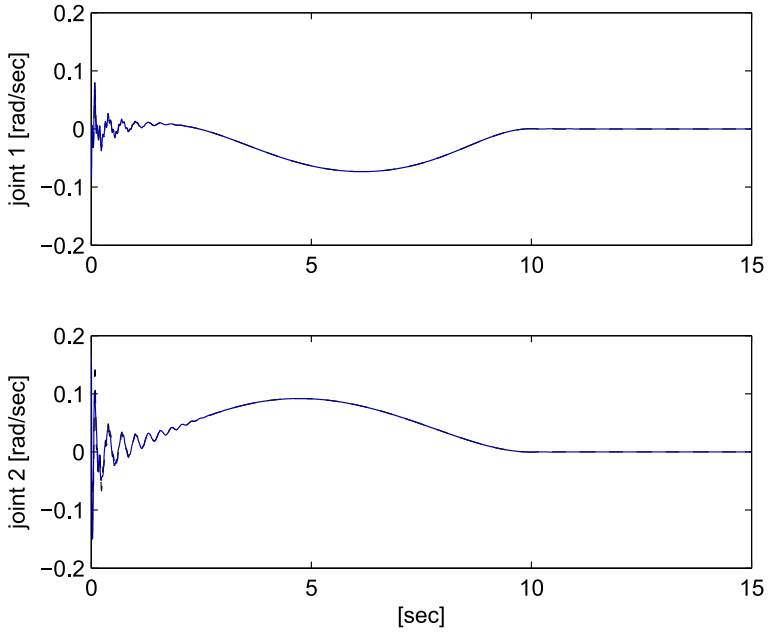

Figure 4.9: Simulation, slave joint velocities estimation: $\boldsymbol{q}_{\mathrm{s}2}$ (- - -), $\hat{\boldsymbol{q}}_{\mathrm{s}2}$ (—).

	a_i	θ_i	α_i	d_i
1	0	θ_1	90°	0
2	0.135	θ_2	0°	0
3	0.1739	θ_3	90°	0

Table 4.1: Denavit–Hartenberg parameters for the *Phantom Touch*® manipulator.

4.2 Experimental Results

An experimental platform was set to test the validity of the algorithm proposed in Chapter 3. The platform consisted of two *Phantom Touch*® manipulators of 3–degrees of freedom each, as shown in Figure 4.10.

The kinematic model for both manipulators was obtained using the Denavit-Hartenberg algorithm. The corresponding kinematic parameters are shown in Table 4.1

On the other hand, the dynamic model for each manipulator, necessary to implement the proposed scheme, is given by

$$\boldsymbol{H}_i(\boldsymbol{q}_i)\ddot{\boldsymbol{q}}_i + \boldsymbol{C}_i(\boldsymbol{q}_i,\dot{\boldsymbol{q}}_i)\dot{\boldsymbol{q}}_i + \boldsymbol{D}_i\dot{\boldsymbol{q}}_i + \boldsymbol{g}_i(\boldsymbol{q}_i) = \boldsymbol{\tau}_i, \tag{4.3}$$

where $i = \mathrm{m}, \mathrm{s}$. This model can be expressed in terms of a set of constant parameters, $\Theta_1, \ldots, \Theta_8$, as

$$\boldsymbol{H}(\boldsymbol{q}) = \begin{bmatrix} c_2^2\Theta_1 + c_2c_{23}\Theta_2 + s_{23}^2\Theta_3 & 0 & 0 \\ 0 & \Theta_1 + 2c_3\Theta_2 + \Theta_3 & c_3\Theta_2 + \Theta_3 \\ 0 & c_3\Theta_2 + \Theta_3 & \Theta_3 \end{bmatrix} \tag{4.4}$$

$$\boldsymbol{C}(\boldsymbol{q},\dot{\boldsymbol{q}}) = \begin{bmatrix} C_{11} & C_{12} & C_{13} \\ C_{21} & C_{22} & C_{23} \\ C_{31} & C_{32} & C_{33} \end{bmatrix} \tag{4.5}$$

$$\boldsymbol{D} = \begin{bmatrix} \Theta_4 & 0 & 0 \\ 0 & \Theta_5 & 0 \\ 0 & 0 & \Theta_6 \end{bmatrix} \tag{4.6}$$

$$\boldsymbol{g}(\boldsymbol{q}) = \begin{bmatrix} 0 \\ g c_2 \Theta_7 + g c_{23} \Theta_8 \\ g c_{23} \Theta_8 \end{bmatrix}, \tag{4.7}$$

where $c_1 = \cos(q_1)$, $c_{12} = \cos(q_1 + q_2)$, $c_{23} = \cos(q_2 + q_3)$ $s_1 = \sin(q_1)$, $s_{12} = \sin(q_1 + q_2)$, $s_{23} = \sin(q_2 + q_3)$, and

$$\begin{aligned}
C_{11} &= -c_2 s_2 \dot{q}_2 \Theta_1 - \frac{1}{2}(c_2 s_{23}(\dot{q}_2 + \dot{q}_3) + s_2 c_{23} \dot{q}_2)\Theta_2 + c_{23}(\dot{q}_2 + \dot{q}_3)\Theta_3 \\
C_{12} &= -c_2 s_2 \dot{q}_1 \Theta_1 - \frac{1}{2}(s_2 c_{23} + c_2 s_{23})\dot{q}_1 \Theta_2 + s_{23} c_{23} \dot{q}_1 \Theta_3 \\
C_{13} &= -\frac{1}{2} c_2 s_{23} \dot{q}_1 \Theta_2 + c_{23} s_{23} \dot{q}_1 \Theta_3 \\
C_{21} &= c_2 s_2 \dot{q}_1 \Theta_1 + \frac{1}{2}(s_2 c_{23} + c_2 s_{23})\dot{q}_1 \Theta_2 - s_{23} c_{23} \dot{q}_1 \Theta_3 \\
C_{22} &= -s_3 \dot{q}_3 \Theta_2 \\
C_{23} &= -s_3(\dot{q}_2 + \dot{q}_3)\Theta_2 \\
C_{31} &= \frac{1}{2} c_2 s_{23} \dot{q}_1 \Theta_2 - c_{23} s_{23} \dot{q}_1 \Theta_3 \\
C_{32} &= s_3 \dot{q}_2 \Theta_2 \\
C_{33} &= 0 .
\end{aligned}$$

An off–line parameter identification based on the standard Least Squares method was carried out to obtain an approximation for the parameters $\Theta_1, \ldots, \Theta_8$. The identified values for these parameters are shown in Table 4.2[1].

For the experimental setup, both manipulators are connected to a PC via *Ethernet*. The control loop for the whole teleoperation system, included the data acquisition for both robots and all the required computations, is executed in the PC with a sample time $T = 2$[msec]. As for the desired contact force, it is given by the operator through a load cell, which in turn is connected to the PC via acquisition hardware.

[1] In this table m_i is the mass of link i, a_i is a Denavit–Hartenberg parameter given in Table 4.1, l_{ci} is the link center of mass distance with respect to a frame fixed on the link i, and cf_i is the viscous friction coefficient of joint i.

Parameter	Physical meaning	Value
Θ_1	$m_2 l_{c2}^2 + \frac{1}{12} m_2 a_2^2 + m_3 a_2^2$	0.000012
Θ_2	$m_3 a_2 l_{c3}$	0.000003
Θ_3	$m_3 l_{c3}^2 + \frac{1}{12} m_3 a_3^2$	0.000015
Θ_4	$c f_1$	0.000005
Θ_5	$c f_2$	0.000006
Θ_6	$c f_3$	0.000006
Θ_7	$m_2 l_{c2} + m_3 a_2$	0.0085
Θ_8	$m_3 l_{c3}$	0.01

Table 4.2: Identified dynamic model parameters of the *Phantom Touch*® manipulator.

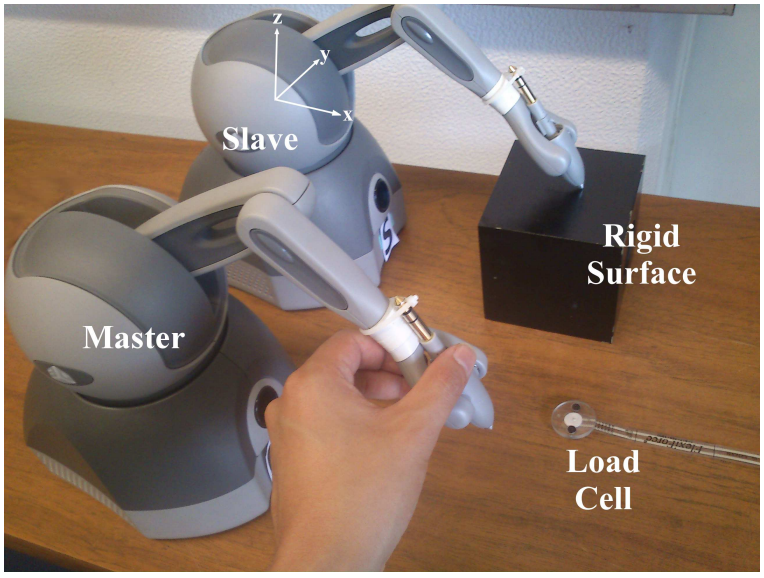

Figure 4.10: Experimental platform.

The controller gains for the master manipulator were $k_{\mathrm{Fv}} = 0.1$ and $k_{\mathrm{Fiv}} = 0.1$, while for the slave were chosen $\boldsymbol{K}_{\mathrm{ps}} = \mathrm{diag}(5,5,5)$, $\boldsymbol{K}_{\mathrm{vs}} = \mathrm{diag}(0.02,0.02,0.02)$, $\boldsymbol{K}_{\mathrm{is}} = \mathrm{diag}(0.25,0.25,0.25)$, and $k_{\mathrm{Fis}} = 2$. For the dynamic extension in (3.5)–(3.7) it was chosen $p = 2$, and the observer gains in (3.8)–(3.12) were $\lambda_0 = 1 \times 10^8 \boldsymbol{I}$, $\lambda_1 = 4 \times 10^6 \boldsymbol{I}$, $\lambda_2 = 60000 \boldsymbol{I}$, and $\lambda_0 = 400 \boldsymbol{I}$, *i.e.*, the poles were located at $p_{\mathrm{o}1} = p_{\mathrm{o}2} = p_{\mathrm{o}3} = p_{\mathrm{o}4} = -100$. For the surface estimator $\gamma = 0.02$ and $\epsilon = 0.00001$ were chosen. It was also set $\eta = 1/T = 500$ in (3.24). Finally, there were chosen $\alpha_{\mathrm{v}} = 0.02$, $\xi = 2$, and $\omega_{\mathrm{n}} = 50$ for the virtual surface construction given by (3.27).

The task consists for the human operator to impose a desired trajectory to the master, which is then followed by the slave manipulator. At the same time, the slave robot exerts the

desired force, commanded by the operator through the load cell, over the rigid metallic cube shown in Figure 4.10.

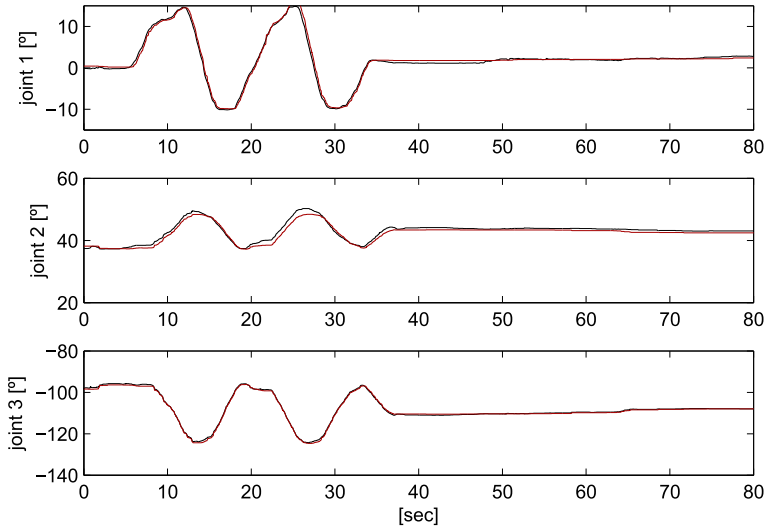

Figure 4.11: Experiment, position tracking in joint coordinates: master (—), slave (—).

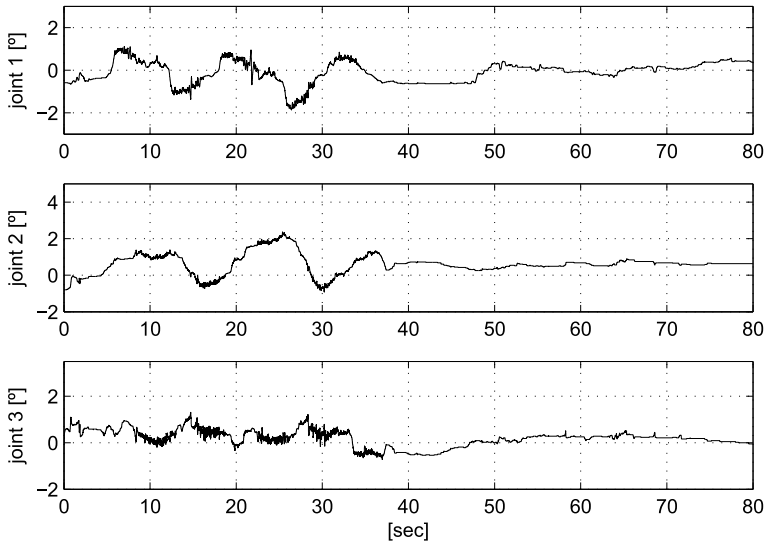

Figure 4.12: Experiment, position tracking error.

The position tracking in joint coordinates is shown in Figure 4.11, while the corresponding tracking error is displayed in Figure 4.12. Notice that the tracking error is ultimately bounded for all joints as guaranteed by the proposed algorithm.

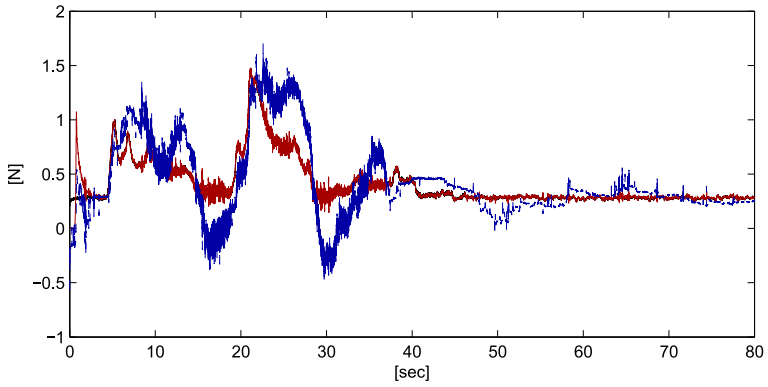

Figure 4.13: Experiment, force tracking and estimation: desired (···), estimated (—), virtual (- - -).

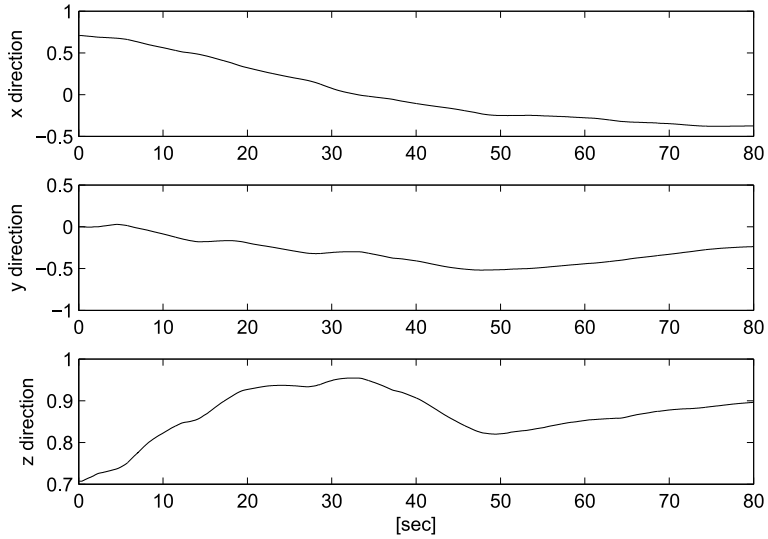

Figure 4.14: Experiment, estimation of the surface gradient $\hat{\boldsymbol{J}}_{\varphi \mathrm{xs}}$.

In Figure 4.13 the desired, estimated and virtual forces are shown. While the desired and estimated forces are practically identical signals, the virtual force is noisier. This noise is due to the tuning and the number of iterations chosen for the Lagrange multiplier computation in (3.27), so there is an application dependent trade-off between the quality of the force reflected to the human and the speed of computation of this multiplier.

Finally, in Figure 4.14 the estimated components of the surface gradient in Cartesian coordinates are shown. The initial condition for the components of this gradient was set to $\hat{\boldsymbol{J}}_{\varphi \mathrm{xs}}(t_0) = \begin{bmatrix} 1/\sqrt{2} & 0 & 1/\sqrt{2} \end{bmatrix}$, *i.e.,* it was set with an approximate initial error of $45[^\circ]$, since the

real surface gradient is $\boldsymbol{J}_{\varphi \mathrm{xs}}(t) = \begin{bmatrix} 0 & 0 & 1 \end{bmatrix}$. The discrepancy between this gradient and the estimated one is mainly due to the unmodeled contact friction.

Chapter 5

Conclusions and Future Perspectives

5.1 Concluding Remarks

In this work, the problem of master–slave bilateral teleoperation with velocity and force observation at the slave side and with estimation of the remote rigid surface geometry was studied. The main results can be summarized as:

1. An extended–state high–gain observer was designed to solve the problem with only joint position measurements. This observer has some advantages over the existing observers in the literature, for example,

    - Its tuning is easy, since the poles of (3.13) should be located as far in the left half of the complex plane as the system bandwidth allows it.
    - The implementation of the observer is straightforward, for it does not require a coordinate transformation and the same observer accounts for velocity and force estimation.

    Some disadvantages of the force/velocity observer are the *peaking phenomena*, noise amplification and the dependency on the slave manipulator model exact parameters. The first two come from the high–gain nature of the proposed observer. With respect to the peaking phenomena at the transient response beginning, a suitable *clutch* can be employed as proposed in Sira-Ramírez et al. [2010]. On the other hand, a first order filter could be used to eliminate the noise from the estimated signals. As for the dependency on the model, it could be obtained by experimental identification. Care should be taken at this point, since any error in the identification or any unexpected disturbance will

affect the observation error. Nevertheless, to the best of the authors' knowledge, there does not exist a force observer that is exempt from this dependency when only joint positions are measured.

2. An estimator of the remote surface gradient was proposed, taking the estimated signals from the force/velocity observer as inputs. This estimator is also easy to implement and its norm was proven to be invariant, which is convenient for the (unitary) gradient vector estimation that emerges from a normalized surface, as the one proposed in this work.

3. The designed velocity and force observer and the surface estimator were included in a teleoperation scheme, which is based in the *virtual surfaces* approach. The main advantages of this approach are the improvement of the bandwidth, the high transparency obtained, and the decoupling of the force and movement subspaces. This decoupling permits an orthogonal decomposition of the task space, which is widely exploited at the dynamical analysis fo the closed loop system. The proposed controllers for both master and slave manipulators make use of the estimated signals and, in accordance with the rest of the design philosophy, are easy to implement.

4. A formal stability analysis was carried out for the whole teleoperation system in closed loop with the velocity/force observer, the surface estimator and the force/position control. The proof guarantees local ultimate boundedness of all the signals of interest. By applying high gains, the ultimate bound for these signals can be made arbitrarily small, which is translated into arbitrarily close tracking of position and force, and convergence of all the estimated signals. Furthermore, high transparency of the teleoperator is also guaranteed.

5. Both simulation and experimental results are utilized to validate the applicability of the proposed scheme. The simulation results show that, under ideal conditions, position and force tracking, velocity and force estimation, surface identification and transparency are reached with an excellent performance. On the other hand, the experimental results corroborated the pertinence of the assumptions made, although the performance is no longer as good as in the simulations.

5.2 Future Directions

As pointed out above, one of the disadvantages of the proposed algorithm is its high dependence on the manipulator model exactitude. Therefore, one natural future direction could be to investigate if it is possible to avoid this model dependency or at least to reduce it. For example, in Arteaga-Pérez and Gutiérrez-Giles [2014] the standard properties of the Lagrangian model were exploited to avoid the estimation of workless forces for their further on line cancellation to solve the robust position tracking problem. This idea could be adapted to the observer design in order to evade the cancellation of some of the signals, and thus reducing the dependence on the model.

Another natural direction for future work is to address the communication delays problem. Due to destabilizing effect of these delays, most of the existing solutions to this problem rely on the controller robustness. In contrast, the goal pursued in this work is to obtain the best possible transparency of the teleoperation system. However, transparency and robust stability are two contradictory goals, so that it is reasonably that some modifications must be done to the algorithm when consider the delayed teleoperation problem.

Finally, the proposed observer is basically a dynamic extension with a high–gain linear observer. The disadvantages of the observer are mainly due to its high–gain nature. Therefore, the dynamic extension could be preserved and the high–gain observer could be substituted with another kind of the state observers available in the literature.

5.3 Summary of journal papers

The following is a list of the journal papers which were written during the author's doctorate period. Some of them contain many results presented in this work, while others were rather part of the learning process to acquire and develop the abilities, skills and know–hw of the techniques which ultimately yield to the solution of the main problem solved in this thesis.

1. Arteaga-Pérez, M. A., Rivera-Dueñas, J. C., and Gutiérrez-Giles, A. (2013). Velocity and force observers for the control of robot manipulators. *Journal of Dynamic Systems, Measurement, and Control*, 135(6):064502

2. Gutiérrez-Giles, A. and Arteaga-Pérez, M. A. (2014). GPI based velocity/force observer design for robot manipulators. *ISA Transactions*, 53(4):929–938

3. Arteaga-Pérez, M. A. and Gutiérrez-Giles, A. (2014). On the GPI approach with unknown inertia matrix in robot manipulators. *International Journal of Control*, 87(4):844–860

4. Arteaga-Pérez, M. A., Gutiérrez-Giles, A., and Weist, J. (2015). On the observability and the observer design of differential pneumatic pistons. *Journal of Dynamic Systems, Measurement, and Control*, 137(8):081006

5. Gutierrez-Giles, A., Arteaga-Perez, M. A., and Sira-Ramirez, H. (2016). Generalized proportional integral observer-based force control in robot manipulators. *Revista Iberoamericana de Automatica e Informatica Industrial*, 13(2):238–246

6. De La Guerra, A., Arteaga-Pérez, M. A., Gutiérrez-Giles, A., and Maya-Ortiz, P. (2016). Speed-sensorless control of sr motors based on gpi observers. *Control Engineering Practice*, 46:115–128

7. Gutiérrez-Giles, A. and Arteaga-Pérez, M. A. (2016b). Velocity/force observer design in the position/force control for robotic manipulators interacting with unknown rigid surfaces. *Robotics and Autonomous Systems(submitted)*

8. Gutiérrez-Giles, A. and Arteaga-Pérez, M. A. (2016a). Transparent bilateral teleoperation interacting with unknown remote surfaces with a force/velocity observer design. *International Journal of Control(submitted)*

Bibliography

Aksman, L. M., Carignan, C. R., and Akin, D. L. (2007). Force estimation based compliance control of harmonically driven manipulators. In *Robotics and Automation, 2007 IEEE International Conference on, Rome, Italy*, pages 4208–4213. IEEE.

Alcocera, A., Robertssona, A., Valerac, A., and Johanssona, R. (2004). Force estimation and control in robot manipulators. In *Robot Control 2003 (SYROCO'03): A Proceedings Volume from the 7th IFAC Symposium, Wrocław, Poland, 1-3 September 2003*, volume 1, page 55. International Federation of Automatic Control.

Anderson, R. J. and Spong, M. W. (1989). Bilateral control of teleoperators with time delay. *Automatic Control, IEEE Transactions on*, 34(5):494–501.

Arimoto, S., Liu, Y., and Naniwa, T. (1993). Principle of orthogonalization for hybrid control of robot arms. In *Proceedings of the 12th IFAC World Congress, Sydney, Australia*, volume 1, pages 507–512.

Arteaga, M. A. (1998). On the properties of a dynamic model of flexible robot manipulators. *Journal of dynamic systems, measurement, and control*, 120(1):8–14.

Arteaga-Perez, M. and Gutierrez-Giles, A. (2014). A simple application of gpi observers to the force control of robots. In *Control, Decision and Information Technologies (CoDIT), 2014 International Conference on, Metz, France*, pages 303–308. IEEE.

Arteaga-Pérez, M. A. and Gutiérrez-Giles, A. (2014). On the GPI approach with unknown inertia matrix in robot manipulators. *International Journal of Control*, 87(4):844–860.

Arteaga-Pérez, M. A., Gutiérrez-Giles, A., and Weist, J. (2015). On the observability and the observer design of differential pneumatic pistons. *Journal of Dynamic Systems, Measurement, and Control*, 137(8):081006.

Arteaga-Pérez, M. A., Rivera-Dueñas, J. C., and Gutiérrez-Giles, A. (2013). Velocity and force observers for the control of robot manipulators. *Journal of Dynamic Systems, Measurement, and Control*, 135(6):064502.

Bayo, E. and Avello, A. (1994). Singularity-free augmented lagrangian algorithms for constrained multibody dynamics. *Nonlinear Dynamics*, 5(2):209–231.

Bayo, E., De Jalon, J. G., and Serna, M. A. (1988). A modified lagrangian formulation for the dynamic analysis of constrained mechanical systems. *Computer methods in applied mechanics and engineering*, 71(2):183–195.

Callier, F. M. and Desoer, C. A. (1991). *Linear system theory*. Springer-Verlag.

Chan, L., Naghdy, F., and Stirling, D. (2013). Extended active observer for force estimation and disturbance rejection of robotic manipulators. *Robotics and Autonomous Systems*, 61(12):1277–1287.

Cheah, C. C., Hou, S. P., Zhao, Y., and Slotine, J.-J. E. (2010). Adaptive vision and force tracking control for robots with constraint uncertainty. *Mechatronics, IEEE/ASME Transactions on*, 15(3):389–399.

Chiu, C.-S., Lian, K.-Y., and Wu, T.-C. (2004). Robust adaptive motion/force tracking control design for uncertain constrained robot manipulators. *Automatica*, 40(12):2111–2119.

Chopra, N., Spong, M. W., and Lozano, R. (2008). Synchronization of bilateral teleoperators with time delay. *Automatica*, 44(8):2142–2148.

Chopra, N., Spong, M. W., Ortega, R., and Barabanov, N. E. (2006). On tracking performance in bilateral teleoperation. *Robotics, IEEE Transactions on*, 22(4):861–866.

Clement, G., Vertut, J., Fournier, R., Espiau, B., and Andre, G. (1985). An overview of cat control in nuclear services. In *Robotics and Automation. Proceedings. 1985 IEEE International Conference on*, volume 2, pages 713–718. IEEE.

Daly, J. M. and Wang, D. W. (2014). Time–delayed output feedback bilateral teleoperation with force estimation for n–dof nonlinear manipulators. *Control Systems Technology, IEEE Transactions on*, 22(1):299–306.

Davila, J., Fridman, L., Levant, A., et al. (2005). Second-order sliding-mode observer for mechanical systems. *IEEE transactions on automatic control*, 50(11):1785–1789.

De La Guerra, A., Arteaga-Pérez, M. A., Gutiérrez-Giles, A., and Maya-Ortiz, P. (2016). Speed-sensorless control of sr motors based on gpi observers. *Control Engineering Practice*, 46:115–128.

de Queiroz, M. S., Dawson, D., and Burg, T. (1996). Position/force control of robot manipulators without velocity/force measurements. In *Robotics and Automation, 1996. Proceedings., 1996 IEEE International Conference on, Minneapolis, MN, USA*, volume 3, pages 2561–2566. IEEE.

Dean-León, E. C., Parra-Vega, V., and Espinosa-Romero, A. (2006). Visual servoing for constrained planar robots subject to complex friction. *Mechatronics, IEEE/ASME Transactions on*, 11(4):389–400.

Doulgeri, Z. and Karayiannidis, Y. (2008). Force/position regulation for a robot in compliant contact using adaptive surface slope identification. *Automatic Control, IEEE Transactions on*, 53(9):2116–2122.

Ferrell, W. R. and Sheridan, T. B. (1967). Supervisory control of remote manipulation. *Spectrum, IEEE*, 4(10):81–88.

Goertz, R. C. (1954). Mechanical master-slave manipulator. *Nucleonics (US) Ceased publication*, 12.

Goertz, R. C. and Thompson, W. M. (1954). Electronically controlled manipulator. *Nucleonics (US) Ceased publication*, 12.

Guizzo, E. and Goldstein, H. (2005). The rise of the body bots [robotic exoskeletons]. *IEEE spectrum*, 42(10):50–56.

Gutierrez-Giles, A., Arteaga-Perez, M., et al. (2013). Velocity/force observer design for robot manipulators. In *Methods and Models in Automation and Robotics (MMAR), 2013 18th International Conference on, Międzyzdroje, Poland*, pages 730–735. IEEE.

Gutiérrez-Giles, A. and Arteaga-Pérez, M. A. (2014). GPI based velocity/force observer design for robot manipulators. *ISA Transactions*, 53(4):929–938.

Gutiérrez-Giles, A. and Arteaga-Pérez, M. A. (2016a). Transparent bilateral teleoperation interacting with unknown remote surfaces with a force/velocity observer design. *International Journal of Control(submitted)*.

Gutiérrez-Giles, A. and Arteaga-Pérez, M. A. (2016b). Velocity/force observer design in the position/force control for robotic manipulators interacting with unknown rigid surfaces. *Robotics and Autonomous Systems(submitted)*.

Gutierrez-Giles, A., Arteaga-Perez, M. A., and Sira-Ramirez, H. (2016). Generalized proportional integral observer-based force control in robot manipulators. *Revista Iberoamericana de Automatica e Informatica Industrial*, 13(2):238–246.

Hacksel, P. and Salcudean, S. (1994). Estimation of environment forces and rigid-body velocities using observers. In *Robotics and Automation, 1994. Proceedings., 1994 IEEE International Conference on, San Diego, CA, USA*, pages 931–936. IEEE.

Hannaford, B. and Kim, W. S. (1989). Force reflection, shared control, and time delay in telemanipulation. In *Systems, Man and Cybernetics, 1989. Conference Proceedings., IEEE International Conference on, Cambridge, MA, USA*, pages 133–137. IEEE.

Hashtrudi-Zaad, K. and Salcudean, S. E. (1996). Adaptive transparent impedance reflecting teleoperation. In *Robotics and Automation, 1996. Proceedings., 1996 IEEE International Conference on, Minneapolis, MN, USA*, volume 2, pages 1369–1374. IEEE.

Hashtrudi-Zaad, K. and Salcudean, S. E. (2002). Transparency in time-delayed systems and the effect of local force feedback for transparent teleoperation. *Robotics and Automation, IEEE Transactions on*, 18(1):108–114.

Hirzinger, G., Brunner, B., Dietrich, J., and Heindl, J. (1993). Sensor-based space robotics-rotex and its telerobotic features. *IEEE Transactions on robotics and automation*, 9(5):649–663.

Hokayem, P. F. and Spong, M. W. (2006). Bilateral teleoperation: An historical survey. *Automatica*, 42(12):2035–2057.

Huang, H.-P. and Tseng, W.-L. (1988). An observer design for constrained robot systems. In *Decision and Control, 1988., Proceedings of the 27th IEEE Conference on, Austin, TX, USA*, pages 2261–2263. IEEE.

Huang, H.-P. and Tseng, W.-L. (1991). Asymptotic observer design for constrained robot systems. In *Control Theory and Applications, IEE Proceedings D*, volume 138, pages 211–216. IET.

Isidori, A. (1995). *Nonlinear control systems*. Springer-Verlag London Limited.

Juárez-Abad, J. A., Linares-Flores, J., Guzmán-Ramírez, E., and Sira-Ramirez, H. (2014). Generalized proportional integral tracking controller for a single-phase multilevel cascade inverter: an fpga implementation. *Industrial Informatics, IEEE Transactions on*, 10(1):256–266.

Karayiannidis, Y. and Doulgeri, Z. (2009). Adaptive control of robot contact tasks with on-line learning of planar surfaces. *Automatica*, 45(10):2374–2382.

Karayiannidis, Y. and Doulgeri, Z. (2010). Robot contact tasks in the presence of control target distortions. *Robotics and Autonomous Systems*, 58(5):596–606.

Khalil, H. K. (2002). *Nonlinear systems*. Prentice Hall.

Kurtzer, I. L., Pruszynski, J. A., and Scott, S. H. (2008). Long-latency reflexes of the human arm reflect an internal model of limb dynamics. *Current Biology*, 18(6):449–453.

Lawrence, D. A. (1993). Stability and transparency in bilateral teleoperation. *Robotics and Automation, IEEE Transactions on*, 9(5):624–637.

Lee, H.-K. and Chung, M. J. (1998). Adaptive controller of a master–slave system for transparent teleoperation. *Journal of Robotic Systems*, 15(8):465–475.

Leite, A. C., Lizarralde, F., and Hsu, L. (2009). Hybrid adaptive vision/force control for robot manipulators interacting with unknown surfaces. *The International Journal of Robotics Research*, 28(7):911–926.

Lippiello, V., Siciliano, B., and Villani, L. (2007). A position-based visual impedance control for robot manipulators. In *Robotics and Automation, 2007 IEEE International Conference on, Rome, Italy*, pages 2068–2073. IEEE.

Liu, X., Tao, R., and Tavakoli, M. (2014). Adaptive control of uncertain nonlinear teleoperation systems. *Mechatronics*, 24(1):66–78.

Liu, X., Tavakoli, M., and Huang, Q. (2010). Nonlinear adaptive bilateral control of teleoperation systems with uncertain dynamics and kinematics. In *Intelligent Robots and Systems (IROS), 2010 IEEE/RSJ International Conference on, Taipei, Taiwan*, pages 4244–4249. IEEE.

Luviano-Juarez, A., Cortes-Romero, J., and Sira-Ramirez, H. (2010). Synchronization of chaotic oscillators by means of generalized proportional integral observers. *International Journal of Bifurcation and Chaos*, 20(05):1509–1517.

Martınez-Rosas, J. C. and Arteaga, M. A. (2008). Force and velocity observers for the control of cooperative robots. *Robotica*, 26:85–92.

Martínez-Rosas, J. C., Arteaga, M. A., and Castillo-Sánchez, A. M. (2006). Decentralized control of cooperative robots without velocity–force measurements. *Automatica*, 42(2):329–336.

Miyazaki, F., Matsubayash, S., Yoshimi, T., and Arimoto, S. (1986). A new control methodology toward advanced teleoperation of master-slave robot systems. In *Robotics and Automation. Proceedings. 1986 IEEE International Conference on, San Francisco, CA, USA*, volume 3, pages 997–1002. IEEE.

Murray, R. M., Li, Z., Sastry, S. S., and Sastry, S. S. (1994). *A mathematical introduction to robotic manipulation*. CRC press.

Namvar, M. and Aghili, F. (2005). Adaptive force-motion control of coordinated robots interacting with geometrically unknown environments. *Robotics, IEEE Transactions on*, 21(4):678–694.

Nicosia, S. and Tomei, P. (1990). Robot control by using only joint position measurements. *Automatic Control, IEEE Transactions on*, 35(9):1058–1061.

Niemeyer, G. and Slotine, J.-J. E. (1991). Stable adaptive teleoperation. *Oceanic Engineering, IEEE Journal of*, 16(1):152–162.

Niemeyer, G. and Slotine, J.-J. E. (1998). Towards force-reflecting teleoperation over the internet. In *Robotics and Automation, 1998. Proceedings. 1998 IEEE International Conference on, Leuven, Belgium*, volume 3, pages 1909–1915. IEEE.

Nuño, E., Basañez, L., and Ortega, R. (2011). Passivity-based control for bilateral teleoperation: A tutorial. *Automatica*, 47(3):485–495.

Nuño, E., Basañez, L., Ortega, R., and Spong, M. W. (2009). Position tracking for non-linear teleoperators with variable time delay. *The International Journal of Robotics Research*, 28(7):895–910.

Ohishi, K., Miyazaki, M., and Fujita, M. (1992). Hybrid control of force and position without force sensor. In *Industrial Electronics, Control, Instrumentation, and Automation, 1992. Power Electronics and Motion Control., Proceedings of the 1992 International Conference on, San Diego, CA, USA*, pages 670–675. IEEE.

Phong, L. D., Choi, J., and Kang, S. (2012). External force estimation using joint torque sensors for a robot manipulator. In *Robotics and Automation (ICRA), 2012 IEEE International Conference on, St. Paul, MN, USA*, pages 4507–4512. IEEE.

Pliego-Jiménez, J. and Arteaga-Pérez, M. A. (2015). Adaptive position/force control for robot manipulators in contact with a rigid surface with uncertain parameters. *European Journal of Control*, 22:1–12.

Ramírez-Neria, M., Sira-Ramírez, H., Garrido-Moctezuma, R., and Luviano-Juarez, A. (2014). Linear active disturbance rejection control of underactuated systems: The case of the furuta pendulum. *ISA transactions*, 53(4):920–928.

Ramírez-Neria, M., Sira-Ramírez, H., Garrido-Moctezuma, R., and Luviano-Juárez, A. (2016). On the linear control of underactuated nonlinear systems via tangent flatness and active disturbance rejection control: The case of the ball and beam system. *Journal of Dynamic Systems, Measurement, and Control*, 138(10):104501.

Ramírez-Neria, M., Sira-Ramírez, H., Luviano-Juárez, A., and Rodrguez-Ángeles, A. (2015). Active disturbance rejection control applied to a delta parallel robot in trajectory tracking tasks. *Asian Journal of Control*, 17(2):636–647.

Ramirez-Neria, M., Sira-Ramirez, H., Luviano-Juarez, A., and Rodriguez-Angeles, A. (2013). Smith predictor based generalized pi control for a class of input delayed nonlinear mechanical systems. In *Control Conference (ECC), 2013 European, Zurich, Switzerland*, pages 1292–1297. IEEE.

Rivera-Dueñas, J. C. and Arteaga-Pérez, M. A. (2013). Robot force control without dynamic model: theory and experiments. *Robotica*, 31(01):149–171.

Rodríguez-Angeles, A., Arteaga-Pérez, M. A., Portillo-Vélez, R. d. J., and Cruz-Villar, C. A. (2015). Transparent bilateral master–slave control based on virtual surfaces: Stability analysis and experimental results. *International Journal of Robotics and Automation*, 30(2):128–139.

Rodriguez-Angeles, A. and Garcia-Antonio, J. (2014). Active disturbance rejection control in steering by wire haptic systems. *ISA transactions*, 53(4):939–946.

Sira-Ramírez, H., Castro-Linares, R., and Puriel-Gil, G. (2014). An active disturbance rejection approach to leader-follower controlled formation. *Asian Journal of Control*, 16(2):382–395.

Sira-Ramirez, H., Linares-Flores, J., Garcia-Rodriguez, C., and Contreras-Ordaz, M. A. (2014). On the control of the permanent magnet synchronous motor: An active disturbance rejection control approach. *Control Systems Technology, IEEE Transactions on*, 22(5):2056–2063.

Sira-Ramírez, H., Ramírez-Neria, M., and Rodríguez-Angeles, A. (2010). On the linear control of nonlinear mechanical systems. In *Decision and Control (CDC), 2010 49th IEEE Conference on, Atlanta, GA, USA*, pages 1999–2004. IEEE.

Tee, K. P., Burdet, E., Chew, C.-M., and Milner, T. E. (2004). A model of force and impedance in human arm movements. *Biological cybernetics*, 90(5):368–375.

Wang, D. and McClamroch, H. (1994). Stability analysis of the equilibrium of a constrained mechanical system. *International Journal of Control*, 60(5):733–746.

Wang, D., Soh, Y. C., Ho, Y. K., and Müller, P. C. (1998). Global stabilization for constrained robot motions with constraint uncertainties. *Robotica*, 16(02):171–179.

Yokokohji, Y. and Yoshikawa, T. (1994). Bilateral control of master-slave manipulators for ideal kinesthetic coupling-formulation and experiment. *Robotics and Automation, IEEE Transactions on*, 10(5):605–620.

Yoshikawa, T. and Sudou, A. (1993). Dynamic hybrid position/force control of robot manipulators-on-line estimation of unknown constraint. *IEEE Transactions on Robotics and Automation*, 9(2):220–226.